Parametric Development of Wire 3D Printing

by

Jeffrey Scott Gaddes

A thesis submitted to the Graduate Faculty of
Auburn University
in partial fulfillment of the
requirements for the Degree of
Master of Science

Auburn, Alabama
December 12, 2015

Keywords: additive manufacturing, welding, casting

Approved by

Lewis N. Payton, Associate Research Professor, Mechanical Engineering
Ruel A. (Tony) Overfelt, Professor, Materials Engineering
Dan B. Marghitu, Professor, Mechanical Engineering

Abstract

Currently commercialized additive manufacturing techniques offer great detail in small, difficult to produce parts. They are also slow, limited in scale, and expensive. An additive technique that can rapidly produce large parts is under development in the current thesis. The inexpensive Wire 3D printing process in development uses an electric arc to melt and deposit metal alloys at much greater rates than other additive manufacturing techniques. Large parts can be created (replacing a sand or investment casting) directly from drawings more rapidly with less material waste or machining time. Unique metal parts are quickly and economically produced.

A wire 3D printer machine was designed, constructed, and evaluated at Auburn University. The wire 3D printer features a modular, open frame design allowing for easy access and continuous upgrades. A standard parametric data sheet was developed to establish a common data set for future researchers. Voltage and current requirements for different wire diameters were analyzed along with resulting wall widths and heights.

Hollow and solid test geometries were printed in steel, aluminum, and stainless steel. The tensile strength of deposited steel structures was measured in multiple orientations achieving up to 90% of standard material values in one orientation. The microstructure and hardness of deposited structures were examined to determine process consistency. Deposited steel structures were found to be heat treatable.   With improved controls and in-process feedback, custom castings can be easily replaced using this process in a wide array of materials. The wire 3D printing process is a viable option for low cost and rapid manufacture of metallic objects.

Acknowledgments

Many people contributed to this project and deserve recognition for its success. I would like to thank my committee for their guidance. My advisor, Dr. Payton, was especially supportive and provided me the opportunity to work in the Design and Manufacturing Laboratory. Dr. Overfelt contributed technical expertise and guidance. The engineering staff at Auburn University was also very helpful. Mr. Moore performed mechanical testing and contributed welding advice. Mr. Marcell solved many electrical problems.

I am also grateful for my fellow researchers' encouragement and technical assistance. Wesley Hunko's help constructing the printer and troubleshooting issues was invaluable. The project would not have been completed without help from the graduate and undergraduate students in the laboratory.

I would also like to thank my family for their unending love and support. I am especially grateful for my fiancé's encouragement and commitment. Finally, I would like to thank God for blessing me with this opportunity.

Table of Contents

List of Tables

List of Figures

I. Introduction

Metal additive manufacturing can be performed by using a modified Metal Inert Gas (MIG) welder to deposit material using computer control. While traditionally used for joining metals, the MIG process has been coupled with computer controlled machines since the 1990s to additively manufacture parts. With the advent of modern additive manufacturing controls software, MIG additive manufacturing is a viable method for metal 3D printing. The MIG process is advantageous in comparison to other metal additive manufacturing techniques because of its high material deposition rate and low cost.

A MIG based 3D printer was designed, constructed, and evaluated. The machine uses off-the-shelf components and a MIG welder as the power source. Freely available software was modified to print CAD files and control the printer. The proper parameters for machine operation were determined, and a machine operation manual was created.

To evaluate the 3D printer's capabilities, multiple geometries were printed. These include hollow objects, solid objects, and objects with complex curves. These objects were printed with steel (ER70S-6), aluminum (ER4041), and stainless steel (ER308).

In addition to multiple materials, wire diameters ranging from 0.025 to 0.035 in. were used. The influence of wire diameter on both deposited wall width and required welder electrical power was studied. A basic geometric model was created to predict the deposited layer's width based upon wire diameter and feed rates.

The tensile strength of the 3D printed structures in multiple orientations was examined for both steel (ER70S-6) and stainless steel (ER308). The tensile strengths were determined to be nearly the wire manufactures' specification when pulled in the direction parallel to the deposited layers. However, the tensile strength was much less in the direction perpendicular to the layers.

The deposited steel (ER70S-6) microstructure was examined. Additionally, deposited steel (ER70S-6) structures were heat treated to determine if the hardness and grain structure could be desirably modified.

Multiple build plate materials were examined for steel (ER70S-6) and aluminum (ER4041) deposition. A suitable build plate for both materials was determined.

Finally, an experimental record sheet was created for future researchers. This record sheet provides an organized platform for future collaborative research efforts in the field of MIG additive manufacture.

II. Scope and Objectives

The comprehensive literature indicates a lack of uniformity and standards amongst experimentalists as is to be expected in an emerging area of research. Research reports lack the detail needed to exactly recreate any of the experiments to date. A standardized approach needs to be developed in order to report the parameters of the process before researchers can begin to truly optimize the process. This need will be incorporated within the scope of this thesis. Additionally, any demonstrated result that is reported will have been reproduced at least twice.

Specific objectives for the thesis include:

- Construct a precision 3 axis Wire 3D printer (0.001 inches +/- 0.0005 inches) with a large build volume using off the shelf components modified within the laboratory.

- Document the printer's construction (drawings, bill of materials, etc.).

- Develop an operator's manual for subsequent Auburn University investigators.

- Decide what can be measured and reported and develop a standard parametric data sheet for each setup/data run.

- Recreate and improve upon the voltage and current measuring technique developed by Pinar *et, al* [1].

- Study the electrical power demands for three different wire diameters in two different wire materials.

- Develop an optical system for observation and possible future feedback control.

- Instrument the process with thermocouples to document heat history and future in-process thermal feedback.

- Study and compare available "slicing" software.

- Develop strategy to deal with "slumping" reported by researchers.

- Develop a standard solid "wall" from which to machine tensile specimens.

- Study tensile strength of standard walls made with three different materials given uniform wire diameters (0.030 inches). Specimens will be made parallel and perpendicular to the direction of deposition.

- Develop a best fill pattern/building strategy for producing thick walled or solid parts.

- Find a suitable base material which allows for quick removal of the printed parts without the need for sawing, wire EDM, or any other machining technique.

- Develop solid specimen geometry to study the effects of heat treatment including changes in the material hardness and granular structure.

- Compare dimensional accuracy of final product to original drawings.

- Determine and graph how much wire goes into a given height and a given width for three alloys all at a uniform wire thickness (0.030 inches).

- Demonstrate the ability to create this standard geometric shapes in three different alloys all at a uniform wire thickness (0.030 inches):
    o Solid square shapes
    o Solid cylindrical shapes.
    o Hollow rectangular shapes
    o Hollow cylindrical shapes

- o Capped hollow shapes

- o Hollow hourglass shape

- Mill solid squares and turn solid cylinders while examining for internal voids

- Bore and turn hollow cylindrical shapes to a smooth surface finish.

- Print an eight-inch diameter, two-inch-high steel skillet with an eight-inch handle.

- Print the block for a small bore steam engine design.

III. Literature Review

Metal Additive Manufacturing

Metal additive manufacturing systems are classified into three broad categories: powder bed systems, powder feed systems, and wire feed systems [2]. Each type of system and its advantages and disadvantages are described below.

Powder bed systems create objects by applying an energy source (electron or laser beam) to selective points on a consistent leveled bed of powder. After melting or sintering a region of powder, additional powder is then evenly distributed across the build surface. The process is repeated to form an object of multiple layers. Powder bed systems currently have a build volume of less than 10 ft^3 (0.03 m^3). Powder bed systems have the advantage of producing high resolution objects with internal features [2]. However, powder bed systems are costly to purchase and operate. Because the entire machine is filled with material, powder bed systems often waste a large amount of un-sintered powder. Additionally, powder bed systems have low material deposition rates [3].

Instead of selectively melting regions of a bed of powder, a powder feed system melts powder as it is deposited. Powder feed systems create objects by depositing a fed powder which is melted or sintered by an energy source. The process is repeated to form multiple layers upon the previous deposit. This type of system currently has a build volume of less than 55 ft^3 (1.5 m^3). Powder feed systems have the advantages of producing large objects and only depositing powder where it is need to build the object.

However, powder feed systems are not capable of producing internal passages like powder bed systems and have relatively low material deposition rates [2].

Wire feed systems create objects by depositing a fed wire of material. The fed wire is melted by an electron beam, a laser beam, or a plasma arc. The process is repeated to form multiple layers upon the previous deposit. This method has the advantage of high deposition rates and large build volumes. Additionally, wire fed machines may be created for less than $2000 which is approximately ten times less costly than other metal manufacturing systems [4]. Another advantage of wire fed machines is the economic use of material. Wire feed systems only deposit object material without waste and have low raw material costs when compared to powders. This makes wire fed machines ideal for near net shape manufacturing of large structural objects with low material waste which greatly reduces the amount of subtractive machining post processing. Additionally, wire feed systems do not require complex powder distribution hardware and are easily integrated to a gantry style CNC machine. This results in easy integration into existing hardware and almost no limit on build volume [3]. Most frequently however, this method is used to create a net shape object that requires a machining post process [2]. In this regard, the wire and arc additive manufacturing process is similar to a sand casting which also requires a machining post process.

Wire and Arc Additive Manufacturing

The wire fed additive manufacturing process can be further classified into multiple types dependent upon the wire melting method. The two types of wire fed additive manufacturing systems use a repurposed and modified Tungsten Inert Gas (TIG/GTAW) or Metal Inert Gas (MIG/GMAW) welding power source [3]. The TIG

process uses an energy source (laser, electron beam, or electricity) to melt a fed wire in an inert gas environment. The MIG process uses a consumable wire electrode that is melted by electricity and deposited in an inert gas environment.

Both the MIG deposition process and the TIG deposition process have advantages. The MIG process results in an easier control because it requires less moving components than the TIG process. The TIG process requires movement of an electrode and the deposited metal wire. The MIG process only has one moving component because the deposited metal wire is the electrode. Additionally, the MIG process does not require orientation of the deposited metal wire. The TIG process requires appropriate orientation of the wire as well as the arc source which results in complicated toolpath generation. The TIG process, however, is less prone to electric arc wandering and a better surface finish is consequently easier to achieve [3].

MIG Welding Processes Applied to Additive Manufacturing

When considering MIG welding deposition, there are multiple methods of metal transfer depending upon process and control variations. Metal transfer is the process by which the fed wire is melted by electricity and deposited on the substrate. These methods include Short Circuit Transfer, Globular Transfer, Spray Arc Transfer, and Cold Metal Transfer (CMT) [5][6].

Short Circuit Transfer is the traditional MIG process as illustrated in Figure 1. During the Short Circuit Transfer process, the welding wire contacts the base metal between 90-200 times per second. While Short Circuit Transfer is not capable of as high deposition rates as Spray Arc Transfer, it does have several advantages. Short Circuit Transfer requires relatively low voltages and consequently lower heat is put into the

welded object. A potentially negative consequence of this behavior is a lack of complete weld fusion when attempting to weld thick metals [5]. However, the additive manufacturing process requires less heat input than a traditional weld which requires full heating and penetration of two pieces of base metal. In the additive manufacturing process, only enough energy to penetrate the relatively thin previously deposited layer is required. This makes the Short Circuit Transfer mechanism capable of high deposition rates.
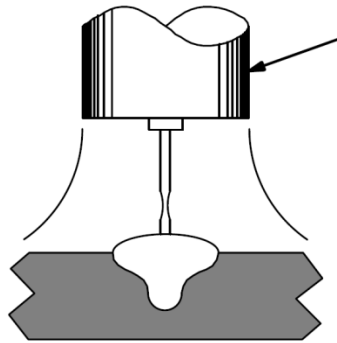
Figure 1: MIG Short Circuit Transfer [5]

An intermittent mode of transfer between Short Circuit Transfer and Spray Arc Transfer is Globular Transfer. Shown in Figure 2, Globular Transfer occurs when globs of hot metal accumulate on the fed wire electrode and are discharged onto the base metal. Instead of a small amount of metal being deposited during a brief short circuit, a large amount of metal accumulates on the electrode before it is deposited. Globular Transfer is not a preferred mode because it creates large amounts of spatter, a large weld, and a poor weld appearance [5]. This makes it a poor choice for application in additive manufacturing.
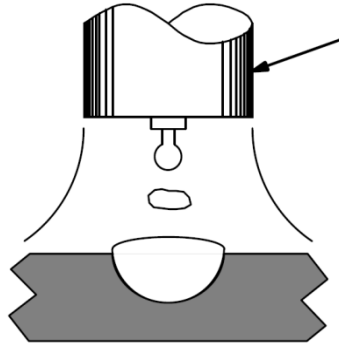
Figure 2: MIG Globular Transfer [5]

As shown in Figure 3, Spray Arc Transfer occurs when a stream of tiny drops flow from the fed wire electrode to the base metal. Spray Arc Transfer has the advantage of a high deposition rate and good weld penetration. However, Spray Arc Transfer does require higher power input to the weld and consequently adds more heat to the deposit [5]. This behavior makes Spray Arc Transfer not conducive to the ideally low thermal input additive manufacturing process.
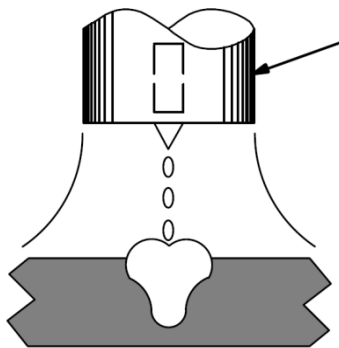
Figure 3: MIG Spray Arc Transfer [5]

The final MIG welding technique is Cold Metal Transfer (CMT) and as illustrated in Figure 4. Developed by the Austrian company Fronius, CMT is a relatively novel welding technique which involves a controlled dip transfer. During the CMT process, wire electrode is fed towards the base metal. Upon contact of the base metal, the electric current is reduced and the wire fed upward to deposit a small drop of material. The

process is then repeated. This process has the advantage of lower thermal input than other MIG welding techniques. The electrical power melting the wire is more precisely controlled which results in an overall lower process temperature. However, this process requires expensive equipment and proprietary control schemes [3].
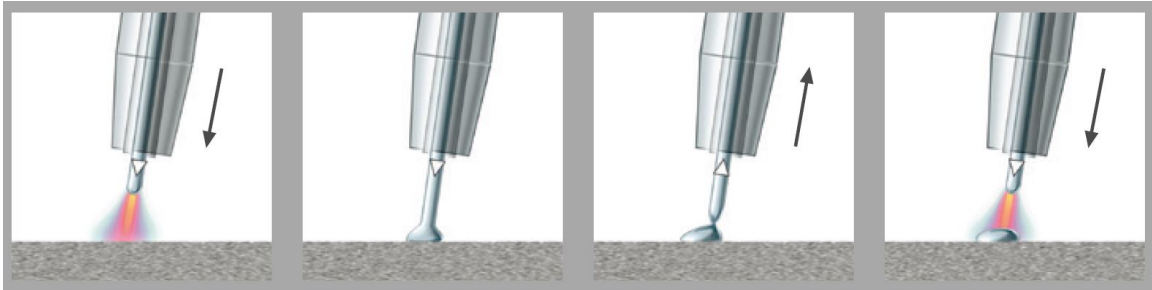
Figure 4: MIG Cold Metal Transfer [6]

The least costly, most researched type of MIG welding is the short circuit transfer process. Therefore, this review will hereafter focus upon the application of the short circuit transfer method to additive manufacturing.

Wire and Arc Additive Manufacturing using Short Circuit Transfer MIG

Short circuit transfer MIG welding has been applied to additive manufacturing in several research attempts which are discussed below. Major contributors to the field include researchers at Cranfield University, UK, University of Nottingham, UK, University of Minho, Portugal, and Southern Methodist University, Dallas, Texas [7]. The development of the short circuit MIG based additive manufacturing process is outlined in Figure 5.

```
            ┌─────────────────┐
            │ Patents for metal│
            │ layer deposition │
            │      (1925)      │
            └────────┬─────────┘
                     │
            ┌────────┴─────────┐
            │   SAW Research   │
            │   (1943 -1986)   │
            └────────┬─────────┘
                     │
            ┌────────┴─────────┐
            │   MIG Research   │
            │   (1990-Now)     │
            └────────┬─────────┘
                     │
     ┌───────────────┴──────────────┐
┌────┴──────────┐          ┌─────────┴──────┐
│ MIG and Milling│          │  Low Cost MIG  │
│ Research (1998-│          │ Research (2013 -│
│     2004)      │          │     Now)       │
└───────────────┘          └────────────────┘
```
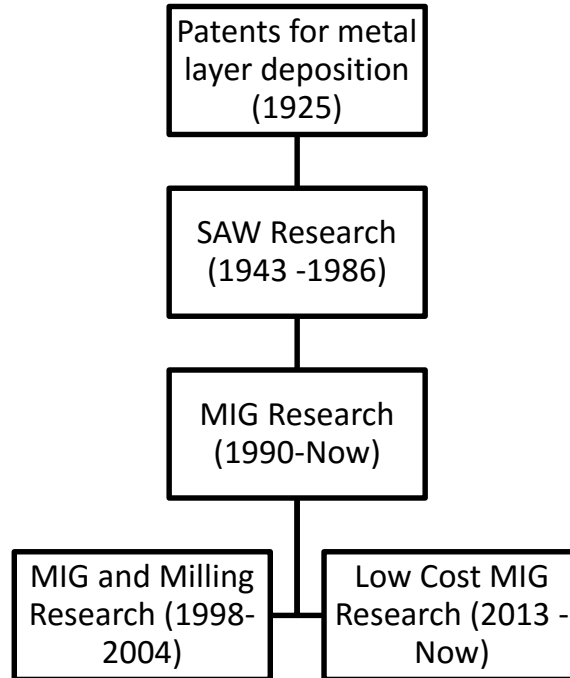
Figure 5: History of Cold Metal Transfer MIG AM Techniques

As shown in Figure 5, wire and arc additive manufacturing was first recorded in a patent by Baker in 1925. The patent, entitled Method of Making Decorative Articles presented a novel method of creating objects using a fusible metal electrode and electricity to deposit material in fused subsequent layers to form an object. The patent included drawings of two objects and a close up of built up layers as shown in Figure 6. In the patent text, Baker identified that the current was related to the speed of the moving electrode and the thickness of the layer. Additionally, Baker moved the electrode in a tight circular manner to create the deposit. Baker focused on creating decorative objects that did not have any mechanical value. The process was not mechanized and relied upon the operator for movement of the welding tip [8].
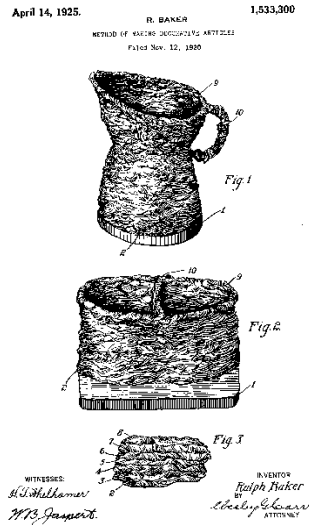
Figure 6: Baker's Patent [8]

Additional research in the wire and arc additive manufacturing field in subsequent years (prior to CNC) is evidenced by the filing of several patents. In 1925, Eschholz deposited single layers of metal to form ornamental letters. Eschholz determined that the important process parameters were substrate material, arc current, travel speed, bead width, bead height, and penetration depth [9].

Shockey in 1932 used the novel wire and arc deposition method in his patent for *Machine for Reclaiming Worn Brake Drums*. In the patent, one layer tall weld beads were deposited on worn brake drums so they could be returned to service. After depositing the material, the brake drum was machined to the correct size. The mechanization of the deposition process instead of manual operator movement of the weld head was the major improvement in this patent method. As a result, Shockey noted the impact of travel speed and electrical current on the geometry of the deposited bead. Although investigated, Shockey's technique determined to not be economically viable

13

because the refurbishment process was costly compared the cost of new brake drum [10]. In 1933, Noble filed a similar patent for a cost effective method of enlarging shaft diameters. Noble proposed near net shape manufacturing of a collar on a shaft instead of machining a large diameter shaft with great material waste [11].

In 1943, a significant development was made as evidenced in a patent by Carpenter and Kerr. This invention used the relatively new high deposition rate Submerged Arc Welding (SAW) process to deposit alloys with a significant percentage of chromium (24-27%) and nickel (19-22%). Their objective was to manufacture large shafts with increased strength when compared to traditionally manufactured objects. As a factor, the team considered the amount of granular flux used to prevent oxidation. It was determined that the substrate must be preheated to permit a high rate of metal deposition. Preheating seemed to allow a greater feedrate [12].

The SAW process continued to be refined in a 1962 patent by White in which rollers were used to apply pressure to the previously deposited layer. White observed large variability in the process which prevented its application in food processing industry. The pressure roller improved the surface of the layer and created a more consistent process. For future work, White proposed that pre-heating the roller improved the deposit quality and recommended a post process of gradual cooling for internal stress relief [13].

In patents filed in 1967 and 1970 by Ujiie, large thick-walled pressure vessels were created. In addition to the flux shielded SAW process, Ujiie used an inert shielding gas and multiple welding nozzles. To achieve a high deposition rate, three simultaneous parallel wire electrodes were used. This created a larger weld pool than previous

researchers. However, the large weld pool had degraded grain structure and voids when compared to the single wire electrode objects using a smaller weld pool. When using a smaller weld pool resulting from a single welding nozzle, Ujiie hypothesized that the pressure vessel's good mechanical properties resulted from the tempering effects of subsequent layer deposition [14].

A patent filed in 1974 by Brandi and Luckow, featured fabrication of large shafts and rotors for turbines and electric generator applications requiring high strength and durability. They compared the near net shape manufacturing process to the traditionally used forging process and concluded that the novel method had only slightly less mechanical properties and isotropicity. Additionally, they determined that the welding power and temperature of the substrate and subsequent layers were critical factors that could be controlled [15].

The SAW additive manufacturing process continued to be developed and studied with multiple welding heads and steel alloys. Significant improvements in mechanical properties were observed with comparing deposited parts to forged and rolled objects. Prior to the Chernobyl disaster in 1986, German researchers at the large steelmaker *Thyssen-Hutte AG* were focused on applying near net shape additive manufacturing techniques to produce nuclear boilers or pressure vessels. After 1986, the rapid SAW additive manufacturing research powered by a high market demand for nuclear energy was refocused on production of pressure vessels for the chemical industry or heavy turbine shafts. However, funding for these industries was not sufficient for the previous research rate [16].

In 1990, Acheson was granted a patent titled *Automatic Welding Apparatus for Weld Build-up and Method of Achieving Weld Build-up*. He included a nozzle for a shielding gas that moved with the fed arcing wire in a process similar to the Gas Metal Arc Welding (GMAW) also known as Metal Inert Gas (MIG) welding. Acheson focused on the mechanical design of nozzle with shielding gas to additive manufacturing but did not provide any testing or evaluation of his invention [17]. However, this patent marked the beginning of the current trend of focused research of the MIG based wire and arc additive manufacturing process.

With the proliferation of Computer Numerical Control (CNC), the wire and arc additive manufacturing process has been increasingly researched and developed focusing on the GMAW process. Recognizing the potential of this additive manufacturing technique to be a disruptive technology, Rolls-Royce in the early 1990s internally investigated the application of this technique to the aerospace industry. The focus of the research was on lowering cost by producing near net shape high performance alloys with low waste [16,18].

At the University of Nottingham in 1992, UK, Dickens, *et al.* conducted a notable preliminary study of additive manufacturing using MIG based methods. A commercially available welding robot was used, and the researchers noted significant advantages to the process when compared to conventional manufacturing techniques. These techniques included robotic control and automation, consistent material properties, rapid manufacturing times, and material efficiency. The team used mild steel welding wire based on Fe-C (0.08%) - Si:(0.9%) Mn(1.5%). As shown in Figure 7 and Figure 8 the authors achieved production of a square box and a truncated pyramid [18].
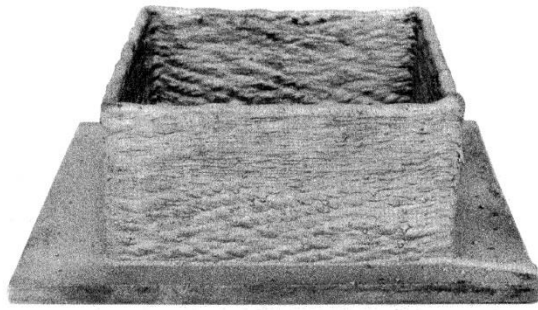
Figure 7: Box produced by Dickens, et al. using MIG Process [18]
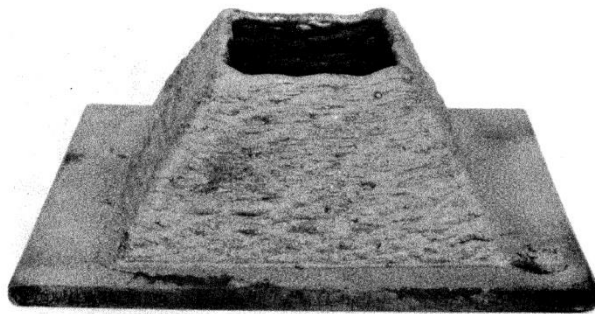
Figure 8: Truncated hollow pyramid produced by Dickens, et al. using MIG process [18]

Dickens, *et al.* emphasized the importance of geometry of the produced weld bead and conducted numerous trials of singular weld beads with varying parameters. The authors observed that the geometry of the weld bead was dependent upon several factors. The authors studied voltage, wire feed rate, wire stickout distance from the nozzle, wire diameter, and welding velocity in observing their effect on arc voltage, arc current, layer width, and layer height. The general trends were presented in the table shown in Table 1. It was observed that the shape of the weld bead could be modified from a wide and flat bead to a narrow bead when producing vertical walls by varying the velocity of the welder [18].

Table 1: Interactions observed by Dickens, et al. [18]

Increasing Variable	Effect on Measured Variable			
	Arc Voltage	Current	Bead Width	Bead Height
Voltage	↑	=/↑	↑	↓
Wire Feed	↓	↑	↑	↑
Stickout	↑	↓	↓	↑
Wire Diameter	↓	↑	↑	↑
Velocity	=	=	↓	↓

Dickens, *et al.* also conducted a brief (not statistically significant) post process mechanical and microstructure evaluation of the manufactured square box wall sections. Hardness tests showed an increase in hardness from the base of the wall to the top of the wall. They hypothesized that this was the result of tempering of the lower layers due to heating during deposit of subsequent layers. Tensile test were conducted parallel and orthogonal to the layers. There was very little difference in ultimate tensile strength in the two directions; however, a statistical study was not performed [18].

When examining the microstructure, the wall was largely equiaxed ferrite and perlite with a grain size of approximately $60\mu m$. It was observed that the structure was much less equiaxed and more columnar in the top layers of the wall that were not subjected to reheating during the additive manufacturing process. As subsequent layers are deposited, the previous layers are repetitiously reheated and consequently tempered during the process. The researchers recommended heat treating the object to ensure a uniform microstructure, but they did not test this hypothesis. Additionally, there were no voids or cavities in the material when a sample was polished and observed under a microscope. The part was concluded to have good mechanical properties.

Dickens *et al.* concluded that to further develop the MIG based additive manufacturing technique there must be significant software development. Additionally, a

sensing feedback loop between the welder and the robot controller was identified as necessary to improve the consistency of the process and create surface finishes similar in quality to cast objects. The authors recommended that the sensing feedback loop provide the wire offset distance to the controller. The controller would then maintain the wire offset distance to a constant value [18].

Further research at the University of Nottingham of the MIG additive manufacturing technique was published by Spencer *et al.* in 1997. The team used a commercially available three axis MIG welder with a Siemens controller to build layers on a platform that could tilt and rotate. The platform was manually moved before the additive manufacturing operation. This allowed orientation of the part at different angles to the welder so geometries could be made without supports [19].

Three test parts, a hollow box, a vertical wall, and a horizontal slab, were studied and are shown in Figure 9. The geometries consisted of 82 layers totaling 100 mm high. The test parts were made from a copper coated mild steel wire that was 1 mm in diameter. The parts were manufactured on a 12 mm thick mild steel build plate. The layer width of the resulting weld bead was 3.5mm. It was found that the layer widths between 3 and 6 mm were possible. Attempting to build walls of thicknesses greater than 6mm resulted in excessive heat input and poor bead profile to due to insufficient cooling of built up heat [19].
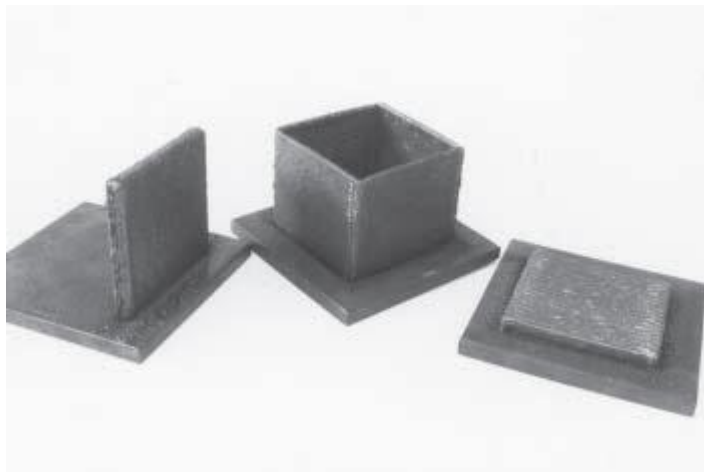
Figure 9: Geometries studied by Spencer et al.[19]

Spencer *et al.* attempted to manufacture thicker walls by placing multiple beads beside each other. However, this resulted in incomplete penetration of the substrate and neighboring bead. Attempts to angle the welding torch to deposit multiple adjacent beads were unsuccessful due to an unpredictable bead profile. The dye penetrant test shown in Figure 10 demonstrated the lack of fusion when attempting to deposit adjacent beads. Instead of attempting to deposit the beads directly next to each other, the authors deposited beads at a pitch approximately double the width of the weld bead crest. As illustrated in Figure 11, material was then deposited in the root channel formed by the two beads separated by the pitch distance. According to tensile tests, the researchers concluded that this method of adjacent layer deposition created excellent mechanical properties. The tensile test standard used was not recorded.
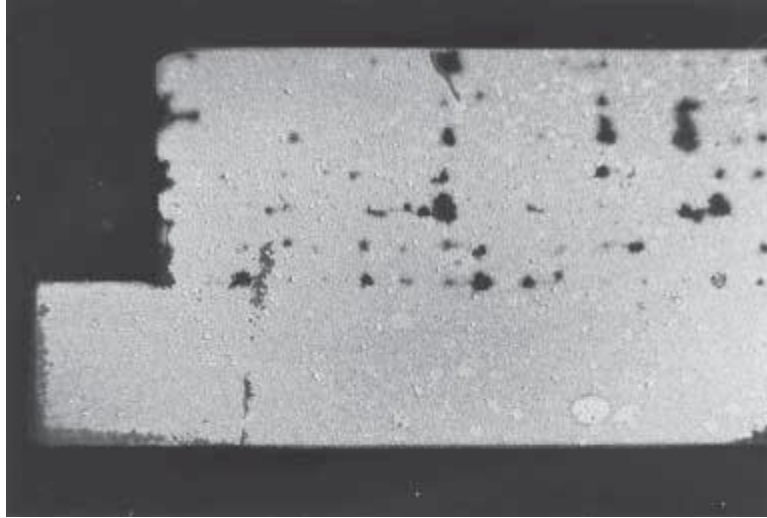
Figure 10: Voids in adjacent beads as shown in dye penetrant test by Spencer et al. [19]
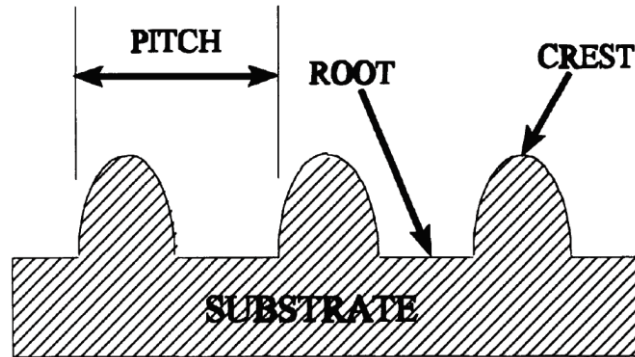
Figure 11: Procedure for depositing adjacent layers by Spencer et al.[19]

Spencer *et al.* also implemented temperature control to ensure the previous layer had sufficiently cooled before depositing the next layer. An infra-red sensor was used to measure temperature. The operators set a maximum allowable temperature at which welding was to be performed. The computer prevented welding until the part reached an acceptable temperature. After implementing temperature control, the authors achieved an improved surface finish at the cost of over doubling the build time [19].

When examining the microstructure of a cut, polished, and chemically etched sample, Spencer *et al.* observed that the upper surface had a martensitic structure due to

rapid cooling. However, the recrystallization and slower cooling of the lower layers resulted in finer ferrite/pearlite grain structure. Aside from the top layer, Spencer *et al.* achieved uniform grain structure and fusion between layers throughout the created sample [19].

Additionally, Spencer *et al.* conducted stress tests on the finished parts to determine the residual stress and compared the results to the previous layer temperature. The residual stress measurements were performed using the center hole method [20]. A three strain gauge rosette was used to measure the change in stress when the material removed by drilling a whole through the sample. The results varied greatly between the different geometries and the sample size was small so there were no significant conclusion [19].

The work of Dickens, *et al.* and Spencer *et al.* did not include Computer Aided Design (CAD) integration [21]. Rather, the researchers wrote the machine code by hand and only created simple objects. Ribeiro *et al.* at Canfield University in 1994 developed a process for transferring a CAD drawing to the MIG technology based additive manufacturing equipment. Their proprietary, unpublished software package translated a CAD file created with AutoCAD into movements interpreted by the software controlling the industrial robotic arm welder. The weld parameters were kept at predefined constants and were controlled by the internal circuitry of the welding robot. Ribeiro *et al.* successfully produced a circular metal vase out of mild steel with this process as shown in Figure 12 [22][23].

Figure 12: First successful integration of CAD and welder controls [22]

Although he was just performing a software process evaluation, Ribeiro, *et al.* recorded conclusions from the brief experiment. The authors identified that the curved geometry of the vase created a variable distance between the arcing wire and the previous layer during deposition. Additionally, it was observed that the quality decreased with time which was likely due to latent heat buildup. Finally, Ribeiro, *et al* recommended weighing the base plate before building an object to calculate how much material was deposited [22][24].

To illustrated the software capabilities and evaluate the geometric accuracy, an additional hollow object was created with refined software by Ribeiro, *et al* in 1996 and is shown in Figure 13. The authors concluded that bead geometry (layer height and width) was of utmost importance and must be properly estimated for the slicing parameters to function correctly. Additionally, during the build process, the distance between the arcing wire and the previous layer was variable and required manual adjustment during the process. The inward taper of the component was considered to be the cause of this issue and closed loop control was recommended as the solution [25][26].

23

Figure 13: Complex geometry produced by Ribeiro, et al. [26]

For greater control of the MIG arc welding process, Ribeiro, *et al.* developed a mathematical model to determine the appropriate welding parameters to input into the previously developed unpublished slicing software. The welding parameters inputted into the slicing software were layer width, layer height, welding current, and welding voltage. To evaluate the feasibility of creating a schedule for additive manufacturing, Ribeiro, *et al.* created cylindrical test pieces ten layers high. The machine travel speed was varied between 500and 2500 mm/min, and the welding current was varied between 120 and 160 Amps [21].

The welding robotic arm used by the authors used a synergic algorithm to control the pulsing of the power source and the wire feed speed. The synergic algorithm was a control scheme internal to the welder that varied the welding power based upon the wire feed rate. The robotic welding arm used a short circuit MIG process with a synergic

algorithm and the internal controls were not studied [27]. Therefore, the wire feed speed was not considered [21].

Ribeiro *et al.* performed their experiments with Inconel 718 wire of 1.0 mm in diameter and used a shielding gas of commercial argon. During the experiments, the layer width varied between 3.8 and 10 mm and the layer height varied between 0.44 and 1.24 mm. The authors observed a relationship between welding speed and layer width as shown in Figure 14 [21].
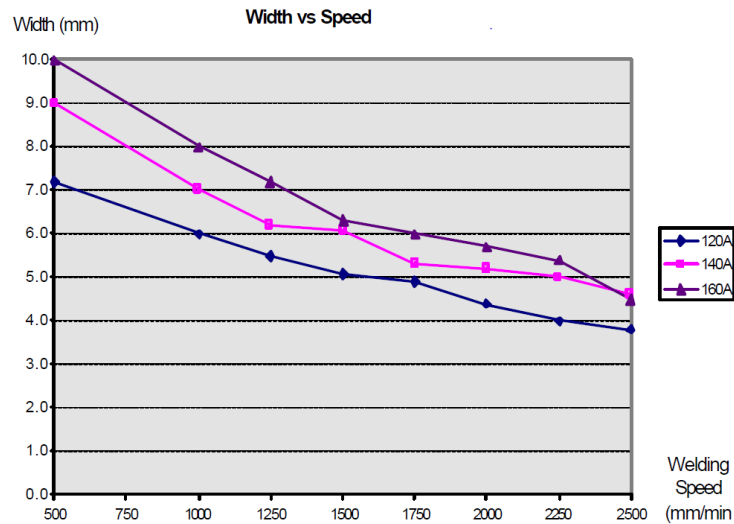
Figure 14: Relationship between layer width and travel speed by Ribeiro et al.

To develop the parameter input algorithm for the slicing software, Ribeiro *et al.* used empirical results as inputs for a regression analysis to determine the relationship between four measureable coefficients of welding speed, welding current, layer height, and layer width. The created mathematical model was incorporated into the software so the user could input a desired layer height, and the computer would automatically set the welding speed and current. To evaluate the software, three test objects of desired layer width were manufactured. The greatest observed absolute layer width error was 0.4mm

with an expected layer width of 8.0 mm. The authors considered this layer width error to be relatively small [21].

While Ribeiro *et al.* were successful in creating an appropriately sized geometry, their preliminary study failed to consider many parameters (*e.g.* wire feed speed, weld characteristics, wire offset, wire diameter) previously identified as important by other researchers [16]. Additionally, the authors failed to study the influence of the internal controls of the welder. Finally, the model was purely based upon empirical data for Inconel 718 deposited by the studied welder, and generalized equations that could be applied to other materials and hardware were not created.

In 1998, Kovacevic, *et al.* at Southern Methodist University used a high speed vision system to study the formation of droplet parameters and resulting weld penetration of MIG based additive manufacturing. Additionally, the researchers performed a finite element analysis to simulate the cooling characteristics of the process. The end goal of the research was to create a sensing system that could improve the process consistency; however, the research was not completed [28].

Kovacevic, *et al*. used a 24 Volt MIG welder with ER70S-6 mild steel wire. A shielding gas of 95% Argon and 5% CO_2 was used and the machine traveled at a constant speed of 6.4 mm/sec. The researchers proposed controlling the metal transfer process by turning the electrical current to the welder on and off based upon the size of the metal droplet formed at the end of the electrode. To observe the metal transfer process, a high speed digital camera capable of 800 frames per second with a resolution of 128X128 pixels was used [28]. Kovacevic, *et al*. determined that the deposited metal bead size and

penetration could be controlled by the pulsing electrical current. Therefore, this strategy could be used for increased control and consistency during the deposition process [28].

In 1999, Kmecko, *et al.* continued to research the MIG based additive manufacturing technique at Southern Methodist University by applying real time image processing to the system in an effort to reduce welding spatter. The developed system measured the voltage and current used by the welder. In addition, the system featured an infrared pyrometer and a light sensor. However, while the system was capable of real time image capture, no reference of successful closed loop control was presented. However, Kmecko, *et al.* were convinced that the closed loop control was necessary to improve the process and reducing welding spatter [29].

In 2002, Zhang, *et al.* at the University of Kentucky published an improved MIG based additive manufacturing process with a more sophisticated CAD model slicing strategy. The team developed unpublished slicing software that could vary the infill method and vary the layer height throughout different sliced regions of the CAD model. Additionally, the author's software was capable of varying the start point of each deposited layer [30].

Zhang, *et al* used two different steel based wires of E70S-6 and SS308 to evaluate the novel CAD model slicing software. For both materials, the wire was fed at a speed of 160 in/min and the 3 axis CNC machine travel speed was 0.2 in/sec. The welding voltage was 25 Volts for both materials and the welding current was 125 Amps for the E70S-6 wire and 110 Amps for the SS308 wire. The shielding gas was a composition of argon and CO_2 with 25% CO_2 for the E70S-6 wire and 5% CO_2 for the SS308 wire.

In order to evaluate the slicing software varying start point strategy, Zhang *et al.* created tube shaped parts with and without varying start points. As shown in Figure 15, the accumulated error from buildup at the start point of the deposited layer path is significant. Figure 16 presents a tube shaped part with a varied layer start point. As a result, the effects of the accumulated start point error are mitigated [30].
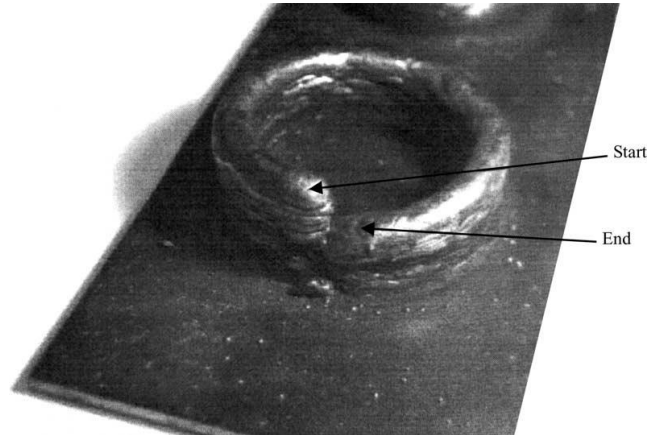
Figure 15: Tube shaped part with the same layer start point by Zhang, et al.[30]
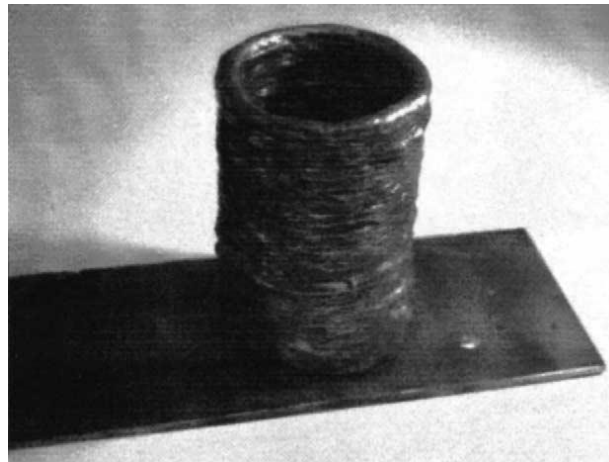
Figure 16: Tube shaped part with varied layer start point by Zhang, et al.[30]

The software was also capable of speed control over the start and end point of a deposited line. The researchers observed buildup of the layer at the start of the path and a decreased amount of material at the end of the path. To counteract this effect, the authors

increased the machine travel speed at the beginning of the path and slowed the machine

travel speed at the end of the path while the wire feed speed was kept constant as shown

in Figure 17.   Additionally, a second pass was added to the end region of the path to

further level the deposited layer [30].
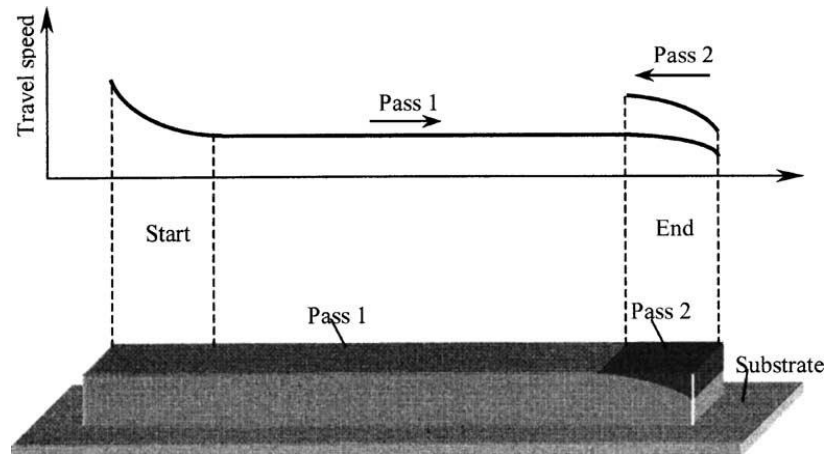
Figure 17: Speed control for the start and stop of the path by Zhang, et al. [30]

To evaluate this control strategy, Zhang, *et al.* deposited a sample wall section

with and without the start and end point speed control. As shown in Figure 18, the wall is

not level with material buildup at the start point of the path and lacking material at the

end point of the path. Figure 19 presents a wall section with control of the start and end

points. As a result, the build up at the start point is decreased, the end point is not lacking

material, and the wall section is more even [30].
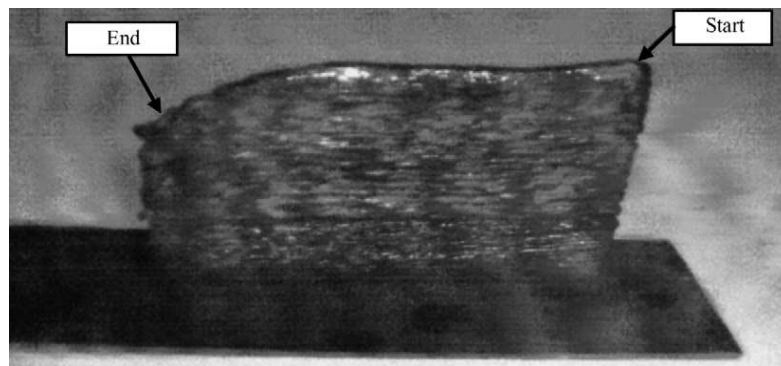
Figure 18: Wall section without start and end point control by Zhang, et al. [30]
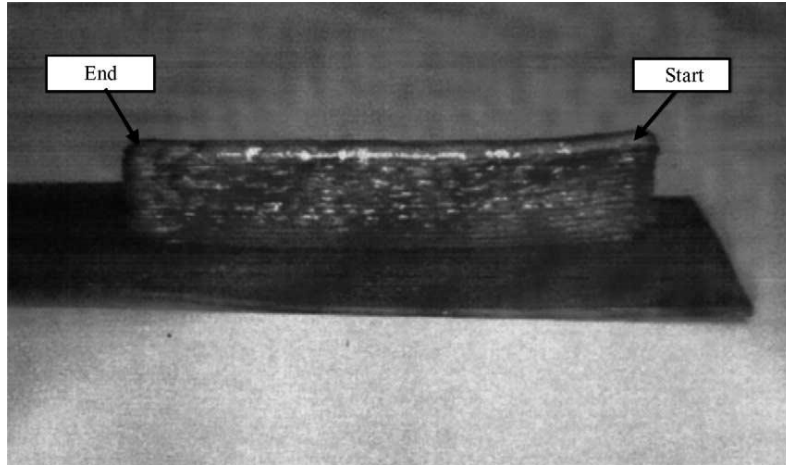
Figure 19: Wall section with start and end point control by Zhang, et al.[30]

While successful in implementing effective slicing software with better start and endpoint geometry, Zhang, *et al.* identified future work was still necessary to manage the heat input to the deposited part. Additionally, the team recommended further development using thinner wire with a higher material transfer stability [30].

In 2004, Song, *et al.* published a technique based upon MIG additive manufacture coupled with a subtractive manufacture milling machine [31]. The authors proposed a machining post-process after each additive manufactured layer was deposited. As shown in Figure 20, the research was performed on a 3-axis CNC milling machine to which a laser welding unit and two arc welding guns had been added. Additionally, the build plate was heated to 200 ^{0}C with a built in heater. The researchers hypothesized that preheating the build plate would reduce thermal stress build up during deposition but did not perform experiments to confirm this [32].

Song, *et al.* confirmed that several factors greatly influenced the process. These factors were layer height, layer width, welding speed, welding voltage, welding current, and distance between adjacent layers.
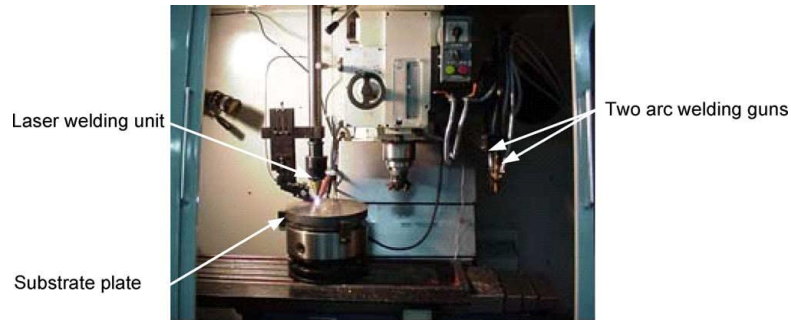
Figure 20: Integrated welding and milling machine created by Song et al.[32]

To evaluate the welding and milling process, the authors constructed test parts with a constant welding voltage of 19 volts and a constant welding current of 120 Amps with a welding speed of 1.2 m/min. The material used in the experiments was mild steel wire 0.9 mm in diameter. During the process, the authors deposited layers and then milled the created object as shown in Figure 21. The object had a layer height of 0.8 mm, a layer width of 4 mm, and a surface roughness of R_a=150 μm. After machining, the object had a wall thickness of 1 mm and a surface roughness of R_a=2 μm. The layers shown in Figure 21 are uneven. This is from poor control of the process; however, Song, *et al.* successfully machined an object after additive manufacture [32].
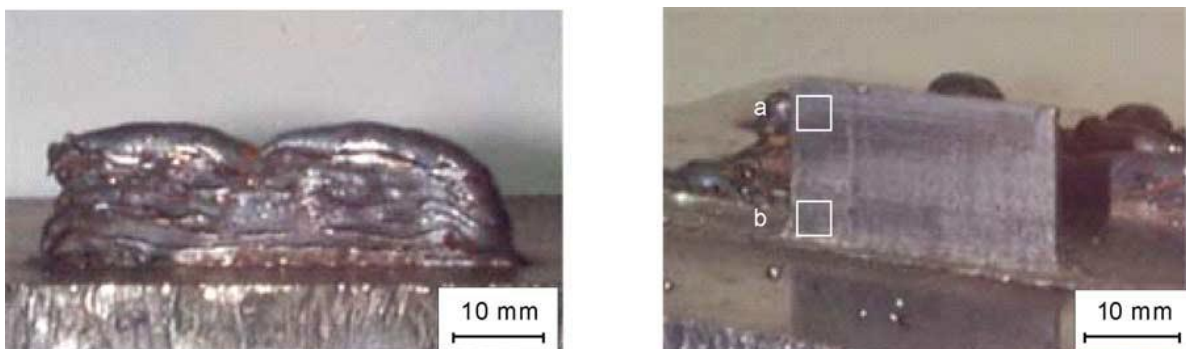
Figure 21: Thin-walled part before and after machining by Song et al. [32]
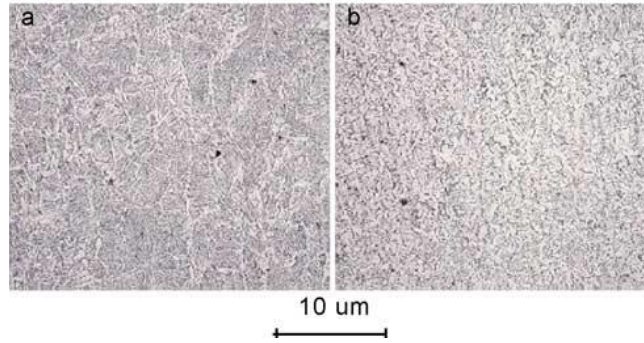
Figure 22: Microstructure observed by Song et al. [32]

Song, *et al.* examined the microstructure of a machined and polished sample. As shown in Figure 22, the sample had large grains in the upper region of the wall (region a) and fine grains in the lower region of the wall (region b) [32]. This is consistent with the observations of Ribeiro, *et al.* [32].

In addition to a thin wall, Song, *et al.* manufactured a test rectangular solid object as shown in Figure 23. The object had a layer height of 0.8 mm and a deposited layer offset of 2.8 mm. The solid test object was measured to have a dimensional accuracy of ± 0.5 mm before machining and a dimension accuracy of 20 μm after machining. When examining the microstructure, the solid part had similar results as the thin wall part with a microstructure that was finer at the base due to the reheating effects [32].

Song, *et al.* also performed a tensile test parallel to the layers of the deposited material and observed that the object had a tensile strength of 620 MPa which was compared to the deposited wire material which had a tensile strength of 550 MPa. However, Song, *et al.* did not perform a tensile test normal to the direction of deposited layers of material [32].
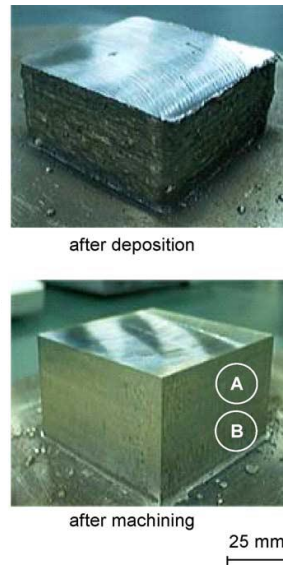
Figure 23: Solid part before and after machining by Song, et al. [32]

In a continuation of the previous study, Song, *et al.* published an additional paper in which the authors optimized their welding and milling technique using statistical methods. The authors chose to optimize four welding parameters which were the welding voltage, wire feed speed, wire offset (distance between the tip of wire and the substrate), and the shielding gas composition. The welding voltage was varied between 14 and 26 volts. The wire feed speed was varied between 3 and 8 m/min. The wire offset was varied between 6 and 8 mm. The shielding gas was composed of CO_2 and argon with the amount of CO_2 varying from 30 to 10%. The weld spatter and deposited layer width were chosen as the two main functions of the welding parameters [33].

To quantify the weld spatter, a spatter index was created which was the ratio of the mass of the spatter divided by the mass of the welded wire. The mass of the spatter was determined by collecting and measuring the spatter beads after the completing the deposition. The mass of fed wire was determined based upon the fed wire speed [33].

Performing an analysis of variance, Song, *et al.* determined that the welding voltage, wire feed speed, and wire offset have a high impact on the spatter formation. However, the shielding had a negligible effect on spatter formation. When examining deposited layer width, the welding voltage and wire feed speed had significant impact. However, the wire offset and shielding gas composition have a small impact on the deposited layer width [33].

From these results, the authors concluded it was best to use the least expensive shielding gas with a CO_2 composition of 30%. Additionally, the wire offset only had a small impact on layer width, so the wire offset was reduced to the minimum of 6 mm to reduce spatter [33].

In addition to studying the factors effects on weld spatter and deposited layer width, Song, *et al.* studied the distance between adjacent layers (bead offset), the direction of layer deposition, and alternating the direction of layer deposition. The direction of layer deposition options studied is shown in Figure 24. To measure the studied factors, tensile tests and hardness tests were performed to see which building strategy had the best performance [33].
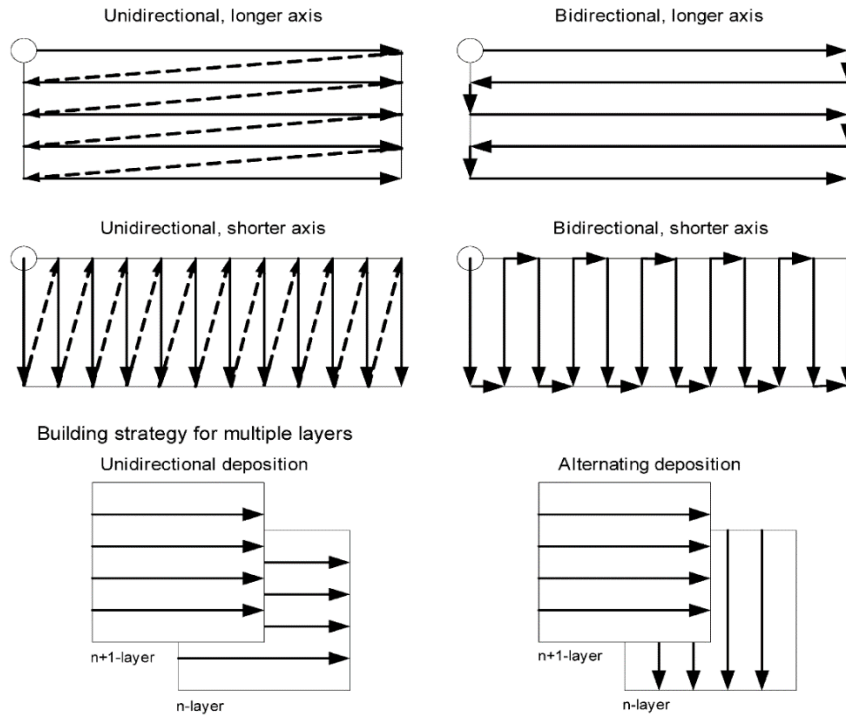
Figure 24: Building strategies for solid layers by Song et al. show how subsequent layers can have different infill directions [33]

Performing an analysis of variants indicated that the deposition parameters have a negligible effect on the surface hardness. However, the team did not examine the surface hardness at different heights of the object. The researchers concluded that the orientation of the depossited layer determines the tensile strength and alternating the deposition direction between layers increases the tensile strength. The authors proposed that the method of alternating deposition direction between layers was stronger because voids were filled in the previous layer and increased the surface quality and density of the layer [33].

In 2007, Clark, *et al.* with Rolls-Royce researched the viability of MIG based additive manufacturing of the nickel-based polycrystalline superalloy Alloy 718 for aero engine applications. The researchers used a synergetic MIG power source with argon

shielding gas. The welder was set to 35 volts, the wire sickout was 20 mm, the travel speed was 20 mm/s , and the wire feed speed was 10 mm/s. The deposited layers had a nominal width of 12.8 mm and nominal height of 1.7 mm [34].

Clark, *et al.* performed multiple deposition geometries and examined the polished and etched samples with a scanning electron microscope for microstructural analysis and x-ray for chemical analysis. The first deposition trial was construction of a thin wall of multiple layers. The second deposition trial was construction of two adjacent beads of a single layer. The final deposition trial was construction of two adjacent beads for multiple layers. When performing the trials, the authors waited until the previous layer had cooled to 80^0C before deposited the subsequent layer. This was to prevent latent heat buildup in the deposited object and a created approximately a 10 minute cooling duration between welds. The resulted in lengthy build times because each deposited layer required over 10 minutes [34].

When examining the microstructure, Clark, *et al*. concluded that the results were highly dependent upon the deposition factors. The authors concluded that controlling the cooling rate in particular was necessary for a uniform part and the prevention of crack formation. Additionally, the authors recommend further study of the MIG additive manufacturing process to further qualify the mechanical properties of the process for aerospace applications [34].

In 2013, Anzalone, *et al.* at Michigan Technological University developed a low cost (less than $2000) open-source metal 3-D printer that used the MIG based additive manufacturing process. The machine used open-source controls and is shown in Figure 25. The machine was a three axis delta robot that was designed for Fused Deposition

Modeling (FDM) plastic extrusion 3-D printing without any feedback (open loop control). The authors used readily available open-source Cura software created for Fused Deposition Modeling (FDM) additive manufacturing. The system used a shielding gas composed of 75% Argon and 25% CO_2 at a rate of 20 CFH. The distance between the build surface and the welding tip was 6 mm. The wire used was 0.024 in. diameter ER70S-6 wire [4].
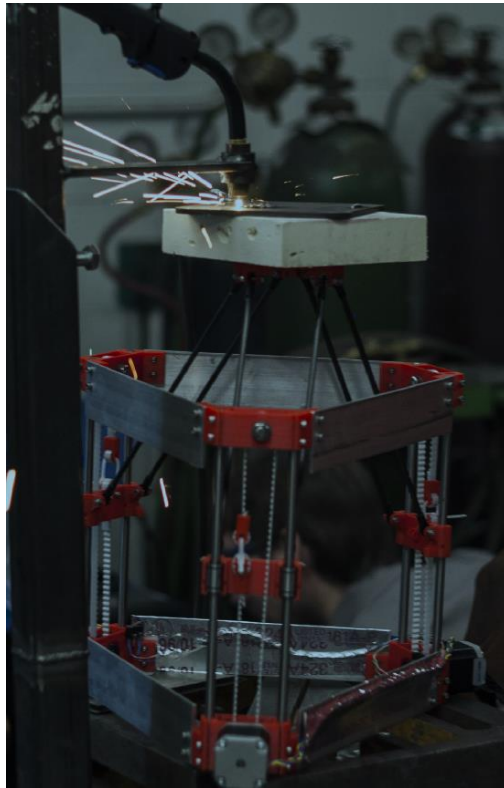
Figure 25: Low-cost open-source MIG printer by Anzalone, et al. [4]

As a proof of concept, the sprocket shown in Figure 26 was created by the authors. The object had a layer height of 1.75mm and was created with a wire federate of 3.5 cm/s [4].

Figure 26: Sprocket manufactured by Anzalone, et al. [4]

Additionally, Anzalone, *et al.* examined the microstructure of a polished and etched sample. Like previous researchers, the Anzalone, *et al.* concluded that the microstructure was finer at lower layers when compared to upper layers. This was due to reheating of the lower layers during the deposition of consecutive layers. The researchers concluded their results proved that this was a feasible process for the economical production of metal parts [4].

Researchers at Michigan Technological University also created a voltage and current monitor for use with the MIG based additive manufacturing process. This low-cost, open-source monitor was used to measure and record the welder's current and voltage. An Arduino Uno microcontroller was used to record the information measured by the monitor. The researchers concluded that the voltage and current monitor would be useful for further evaluation of the MIG based additive manufacturing process [1].

Commercial MIG Additive Manufacturing

Currently, there are two companies pursing MIG based additive manufacturing technologies. The first company, *Keystone Synergistic Enterprises, Inc.,* is located in

Florida and performs additive manufacture of parts using a MIG processes with a robotic arm [35]. An additional company is the startup company *Weld3D* located in Alabama [36]. *Weld3D* uses a MIG process and open source software to create near net shape metal parts.

Software Options

Generating the commands to move the CNC robot or machine was done by hand calculations or a software package. For basic shapes, the machine code was written by hand. More complicated structures were created when computers were used to generate the machine code (g-code). Ribeiro, *et al.* created a unpublished software package to create the machine code [24]. Anzalone, *et al.* used a slightly modified freely available open-source slicing software called *Cura*. *Cura* was designed to generate g-code for FDM 3-D printers [4]. There are no dedicated software packages for wire and arc additive manufacturing.

Evaluation Techniques for MIG Additive Manufacturing

The American Society for Testing and Materials (ASTM) has published the *Standard Guide for Evaluating Mechanical Properties of Metal Materials Made via Additive Manufacturing Process* in 2014. The standard outlines applicable procedures for measuring deformation properties and material fatigue properties [37].

When measuring deformation properties, the tension, compression, bending, modulus, and hardness are to be considered according to the previously published procedures common to materials manufactured by conventional processes. Fatigue properties also use conventional processes for measurement of fatigue, fracture toughness, and crack growth [37].

When reporting results, the ASTM requires previously published guidelines for the individual test to be followed. However, additional information about construction procedure for the additive manufactured part must be reported. The information reported must include location and orientation of the part in the additive manufacturing system build volume. This is due to the potential anisotropic behavior of additive manufacturing [38].

Since the process can be used as a replacement for sand casting in industry, sand casting standards can be used to evaluate parts produced by MIG additive manufacturing. The ASTM *Standard Practice for Steel Castings Surface Acceptance Standards Visual Examination* establishes surface texture criteria. The surface texture should be between A1 to A4 in the Steel Castings Research and Trade Association (SCRATA) graded reference comparators [39]. When examining mechanical requirements, the ASTM *Standard Specification for Common Requirements for Iron Castings for General Industrial Use* contends that the mechanical properties of the part should be sufficient for the need of the particular application. Additionally, the standard provides a list of specifications for specific type of castings. The evaluation techniques used for castings are techniques common to other processes and referenced inside the standard [37].

Previous researchers of MIG based Additive Manufacturing have used tensile tests machined from manufactured wall sections to measure strength [18][19][32][33]. The surface hardness was measured by multiple researchers [4][32][33]. The microstructure of a polished and etched sample was examined under an optical microscope [19][21][28][32][4], a scanning electron microscope [34], and by an x-ray [34]. The surface finish was assessed by laser optical systems [19] and profilometers

[32]. Internal stress was measured by the center hole method [19]. Geometry was measured by image processing systems [22][26]. Finally, the amount of weld spatter was measured by weighing the mass of spatter collected after the completed process [33]. Each researcher additionally visually assessed the quality an appearance of the manufactured part.

Summary of Research Oppurtunities

While the Short Circuit Transfer MIG additive manufacturing process has been considered since 1925 [8], there are many opportunities for process improvement.

When considering build materials for the process, Mild steel welding wire was the most common choice of material [4][18][26][28][30] and proven to be a viable. Inconel 718 has been investigated and considered a feasible material require further study [21][34].   Titanium has been researched extensively by researchers at Cranfield University using the CMT MIG variant [3]; however, titanium has not been investigated using the economical Short Circuit Transfer MIG process. Schedules for previously studied materials need to be further developed and the viability of novel materials like Copper, Aluminum, and various aerospace and nuclear materials should be investigated.

Researchers have investigated the construction of basic geometries including single wall sections [19][32][30], hollow, open top squares [18], hollow open top pyramidal structures [19], hollow, vase shaped cylinders [24] of variable profile, hollow cylinders [30], and hollow transition shapes from square to circular profile [25]. Additionally a more complex sprocket shaped object was created [4]. Methods to create adjacent beads were examined and slicing software parameters for solid objects were

investigated [19][33][30]. The construction of more complex geometries with bridgings, overhangs, and complex details require investigation.

A majority of the researchers have conducted preliminary studies using commercial welding equipment mated to a CNC milling machine [30] or a commercial welding robot [18][19][23]. There has been no purpose built hardware and software for the process [3]. The commercial welding hardware was not modified or purpose built for the application. This results in a lack of control of the process. Additionally, software development for the process has been unpublished and compatible only with the researcher's hardware [21][30]. There is a need for purpose built dedicated hardware and software.

Because of the lack of purpose built hardware, researchers have limited control of the internal circuitry of the parameters internally managed by the welder. Many researchers identified the need for machine control software improvement. Additionally, researchers identified the need for closed loop control for greater consistence in the process [19][30][28]. Kovacevic, *et al* performed a preliminary study of the application of closed loop control hardware; however, the authors failed to fully implement the strategy [28]. Therefore, purpose built hardware with easily modified parameters and closed loop controls should be developed.

Researchers also noted the need for developing post processing procedures. Some researchers have successfully performed milling operations after the deposition of layers [32]. Additionally, researchers hypothesized varied grain structure throughout the part that could be normalized through heat treatment processes [18]. A post processing schedule should be developed for various materials and geometries.

Important Process Factors

Researchers noted complex interactions between process factors. Important factors identified by researchers were welding voltage, welding current, wire feed rate, machine travel rate, wire stickout, wire offset, wire diameter, layer width, and layer height. Additional environment factors such as shielding gas composition [33] and deposition temperature [19][22][30][32][34] were observed. However, the interactions between process factors were not significantly investigated, and every researcher reported different process factors. A summary of the process factors found in the literature review are listed in Table 2. For future researchers use, an experimental data sheet with these factors was created and is found in Appendix 4.

Table 2: Important Process Factors

Factor	Units
Welding voltage	Volts
Welding current	Amps
Wire feed rate	mm/min
Machine travel rate	mm/min
Wire stickout	mm
Wire offset	mm
Wire diameter	mm
Layer width	mm
Layer height	mm
Shielding gas	Material composition percentage
Deposition temperature	^0C
Wire material	Material composition
Base material	Material composition

IV. Design and Construction of Equipment

The machine was efficiently designed and constructed in the Design and Manufacturing Laboratory. The bill of materials used for purchasing is available in Appendix 1.

Previous Machine Designs

Machines used by previous researchers at other institutions included robotic welding arms, repurposed CNC milling machines, and a purpose built low-cost delta robot. While very capable, robotic welding arms were considered too expensive for the beginning stages of this project. Additionally, robotic arms have difficult software and control requirements. A repurposed CNC milling machine was considered, but deemed unnecessarily complicated and not optimized for the 3D printing process. A purpose built machine allowed the greatest flexibility and control for research purposes. Additionally, a purpose built machine could be manufactured for relatively low cost.

Equipment Requirements

Discussions with multiple stakeholders and the literature review dictated requirements that drove the equipment design. The requirements and their justification are identified below.

The first requirement was for a machine that was readily expandable and easily modified by subsequent researchers. It should be relatively simple to implement new hardware and software during the learning process. Additionally, it should be easy to observe the build process from multiple angles. A modular design using aluminum extrusions was chosen.

Another requirement was for the machine to have a build volume of 18" x 18" x 18". This relatively large build volume was required to evaluate the construction of large objects while providing room for future expansion. With a build volume of this size, it was important to consider the increasing weight of the deposited material. A Cartesian style machine was chosen with a build plate that traversed horizontally (y) and not vertically (z). Although this created a larger machine footprint, it prevented having to vertically move the increasing mass of built object. Because the build plate was moving in the horizontal direction (y), the nozzle depositing the material was required to traverse in the vertical axis (z).

Another important requirement was for the machine to have precise and repeatable motion. Consistent motion allowing researchers to focus on the additive manufacturing process and not on the motion controls requires extremely low backlash to ensure high repeatability. This requirement justifies the selection ball screws and linear rails were chosen. The ball screws chosen had a diameter of 16 mm with ball screw nuts having a load rating of 2900 lbs. The linear rails chosen were 20 mm wide and the linear carriages had a load rating of 2500 lbs. Although this was greater capacity than initially necessary, it allowed the machine to be expanded and adapted for future researcher projects.

A commercially available and reliable welder with known safety features was chosen. The welder was a Miller model 190 capable of producing 140 amps at 40% duty cycle and 100 amps at 100% duty cycle as shown in Figure 27. The power source was capable of continuous and reliable operation during lengthy deposition operations. The welding unit operated between 10 at 45 Volts as shown in Figure 28. The welder utilized

a shielding gas and could feed wire between 0.025 and 0.035 in. diameter. The welder

was capable of operating in manual mode with a variable voltage and a variable wire

speed between 60 and 600 in/min.
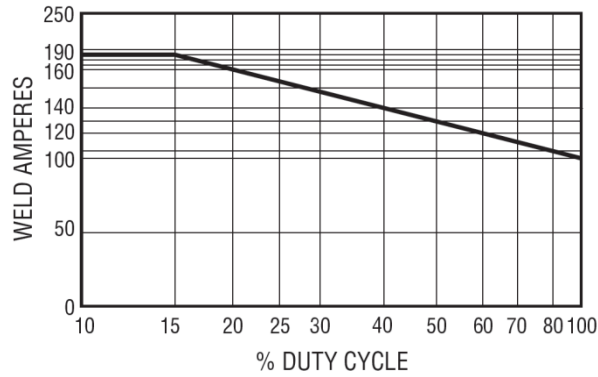
Figure 27: Miller 190 Welder Duty Cycle Chart
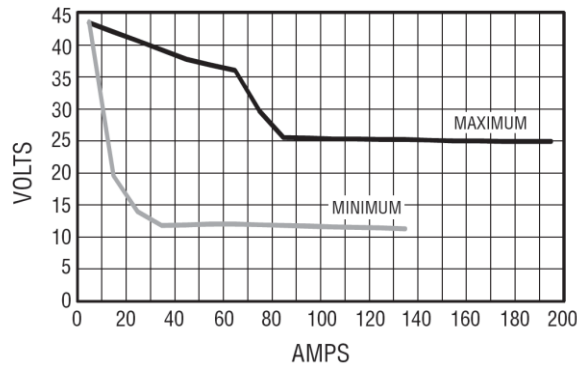
Figure 28: Miller 190 Welder Volt/Amp Curves

The welding process creates bright electrical arc that could blind casual,

unprotected observers. Welding masks were required to prevent eye damage. A fire

watch was used in case of emergency. Electrical isolation and the automatic welder

shutoff features in case of an electrical short or overload were essential considerations.

The machine was housed in a large room with high ventilation turnover rates to preclude

fume accumulation.

Machine Construction

The machine was designed using *SolidWorks* CAD software (Figure 29). The frame was constructed from aluminum 80/20 extrusions that allowed easy assembly and modification. Great care was taken to create a rigid, precise frame to ensure an accurate coordinate system. The motor mounts and bearing block holders were constructed from aluminum bar stock using precision CNC machining. The build plate traversed on two linear rails and four carriages in the *y-axis* direction and was driven by a single ball screw. The vertical, *z-axis* moves upon four linear carriages and is driven by two ball screws connected by an L-series belt and timing pulley. The welding gun is carried upon the *x-axis* and is driven by a single ball screw between two linear carriages. All of the custom ball screws are 16 mm in diameter and all of the linear rails are 20 mm wide.
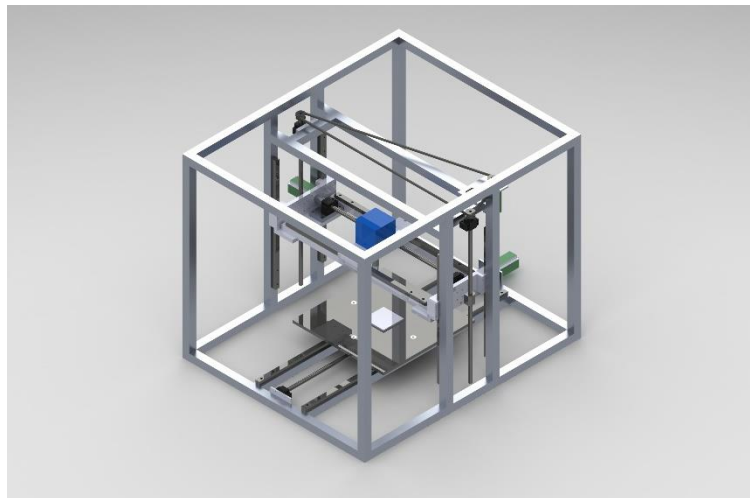
Figure 29: SolidWorks CAD model
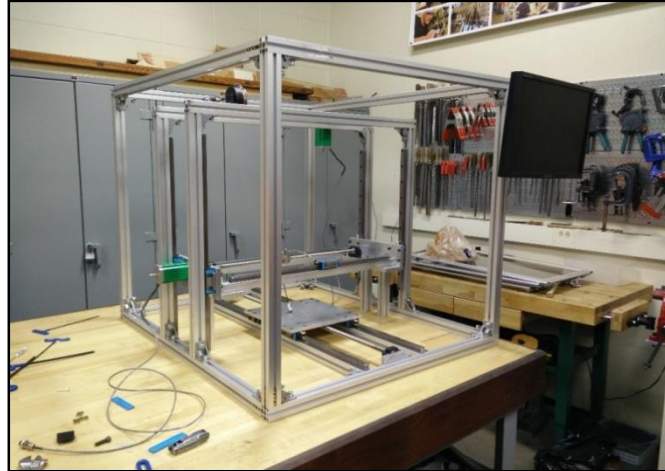
Figure 30: Bare machine frame during Construction

The frame was assembled on a large surface plate to ensure alignment and the bolts used featured locking washers to prevent misalignment during the life of the machine. The linear motion systems were precisely aligned and lubricated. There was no observable backlash in the ball screws when testing their performance with a 0.001 in. precision dial indicator. Repeatability studies show that the machine is accurate to ±0.0005 in. The finish machine is shown in Figure 31.

Figure 31: Finished Printer

Stepper motors were chosen to drive the ball screws because of their relatively low cost and high reliability. The stepper motors chosen were NEMA 23 style with 1.8°/200 steps per Rev. and had 420 oz-in. of holding torque. The stepper motors were connected to the ball screws by an elastomer coupler to prevent binding as shown in Figure 32. If greater precision is required for future research, an optical encoder could be added to the system.

Figure 32: Stepper Motor Drive

The build plate assembly (Figure 33) consists of four layers to provide precision, thermal isolation, electrical isolation, and rapid build substrate replacement. The first layer was a precision machined aluminum plate that rigidly connects the linear carriages and the ball screw nut. Atop the aluminum plate was a 1 in. thick ceramic fiber electrical and thermal insulation board called *Duraboard 3000*. In addition to being an electrical insulator, this ceramic board has a maximum temperature of 3000°F and a very low thermal conductivity of 0.8 at 1000°F. The thermal insulation was important to protect the ball screws and linear carriages from the high heat generated during the metal deposition process. The electrical insulation was important to protect the entire machine from conducting the electricity used by the welder to melt and deposit metal.
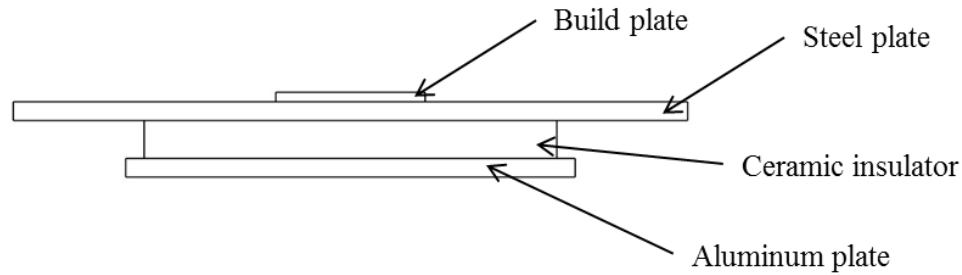
Figure 33: Build Plate Assembly

Above the ceramic insulator was the 18 x 18 x 0.5 in. steel plate which was attached to the aluminum plate with four bolts. However, the steel plate was electrically isolated from the aluminum plate because the four bolts are only contacting counter-bored ceramic inserts. A large, flexible wire fastened with a bolt and locking washer attaches the steel plate to the welder to establish electrical continuity. The steel plate also features threaded holes in a 4 in. spacing pattern to allow attachment of build plates. This permitted build plates to be quickly arranged and replaced.

The nozzle used to deposit the metal wire was created using a modified Miller *Spoolmate 100* MIG welding spool gun. A spool gun which pushes the wire directly into the nozzle was necessary to feed flexible materials like Aluminum. The spool gun was designed by the manufacturer to be used with the Miller 190 welder and is capable of using a shielding gas. The spool gun is capable of feed wires of 0.025 to 0.035 in. by replacing the readily available drive rollers and nozzle. The spool gun was disassembled and mounted in an electrically isolated aluminum and acrylic box (Figure 34). The box was mounted to a precision CNC machined aluminum mount with three equally spaced holes. This allowed relocation of the wire spool holder and secure mounting of the spool gun while maintaining the manufacturer designed feed mechanism and electrical isolation. Additionally, the nozzle could be easily replaced with a milling attachment or

another additive manufacturing head. Eventually there will be both a milling head and printer head working together simultaneously.
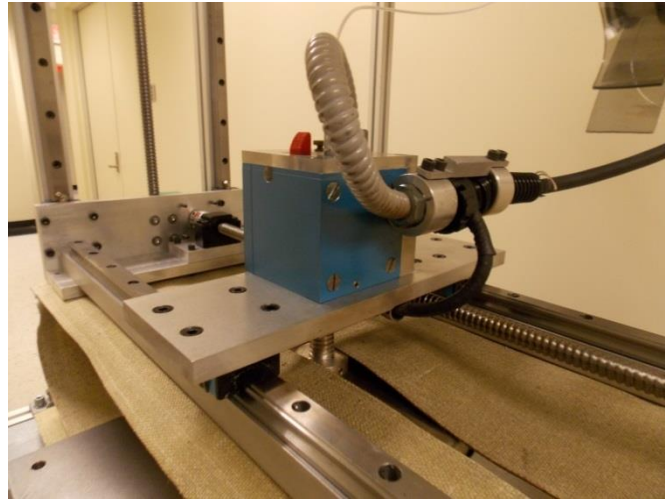
Figure 34: Wire Feed Head

The wire spool holder was relocated to the upper rear of the machine frame and was electrically isolated from the rest of the machine. Two spool holder mounts were created to allow attachment of commercially standard 4 in. diameter spools or 8 in. diameter spools. The wire was fed from the spool to the spool gun feed mechanism through a low friction Polytetrafluoroethylene (PTFE) tube.

To protect the linear rails and ball screws from any welding splatter, vermiculite coated fiberglass fabric curtains were used as shown in Figure 35. The curtains were hemmed to prevent fraying and pleated to allow movement during the machines motion. The curtains are rated for a maximum temperature of 1500°F and were 0.020 in. thick.

Figure 35: Fiberglass Curtains

Machine Controls

The machine was controlled by the readily available and inexpensive CNC control software *Mach3* as shown in Figure 36 [40]. Originally designed for control of CNC milling machines and lathes, *Mach3* was repurposed for controlling the 3D printer because of its stability and flexibility. The software runs on a dedicated computer and is capable of accepting industry standard FANUC G-codes and M-codes. The *Mach3* software was configured to control the three translational axes. The wire feed mechanism was configured as a variable speed spindle. The *Mach3* software was also configured to turn the welding power on and off. An additional benefit was that *Mach3* allowed the operator to change the machine federate and the wire feed rate during the deposition process and provides a visual G-code display.
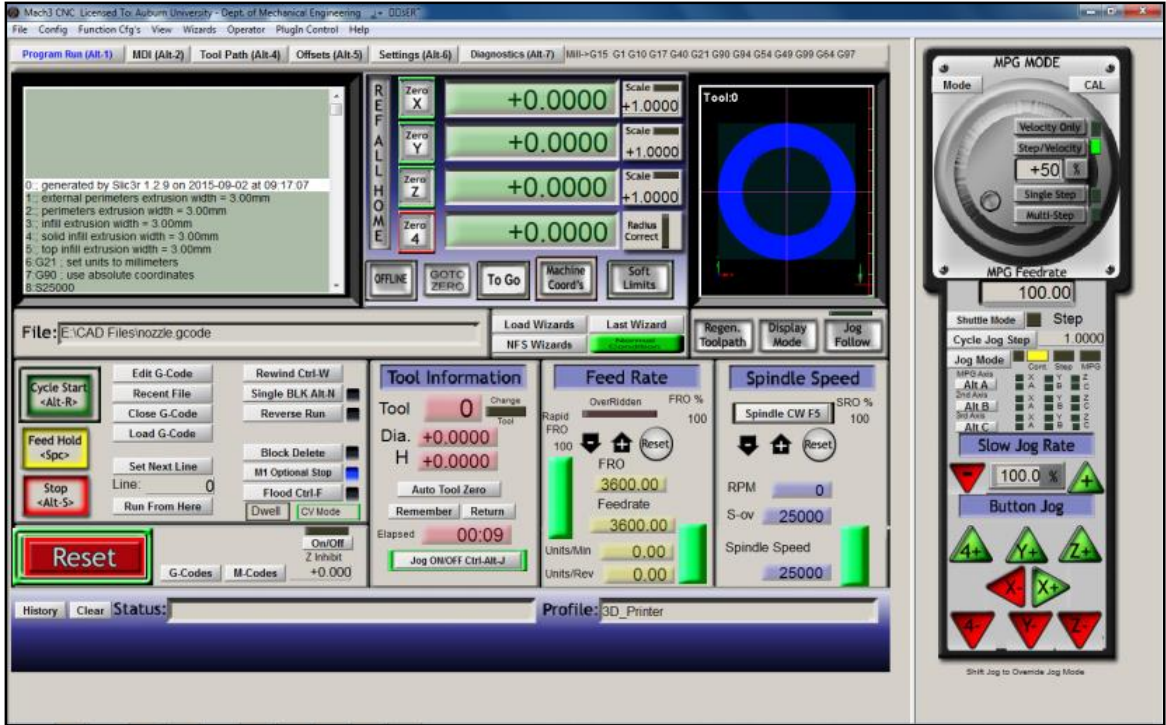
Figure 36: Mach3 CNC Control Software

As shown in Figure 37, the *Mach3* software controls the machine via a standard parallel port. The electrical pulses are transmitted from the computer to the parallel port break-out board. The breakout board distributes the signals to stepper motor drivers which power the motors. The *Mach3* software also controls the relay board and the variable speed control board.
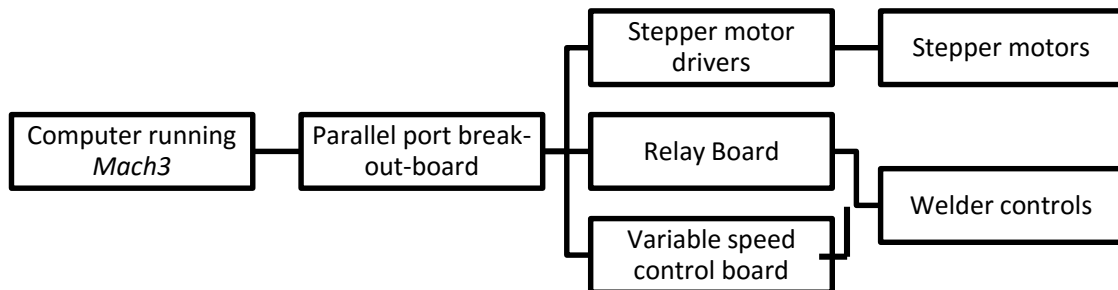
Figure 37: Machine Controls

The Miller 190 welder was modified to allow computer control via the relay board and the variable speed control board. However, care was taken during modifications to ensure that none of the manufacture's safety features were bypassed. The relay board enables and disables the welder by simulating the operator turning the welder on and off. The variable speed control board was used with the pulsed modulation spindle control signal from *Mach3* to control the wire feed speed potentiometer knob on the front of welder. The voltage was controlled manually by the operating turning the knob on the front of the welder. However, the voltage could be controlled by the computer as well.

Software

When creating a 3D printed object, it is necessary to generate the G-code that is inputted into the *Mach3* control software. Two freeware software packages designed for Fused Deposition Modeling (FDM) were configured and used to create the G-code. The first software package used was *KISSlicer* (*kisslicer.com*). The second software package, *Slic3r*, was open source and freely available at *slic3r.org* and is shown in Figure 38. After configuration, both software packages were able to create G-code that could be interpreted by *Mach3*. Both software packages allowed the user to vary important factors including layer height, layer width, print speed, and wire feed speed. Additionally, the software packages used the industry standard *.stl* CAD file format.
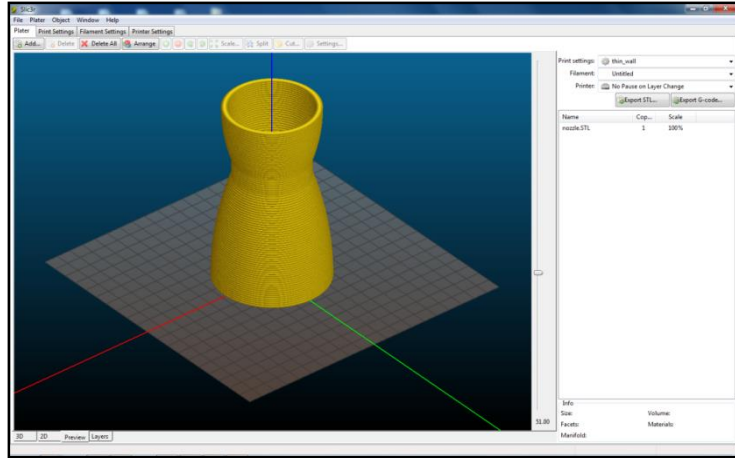
Figure 38: *Slic3r* Software

Voltage and Current Monitor

A voltage and current Monitor as designed by Pinar *et, al.* [1] was created. A custom PCB was purchased and assembled as shown in Figure 39. The voltage and current was powered by a ±15 VDC power supply and featured two green LEDs to indicate power. The monitor sends information to an Arduino Uno microcontroller which processes the voltage and current measurements. The microcontroller then sends the measurements to the computer via the USB serial port. Serial port monitoring software is used record and to plot the voltage and current measurements real time. In addition to recording the voltage and the current, the system includes a time stamp for correlating the data. The Arduino code was included in Appendix 2
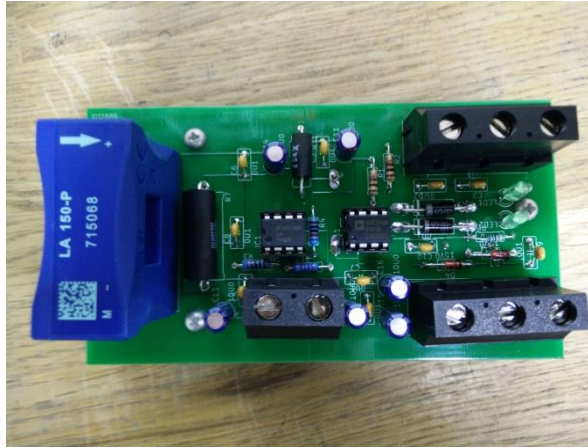
Figure 39: Voltage and Current Monitor

The voltage and current monitor was calibrated using a DC power supply and multimeter using a direct comparison procedure to a known standard [41]. The multimeter had a voltage measurement accuracy of ±0.09% and the current measurement accuracy was ±0.1%. The constant voltage DC power supply was used to supply DC power that was simultaneously measured by the custom build voltage and current monitor and the multimeter. The voltage was increased from 0 to 36 volts in increments of 2 volts while recording the measurements made by the uncalibrated monitor and the multimeter standard as shown in Figure 40. The monitor is very linear in nature until 30 volts is reached which is the peak of the accurate operation range.
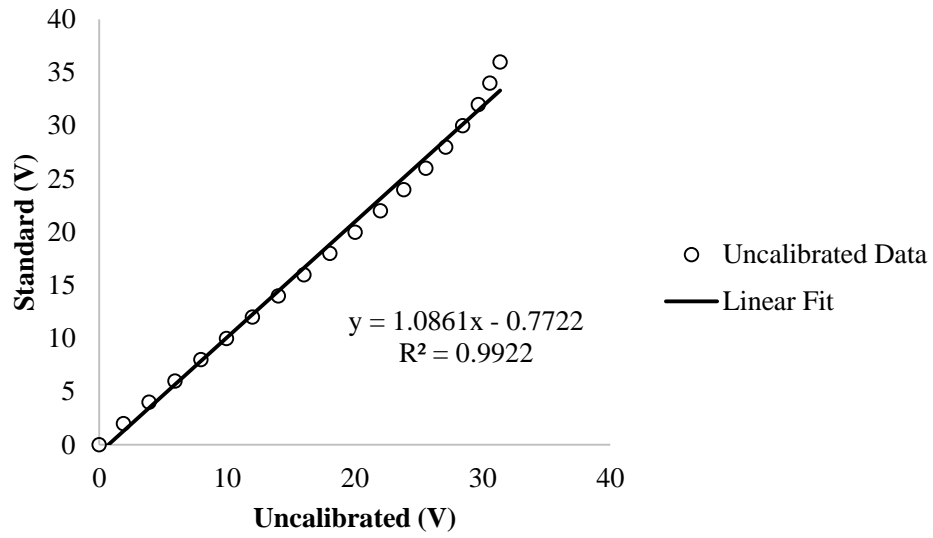
Figure 40: Voltage Measurement Calibration

Similarly, the current was increased from 0 to 10 Amps in increments of 1 Amp as shown in Figure 41.
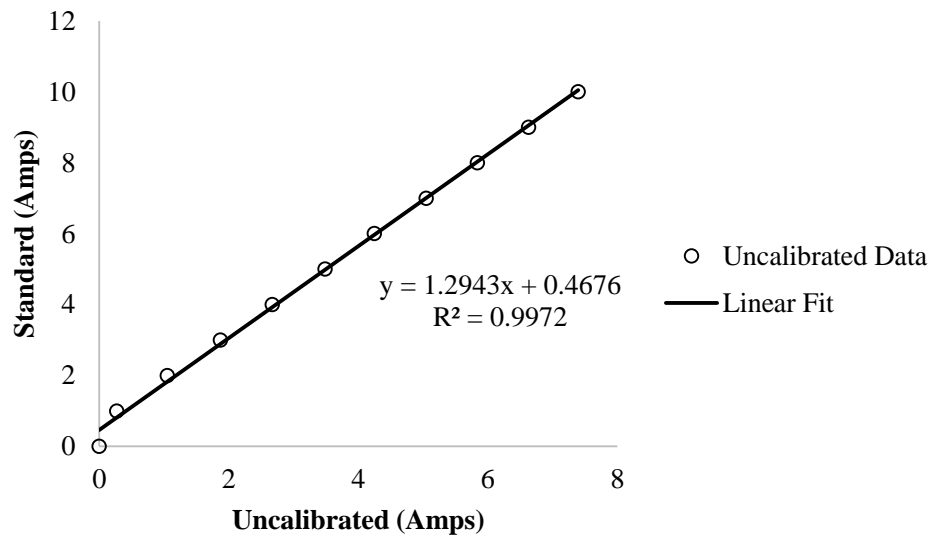
Figure 41: Current Measurement Calibration

According to Beckworth *et, al.*, the voltage and current measurement calibration curves are of the form shown in equations 4.3 and 4.6 [42].

$$f_{cal}(x) = ax + b \pm (\delta_a x + \delta_b + \delta_{std}) \qquad 4.1$$

$$f_{cal,voltmeter}(x) = 1.086x - 0.772(Volts) \pm (0.0490x + 0.979(Volts) + 0.0009x) \qquad 4.2$$

$$f_{cal,voltmeter}(x) = 1.086x - 0.772(Volts) \pm (0.0499x + 0.4945\ (Volts)) \qquad 4.3$$

$$f_{cal}(x) = ax + b \pm (\delta_a x + \delta_b + \delta_{std}) \qquad 4.4$$

$$f_{cal,ampmeter}(x) = 1.294x - 0.4676(Amps) \pm (0.0502x + 0.214(Amps) + 0.001x) \qquad 4.5$$

$$f_{cal,ampmeter}(x) = 1.294x - 0.4676(Amps) \pm (0.0512x + 0.214(Amps)) \qquad 4.6$$

Where δ_a is the scale uncertainty,

$$\delta_a = \pm \frac{t_{\alpha/2,v} S_{y/x}}{S_{xx}} \qquad 4.7$$

$$\delta_{a,voltmeter} = \pm \frac{2.09 \times 1.02}{43.8} \qquad 4.8$$

$$\delta_{a,voltmeter} = 0.00490 \qquad 4.9$$

$$\delta_a = \pm \frac{t_{\alpha/2,v} S_{y/x}}{S_{xx}} \qquad 4.10$$

$$\delta_{a,ampmeter} = \pm \frac{2.201 \times 0.185}{8.09} \qquad 4.11$$

$$\delta_{a,ampmeter} = 0.0502 \qquad 4.12$$

δ_b was the offset uncertainty,

$$\delta_b = \pm t_{\alpha/2,v} S_{y/x} \sqrt{\frac{1}{n} + \frac{\bar{x}^2}{S_{xx}^2}} \qquad 4.13$$

$$\delta_{b,voltmeter} = \pm 2.09 \times 1.02 \sqrt{\frac{1}{19} + \frac{17.3^2}{43.8^2}} \qquad 4.14$$

$$\delta_{b,voltmeter} = 0.978 \qquad 4.15$$

$$\delta_b = \pm t_{\alpha/2,\nu} S_{y/x} \sqrt{\frac{1}{n} + \frac{\bar{x}^2}{S_{xx}^2}} \qquad \text{4.16}$$

$$\delta_{b,ampmeter} = \pm 2.201 \times 0.185 \sqrt{\frac{1}{11} + \frac{3.50^2}{8.09^2}} \qquad \text{4.17}$$

$$\delta_{b,ampmeter} = 0.214 \qquad \text{4.18}$$

and δ_{std} is the uncertainty of the standard. The number of measurements, n, was 19 for the voltage measurement and 11 for the current measurement. The value for $t_{\alpha/2,\nu}$ was found using a Student's t distribution. Student's t distribution was used because there were less than 30 data points. When reading the Student's t table, a 95% confidence interval was used. In the above calculations, $\bar{x}$ was the mean of the data points.

The calibrated voltage and current monitor is installed inside the welder as shown in Figure 42 according to the instructions and electrical diagram by Pinar *et, al*. [1].
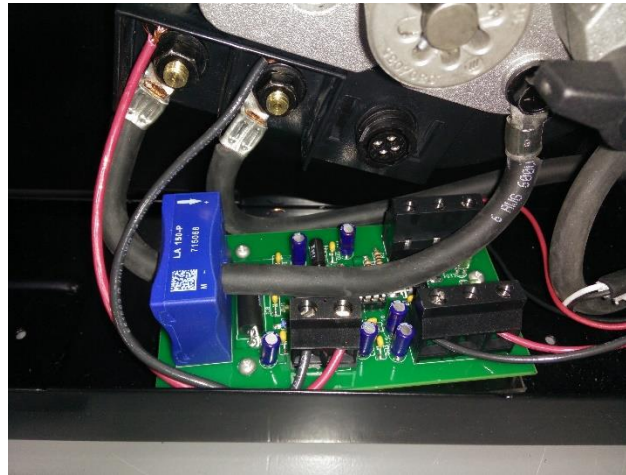
Figure 42: Installed Voltage and Current Monitor

V. Methodology

Geometry Evaluation Methodology

A preliminary evaluation of the 3D printer was a consideration of the geometric structures that the printer was capable of building. Multiple geometries were created and printed at a variety of parameters. Each shape was initially created in *SolidWorks* CAD software. The file was then exported in the Stereolithography (*.stl*) file format that was accepted by the slicing software.

The first shape created was a simple hollow cube with 2 in. wide walls. Hollow cylinders of 2 in. diameter were the second geometry printed. The hollow objects were printed with ER70S-6 steel, ER4043 aluminum, and ER308 stainless steel wires all of 0.030 in. diameter. After printing the hollow objects, some walls were machined on an upright end mill to determine machinability and to inspect for internal voids.

When printing the hollow objects, three different layer change mechanisms were used. The layer change mechanism, which is controlled in the slicing software, determines how the machine will move upwards in the z-axis to deposit the next layer. The three layer change mechanisms considered were (1) changing the layer at the same (x, y) point, (2) changing the layer on randomized (x, y) points, (3) having the layer constantly changing as the machine spiraled upward continuously depositing material.

In addition to hollow objects, solid objects were printed in steel, aluminum, and stainless steel. Multiple infill strategies were considered and evaluated. The infill strategy could be changed with the slicing software. The infill strategies considered were

zigzag and parallel inward spiral as shown in Figure 43. The solid objects were printed in steel, aluminum, and stainless steel and were machined to examine for voids.
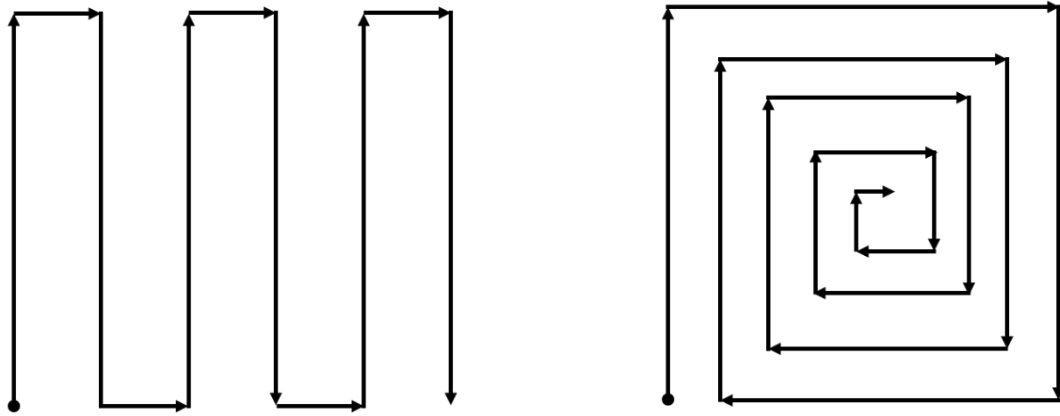
Figure 43: Zigzag and Parallel Inward Spiral Infill Strategies

The ability of the 3D printer to "bridge" over a space between two walls was a critical requirement. This geometry was created by building a hollow object and then depositing a roof over the hollow objects. Because the deposition process requires building upon a previous layer, bridging layers wer deposited starting at the edge of a deposited wall. When bridging, the significant variables that could be controlled in the slicing software were the layer width and bridging speed.

Also considered was the 4 in. tall hollow hourglass shape shown in Figure 44. This geometry was printed to demonstrate ability to create convex and concave overhanging walls. The hourglass shape was printed with the spiraling layer change strategy.

Figure 44: Hourglass Test Shape CAD Model

As a proof of concept of the machine's ability to create a useful part, a nozzle was printed in stainless steel. Two identical objects were printed, and one was post process by turning it on a lathe. The dimensions of the two objects were then compared.

Wire Diameter Study Methodology

Using the calibrated voltage and current monitor, the voltage and current demands for three different wire diameters were measured with two different materials. The same shape was deposited at the same feed rates with the same machine code with three different wires of 0.025, 0.030, and 0.035 inches in diameter. Two replicates were performed at each wire diameter. The voltage, current, and resulting wall width were measured and compared.

The in-situ common study geometry created was a 1 in. tall cylinder of 2 in. diameter. The geometry was tall enough to allow the experiment to reach steady state. Steady state was defined as the point at which the welder's voltage and current was consistent from one layer to the next. The programmed layer height was 1.5 mm (0.059 in.) and the object had a single wall thickness. The first layer feed rate was 2.5 mm/s

(0.492 fpm) and all of the subsequent layers were at a feed rate of 5 mm/s (0.984 fpm). There was no pausing between layer changes except for the brief time the machined moved upward in the vertical (z) axis and the total print time was 9 minutes. Each layer change was performed at the same (x, y) point. The base plate was initially at 70^0C and the environment was a constant 70^0C. The shielding gas used was 100% Argon at a flow rate of 25 CFH. An aluminum build plate was used for the aluminum wire and a steel build plate was used for the steel wire. The welder voltage control knob on the front of the welder was set to "1" for the aluminum wire and "4" for the steel wire. The aluminum wire was ER4043 and the steel wire was ER70S-6.

Two replicates were printed with each wire diameter in each material. A steel print immediately after deposition is shown in Figure 45. The voltage and current was measured and recorded for each specimen. A plot of the measured voltage and current versus time for each specimen was created. A plot of the measurement for steel wire of 0.030 in. diameter is shown in Figure 46 and the other specimens had similar plots. After filtering out measurements taken when the welder was turned off for the layer change, the average voltage and current was calculated for each run.

Figure 45: Steel Wire (ER70S-6) Diameter Study Specimen
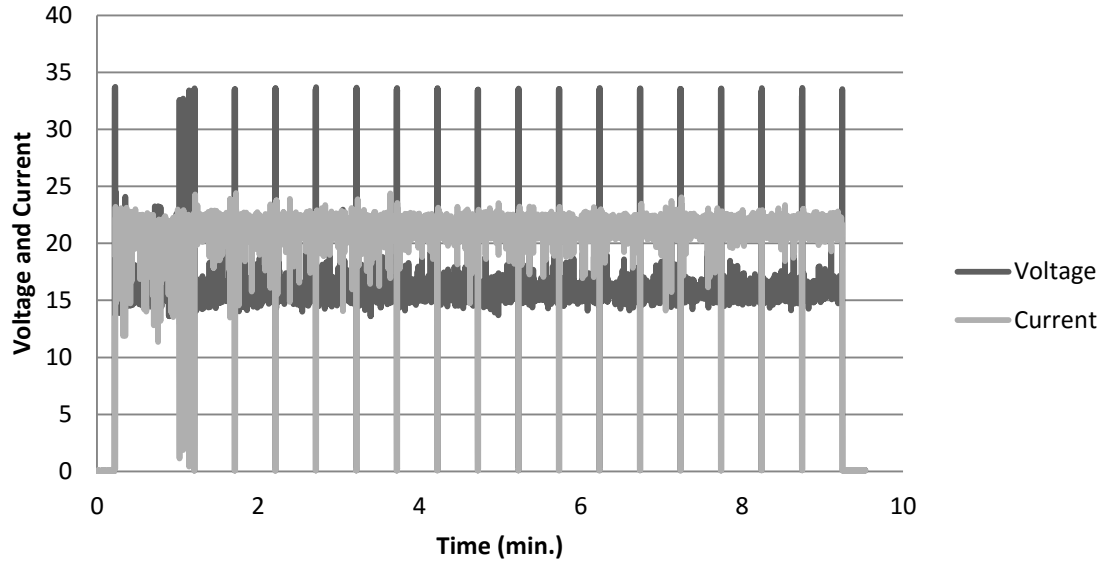
Figure 46: Voltage and Current Measurement for 0.035 in. Diameter Steel Wire

The final wall width for each specimen was measured with dial calipers (accuracy of ±0.001 in.). The wall width was measured at four points around the specimen and the results were averaged to create a final measured wall width for each specimen. The measured wall widths were compared to the hypothetical wall width which was determined using basic geometry. As shown in equation 5.1, the mass of the wire fed into the machine was considered equal to the mass of wire deposited by the machine. For simplicity, the effects of splatter were neglected. The material was said to have the same density before and after the process.

$$\dot{m}_{in} = \dot{m}_{out} \qquad 5.1$$

$$(\rho\dot{v})_{in} = (\rho\dot{v})_{out} \qquad 5.2$$

$$(\rho vA)_{in} = (\rho vA)_{out} \qquad 5.3$$

The density, ρ, of the inputted material was considered to be equal to the outputted material. The velocity, v, of the wire inputted and the velocity of the machine depositing the material were known constants. The cross sectional area, A, of the feed

wire was a constant calculated using the circular wire's diameter. The geometry of the deposited bead was approximated as an ellipsoid with a width of the deposited layer width and a height of the deposited layers height. Therefore, the layer width can be calculated using the formula shown in equation 5.6.

$$(vA)_{in} = (vA)_{out} \qquad\qquad 5.4$$

$$v_{wire}\pi \left(\frac{d_{wire}}{2}\right)^2 = v_{machine}\pi \frac{h_{layer}w_{layer}}{4} \qquad\qquad 5.5$$

$$w_{layer} = \frac{v_{wire}}{v_{machine}}d_{wire}h_{layer} \qquad\qquad 5.6$$

Tensile Strength Evaluation Methodology

Tensile test specimens were created using steel wire (ER70S-6) and stainless steel wire (ER308) of 0.030 in. diameter was deposited on a steel substrate. Four parallel and adjacent beads of steel of 4 in. long were deposited at a spacing of 0.01 in. as shown in Figure 47 in each layer. The layer height was 3.5 mm and there was no pausing between layers. Layer deposition continued until the created walls were 4 in. tall and had a width of 0.5 in.
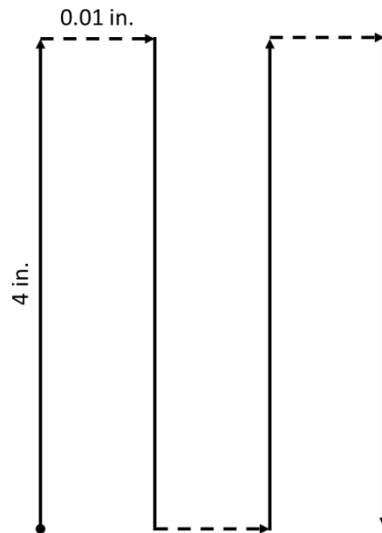
Figure 47: Tensile Test Specimen Build Pattern

The machine was run with a constant feedrate of 3.33 mm/sec (0.66 fpm). The voltage was set to "4" on the welder when depositing the steel and was set to "5" when depositing the stainless steel. The voltage and current monitor measured a resulting steady state voltage of 17.3 Volts and current of 25.3 Amps for the steel and 20.5 Volts and a current 27.0 Amps for the stainless steel. The wire stickout (the distance between the welding tip and the build plate) was 0.25 in. The steel build plate was 0.25 in. thick and at the ambient room temperature of 69^0F. 100% Argon shielding gas at a flow rate of 25 CFH was used. The print time for each wall was 64 minutes.
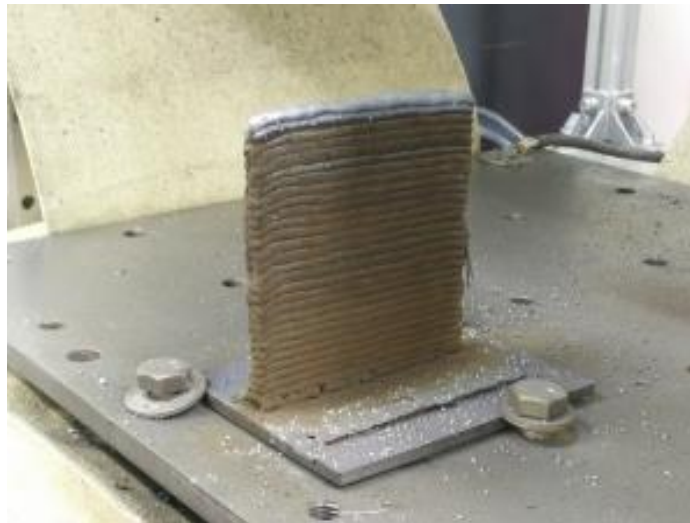
Figure 48: Tensile Test Wall on Machine

After removing the wall from the build plate with a horizontal band saw, the walls were machined square as shown in Figure 49.

Figure 49: Machined Square Tensile Test Specimen Wall

A CNC milling machine with a 0.25 in. diameter end mill was used to machine the tensile test specimens as shown in Figure 50 and Figure 51. Orientation and location of the tensile specimens within the each wall were recorded.

Figure 50: CNC Mill Machining Tensile Test Specimen

Figure 51: Tensile Test Specimens after CNC Machining

The tensile test specimens were created according to *ASTM E8* which dictates a specimen with a gauge length of 1.000±0.003 in., a neck width of 0.250±0.005 in., and a thickness of 0.250±0.005 in. A completed tensile test specimen was shown in Figure 52. Before pulling the specimen, the precise dimensions of the tensile test bars were verified with dial calipers with accuracy ±0.001.

Figure 52: Tensile Test Specimen

Tensile test specimens were created parallel to the layers of deposition and perpendicular to the layers of deposition in both steel (ER70S-6) and stainless steel (ER308). Four walls of each material were created allowing a total of 40 tensile test specimens machined from the walls. Because each created was the same size, there were 16 tensile test specimens parallel to the deposited layers and 24 tensile test specimens

perpendicular to the deposited layers. Aside from the voltage settings for the respective

materials, each wall was printed with the same machine settings.

As shown in Figure 53, the tensile test specimens were pulled on a MTS Q-Test

100 tensile testing machine at a rate of 0.2 fpm. The load, time, and extension were

recorded from which the stress and strain were calculated.
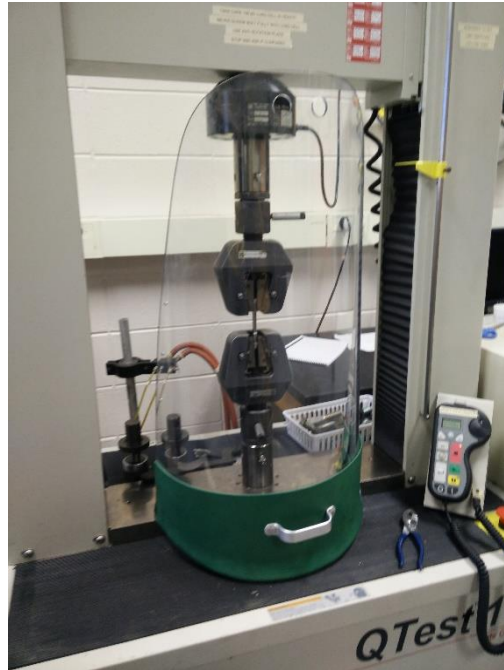
Figure 53: Q-Test 100 Tensile Test Machine

Microstructure Examination Methodology

The metallurgical details of the deposited steel structure were examined using an

optical microscope. The samples to be examined were cut from the walls manufactured

for the tensile test specimens. Samples were selected that would show the microstructure

in the middle of a weld bead or layer in addition to samples that would show the interface

between layers. The samples were polished and etched with a 2% Nital etchant. The

samples were then examined under an optical microscope and the grain structure was

evaluated. Photographs of the microstructure were taken and were compared to the

typical microstructure seen in a traditional steel weld as outlined in *Metallurgy of Welding* by J.F. Lancaster [43].

Slicing Software Comparison

Slicing software refers to the software package that is used to generate the machine code that controls the machine. The input to a slicing software is a CAD file and the output is the machine code. For 3D printing, the CAD file is in the form of the de facto industry standard Stereolithography (*.stl*) file format. Most commercial CAD packages, like SolidWorks and *Solid* Edge, are capable of exporting a drawings as a *.stl* file. From the *.stl* file, the slicing software outputs the G-code in ASCII text-formatted data that is then inputted into the *Mach3* control software.

Several slicing software packages that were developed for the FDM 3D printing process are freely available online. Two pieces of such software are *Kisslicer* and *Slic3r*. Each of these software packages were prepared for use with the weld based 3D printing process and the two software packages were compared.

The first software package considered was *Kisslicer* which is freely available on *kisslicer.com*. As shown in Figure 54, *Kisslicer* has a graphical user interface and multiple slicing parameters. A machine profile was created to allow the software to export the correct G-code and custom machine commands for the machine. *Kisslicer* notably allows the user to vary print speed, layer height, number of layers, layer offsets, infill style, and infill percentage.
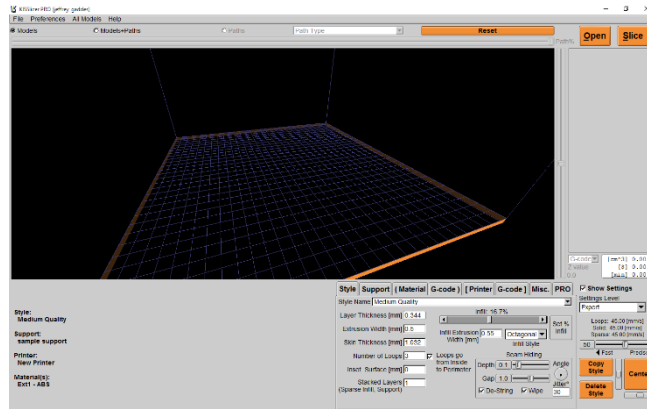
Figure 54: Kisslicer Slicing Software

The second software package considered was *Slic3r* which is freely available on *Slic3r.org*. Shown in Figure 55, *Slic3r* has a graphical user interface. While also having the same features as *Kisslicer*, *Slic3r* had additional features. A notable feature was the ability to vary bridging settings. The bridging variables included the distance between adjacent paths and an independent machine federate setting for bridging. Additionally, *Slic3r* featured a spiral vase mode which allowed seamless printing of a single wall thickness continuous surface. This mode avoided the seam created by moving up one layer at a time. Instead, this mode moved all three axes simultaneously to spiral upward and create a part.
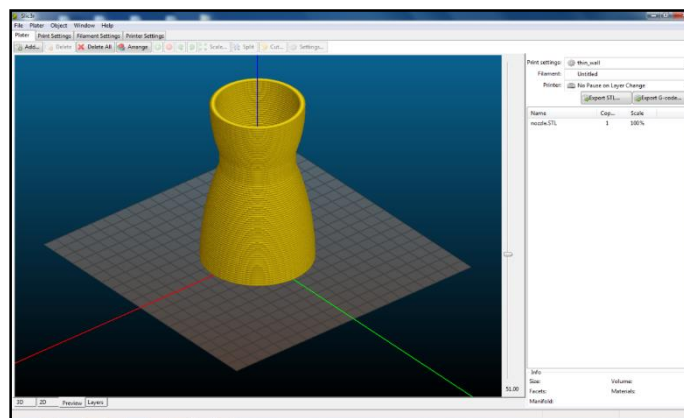
Figure 55: Slic3r Slicing Software

Additional slicing software packages that could be adapted for this process are *Cura* by Ultimaker [44] and *Makerware* by Makerbot [45]. Both of these slicing packages accept a *.stl* file and have the capability to create G-code that could be used by the created 3D printer. However, there has not been opportunity to evaluate these software packages

Heat Treatment Methodology

To further examine the attributes of the deposited material, heat treatment specimens were created. The solid specimens were used to study the effects of heat treatment including changes in the material hardness and the granular structure. Additionally, the specimens were used to examine the influence of latent heat buildup inside of the deposited structure as printing progressed.

Steel wire of 0.030 in. diameter was deposited on a steel substrate. Nine parallel and adjacent beads of steel of 2.4 in. long were deposited at a spacing of 0.01 in. The layer height was 3.5 mm and there was no pausing between layers. This allowed heat buildup inside of the object typical of the deposition process. This heat buildup eventually produces a red hot glow in the part. A finished wall is shown in Figure 56.

Figure 56: Heat Treatment Test Specimen before Cutting

To deposit the metal, the machine was run with a constant feedrate of 3.33 mm/sec (0.66 fpm). The voltage was set to "4" on the welder. The voltage and current monitor measured a resulting steady state voltage of 17.3 Volts and current of 25.3 Amps. The wire stickout was 0.25 in. The steel build plate was 0.25 in. thick and at the ambient room temperature of 69°F. 100% Argon shielding gas at a flow rate of 25 CFH was used.

After printing two walls with the same machine schedule, the two walls were each cut in half with a vertical band saw. The build plate was left attached for to the deposited structures, and each sample was marked to record its orientation and which wall it was cut from. The samples were then machined on the outside and inside surfaces so the material structure could be examined. As shown in Figure 57, this created a total of four samples where half of the samples were from one wall structure and the other half were from the other wall structure.

Figure 57: Separated Heat Treatment Test Wall Structures

One cut sample from each of the two walls was then heat treated simultaneously according to the same schedule as shown in Table 3. The specimens were ramped from

ambient temperature to 1200 °F where the temperature was held for 1.5 hours. The

temperature was then increased to 1500 °F where the temperature was held for 18 hours.

The specimens where then removed from the oven and air cooled.

Table 3: Heat Treatment Schedule

Temperature (°F)	Duration (hours)
1200	1.5
1500	18
69	Until cool

The walls from the cut plane of all four specimens where then polished and etched

with Nital to reveal the microstructure. The microstructure was examined using a 3D

Keyence microscope which stiches together pictures taken at multiple points to create a

3D image. This image allowed inspection of voids and microstructure. The hardness of

each was tested at the bottom, middle, and top locations of the samples as shown in

Figure 58. The hardness of the as printed and heat treated specimens were then

compared. Additionally, the hardness of the different regions was compared to determine

if there was a gradient throughout the sample.
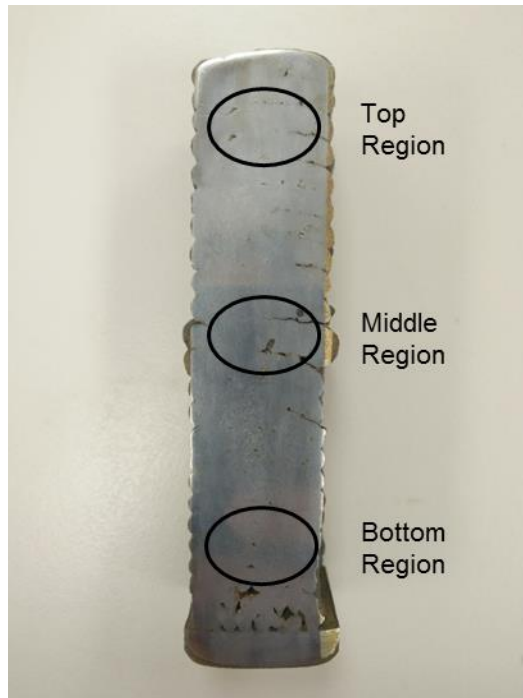
Figure 58: Hardness Test Locations

Build Plate Evaluation Methodology

Multiple materials were considered as build plates for steel and aluminum deposition materials. The objective was to find a build plate material that would allow removal of the metal deposit and that would allow the build plate to be reused for multiple subsequent depositions with minimal processing. As a requirement of the deposition process, the build plate must be a good conductor of electricity. Finally, the build plate should be economically price to avoid high machine operating costs. To evaluate the build plates, material was deposited on the build plate. Attempts were then made to remove the deposit from the build plate. It was then determined if the build plate was suitable for reuse. A list of build plate materials considered is shown in Table 4.

Table 4: Build Plates

Wire material	Build plate material
Steel	Steel
Steel	Aluminum
Steel	Titanium
Steel	Chrome alloy foil
Steel	Tungsten sheet
Steel	Tungsten Bar
Steel	Graphite
Aluminum	Aluminum
Aluminum	Steel

Omitted Objectives

Due to cost and time constraints, the following objectives were deleted by the advisor. These following objectives will be included in future work.

- Develop an optical system for observation and possible future feedback control.

- Instrument the process with thermocouples to document heat history and future in-process thermal feedback.

- Develop strategy to deal with "slumping" reported by researchers.

- Print an eight-inch diameter, two-inch-high steel skillet with an eight-inch handle.

- Print the block for a small bore steam engine design.

VI. Results

Geometry Evaluation Results

The printed geometries were evaluated visually and examined for voids. It was found that hollow squares and cylinders could be deposited in steel (ER70S-6), stainless steel (ER308), and aluminum (ER4043). When varying the layer change strategy, it was found that having the layer changing constantly while spiraling upwards provided the best surface finish. This was because there was a slight buildup of material at the layer start point as shown in Figure 59. Randomizing the start points helped mask this issue as shown in Figure 60.
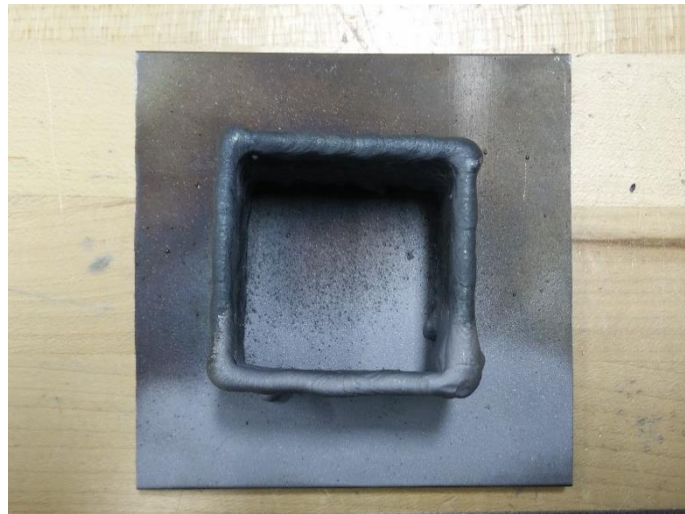
Figure 59: Buildup of Material on Layer Change Corner in Steel (ER70S-6)

Figure 60: Cylinder with Randomized Layer Start Points in Steel (ER70S-6)

As shown in Figure 61, the steel printed geometries were covered in oxide immediately after deposition. This oxide could be removed with a wire brush and was not evident on the two most recently deposited layers. The oxide was not as thick when printing with stainless steel (ER4043). When machining the steel (ER70S-6) and aluminum (ER4043) deposits, it was found that the deposits were machinable with only a few voids observed on a macro scale. No voids were observed when machining the stainless steel (ER308).
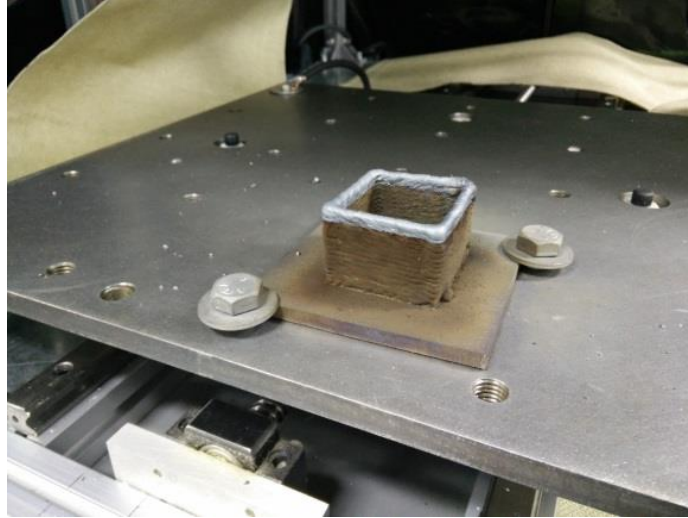
Figure 61: Hollow Steel (ER70S-6) Square after Printing

When depositing solid objects, it was found that the parallel inward constant overlapping spiral method created the most solid object as shown in Figure 62. When using the zigzag infill method, the object was not as solid as shown in Figure 63. The arc was observed to be unstable at the end points of the straight solid infill. Additionally, buildup of material was observed at the end points of the straight solid infill. When creating solid aluminum geometries, it was observed that small (1 in.^{3}) geometries were possible. However, larger geometries were not possible due to the rapid dispersion of heat inside of the part.
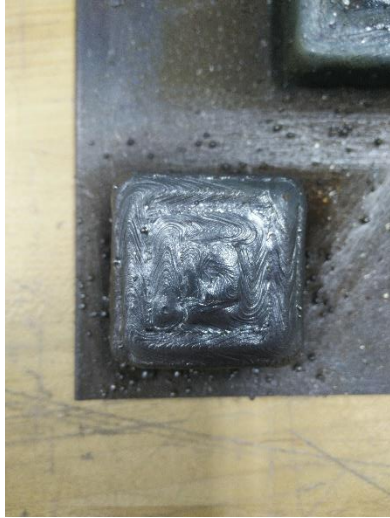
Figure 62: Multiple Perimeter Solid Infill in Steel (ER70S-6)

Figure 63: Straight Solid Infill in Steel (ER70S-6)

Overhanging walls were also printed as shown in Figure 64. However, the overhanging wall geometry was not found to be very repeatable. Additionally, it was only possible to start building an overhanging wall from the edge of a hollow object. It was not possible to bridge between two walls without having a previous layer to build upon regardless of alloy type.

Figure 64: Overhanging Wall in Steel (ER70S-6)

Printing the hollow hourglass shape was a successful demonstration of convex and concave overhangs as shown in Figure 65. Because the object was printed with the spiraling layer change method, the top layer was observed to be angled. Additionally, the spiraling layer change method allowed a large amount of latent heat to accumulate in the top layers. This had the effect that the bottom region layers had a different surface finish than the top region layers.

Figure 65: Hourglass Shape in Steel (ER70S-6)

As a demonstration of a useful part, the two stainless steel printed nozzles are shown in Figure 66. The part on the left was turned on a lathe. The surface finish after turning was excellent and no voids were observed. Before turning, the large diameter of the part was 1.770 in. with a wall thickness of 0.172 in. After turning, the part was 1.667 in. diameter with a wall thickness of 0.087 in.

Figure 66: Stainless Steel (ER308) Nozzles

Wire Diameter Study Results

The voltage and current measurements were averaged for each wire diameter. As shown in Figure 67, the voltage measurements had no significant difference between wire diameters for a given material. The error bars are from the voltage and current monitor's calculated uncertainty.
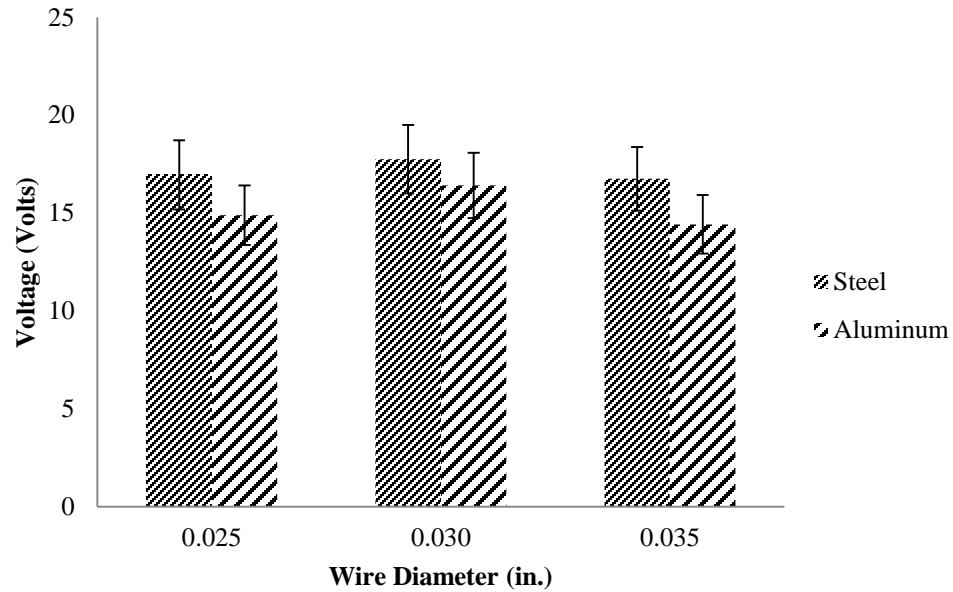
Figure 67: Voltage Measurement Results

When considering the current measurements for the different wire diameters, there was no measureable difference as shown in Figure 68. Although there was greater variation in the current measurement than the voltage measurement, there was no significant difference. A *t-test* was performed between the wire diameters to statistically confirm what was observed in Figure 68, and the *P-values* were all greater than 0.05 for a 95% confidence interval. The samples are statistically equal with 95% surety.
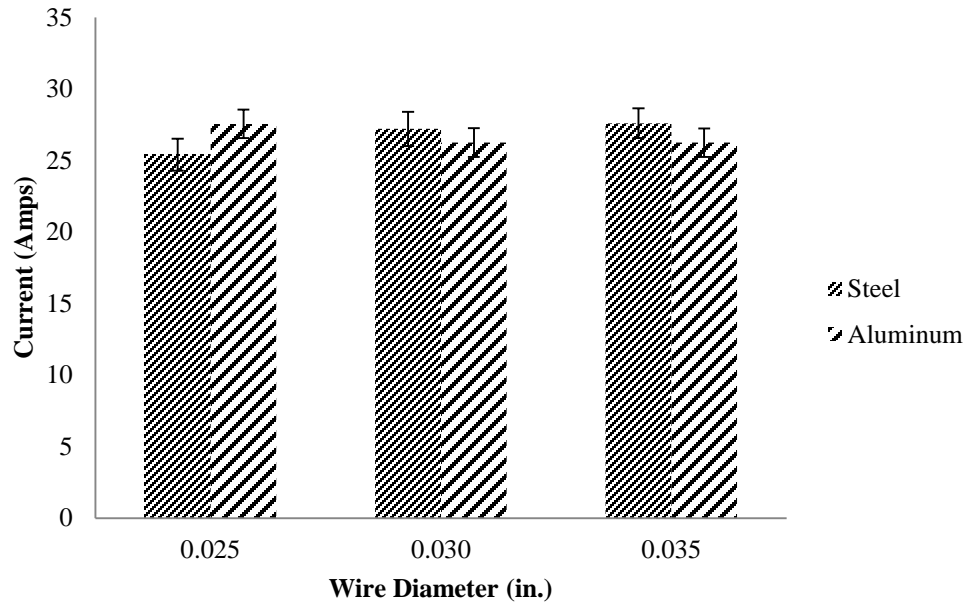
Figure 68: Current Measurement Results

The measured layer widths were compared to the predicted layer widths as shown in Figure 69. The predicted value is greater than the measured values for the 0.030 and 0.035 in. wire diameters. Additionally, the deposited aluminum bead is smaller than the steel bead for the 0.030 and 0.035 in. wire diameters. However, the predicted value is less than the measured value when considering the 0.025 in. diameter wire.
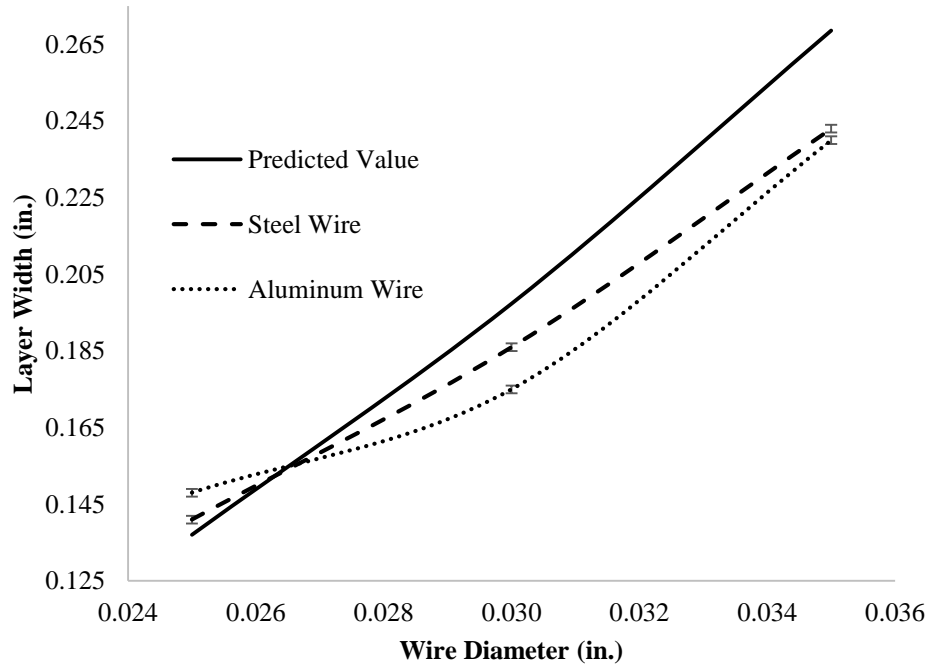
Figure 69: Comparison of Hypothetical Layer Width to Measured Layer Width

Tensile Strength Evaluation Results

When examining the tensile test specimens, the specimens parallel to the deposited layers exhibited different failure modes as compared to the perpendicular specimens. As shown in Figure 70, the horizontal specimens parallel to the layers experienced delamination of the layers. Additionally, the horizontal specimens did not break in middle of the bar.

Figure 70: Steel (ER70S-6) Horizontal Tensile Specimen Failure

86

The tensile test results for the steel specimens that were oriented parallel to the deposited layers are shown in Figure 71 and in Figure 72. The samples are numbered from the bottom to the top region of the deposited wall with the top region being the highest numbered sample. There was no correlation between the tensile strength and the region of the wall from which the sample taken. The samples from Wall 1 had consistent toughness and the samples from Wall 3 had a wide variation in toughness.
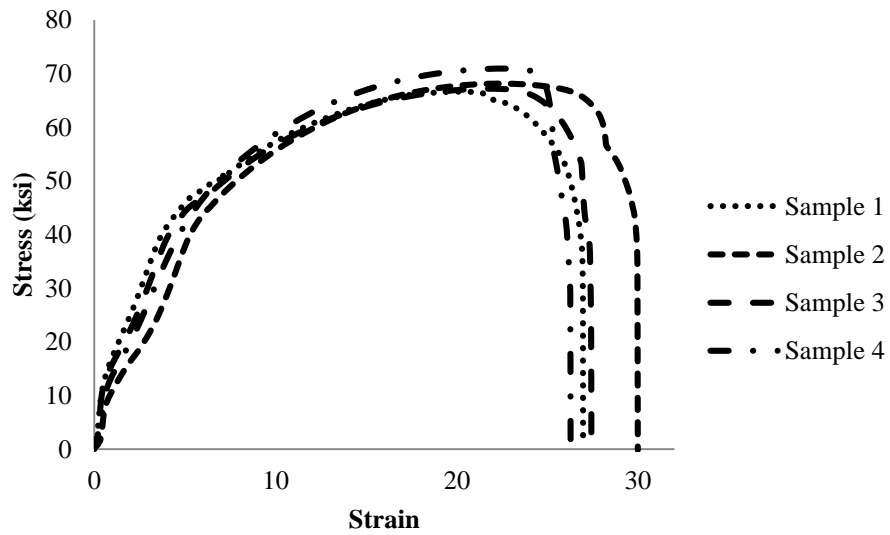
Figure 71: Steel (ER70S-6) Horizontal Tensile Tests - Wall 1
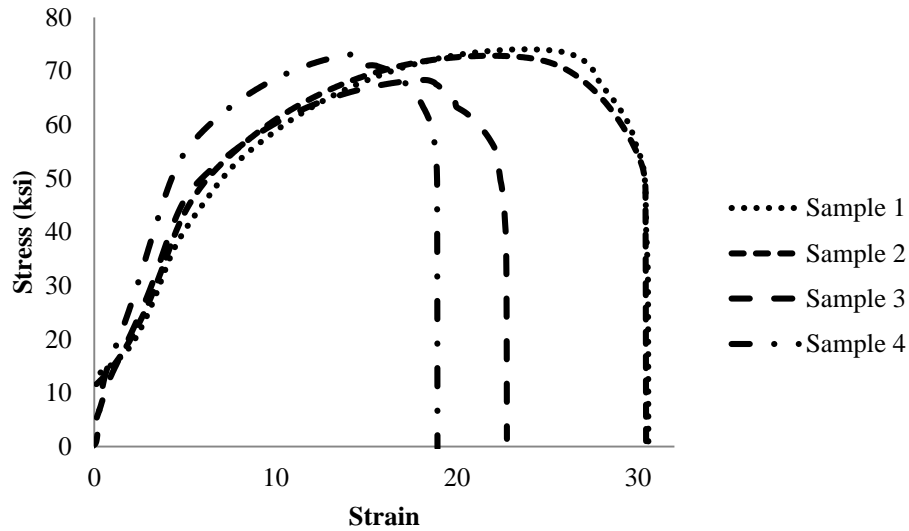
Figure 72: Steel (ER70S-6) Horizontal Tensile Tests - Wall 3

The steel (ER70S-6) horizontal tensile test specimens had an average ultimate tensile strength of 70.1 ksi. A t-test was conducted to compare the horizontal tensile strength in wall 1 and wall 3. There was not a significant difference in the tensile strength in wall 1 (M=68.2 ksi., SD=1.90 ksi.) and wall 3 (M=72.1 ksi., SD=2.56 ksi.); t(3)=2.78, p=0.0690). Therefore, the steel (ER70S-6) deposition process is repeatable when considering tensile strength parallel to the deposited layers.

When examining the steel (ER0S-6) vertical test specimens that were perpendicular to the deposited layers, failure was observed between the layers as shown in Figure 73. The tensile specimens fractured at each deposited layer and failed at the weakest inter layer bond. The fractures at each layer are observable in Figure 73.

Figure 73: Steel (ER70S-6) Vertical Tensile Specimen Failure

The two wall sections for the steel (ER70S-6) vertical test specimens were found to have different ultimate tensile strengths as shown in Figure 74 and in Figure 75. The average ultimate tensile strength of the samples from Wall 2 was found to be 17.8 ksi. and the average ultimate tensile strength of the samples from Wall 4 was found to be 42.3 ksi. After removing the outliers, a t-test was conducted to compare the vertical tensile strength in wall 2 and wall 4. There was a significant difference in the tensile strength in wall 2 (M=17.8 ksi., SD=5.60 ksi.) and wall 4 (M=42.3 ksi., SD=1.65 ksi.); t(3)=10.6, p=0.00182). Therefore, the steel (ER70S-6) deposition process is not repeatable when considering tensile strength perpendicular to the deposited layers. When looking at the results in Figure 74 and in Figure 75, it is readily apparent tensile strength and the toughness is not consistent.
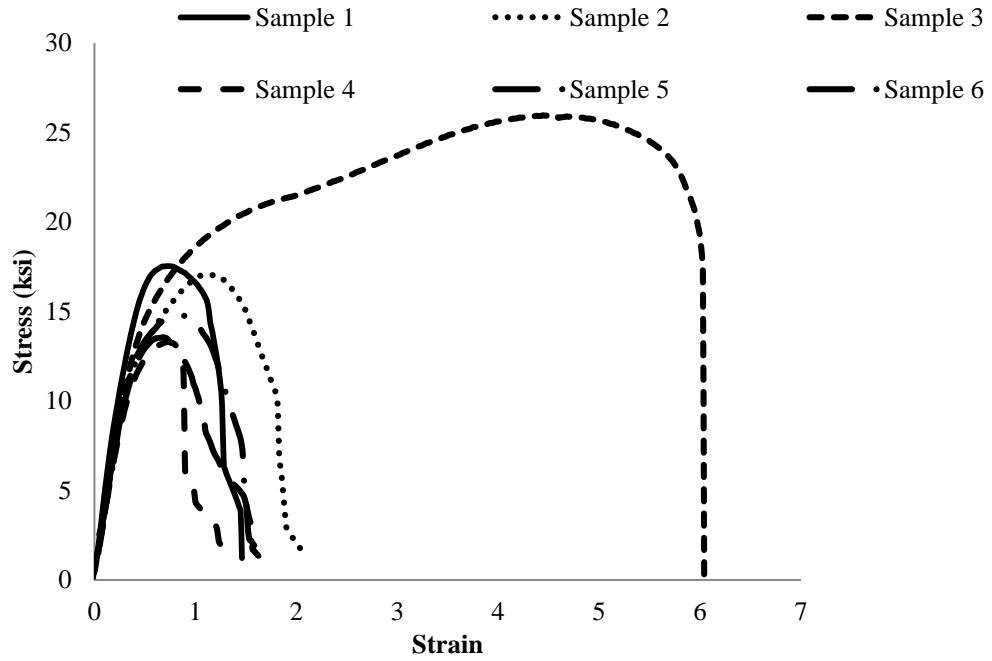
Figure 74: Steel (ER70S-6) Vertical Tensile Tests - Wall 2
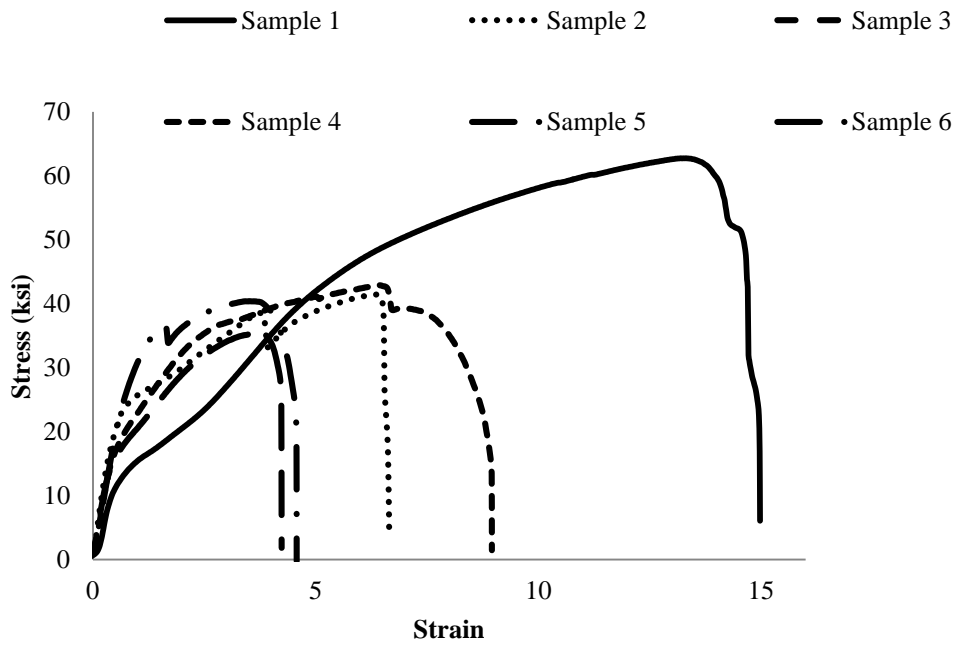
Figure 75: Steel (ER70S-6) Vertical Tensile Tests - Wall 4

All six of the broken steel (ER70S-6) tensile specimens from Wall 2 are shown in Figure 76 and the tensile specimens from Wall 4 are shown in Figure 77. The specimens from the wall that failed at a lower tensile strength all failed in the same manner along the same layer as shown in Figure 76. The specimens from Wall 4, which had a higher average tensile strength, had multiple points of failure but still had a prevailing failure layer as shown in Figure 77. Although the material was able to withstand aggressive machining, it failed easily in perpendicular tensile loading.

Figure 76: Broken Steel (ER70S-6) Tensile Specimens from Wall 2

Figure 77: Broken Steel (ER70S-6) Tensile Specimens from Wall 4

The wire manufacture's specified tensile strength for the steel wire (ER70S-6) after deposition was specified to be 70 ksi. Figure 78 shows the average ultimate tensile strengths for the steel wall sections compared to the manufacture's specification. The horizontal test specimens were at material specification and the vertical test specimens were approximately 50% less.
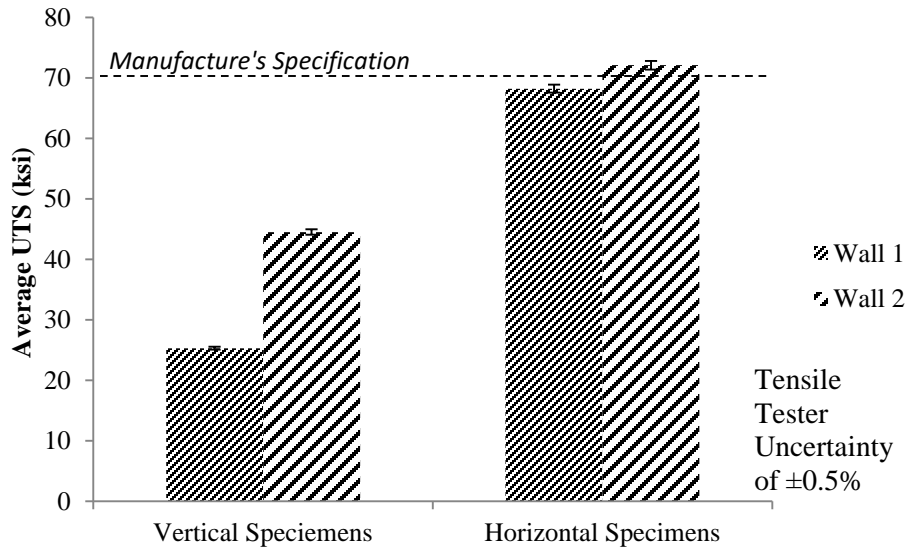
Figure 78: Steel (ER70S-6) Tensile Test Results

The stainless steel (ER308) tensile test specimen results for the specimens that were oriented parallel to the deposited layers are shown in Figure 79 and in Figure 80. The samples are numbered from the bottom to the top region of the deposited wall with the top region being the highest numbered sample. There was no correlation between the tensile strength and the region of the wall from which the sample was taken.
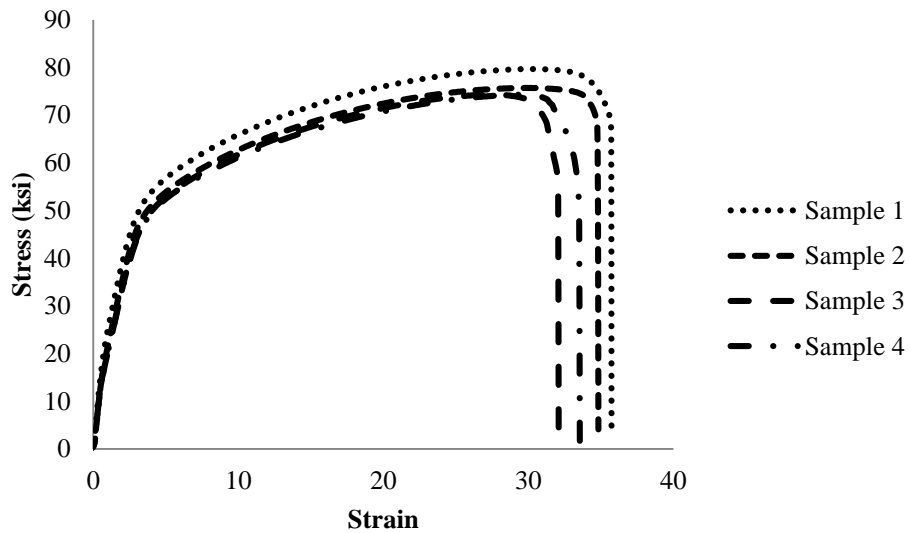
Figure 79: Stainless Steel (ER308) Horizontal Tensile Tests - Wall 1
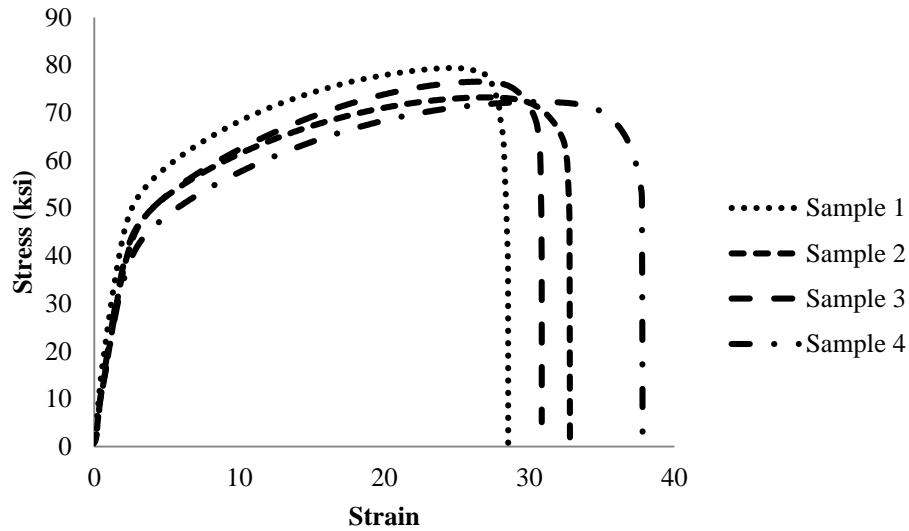
Figure 80: Stainless Steel (ER308) Horizontal Tensile Tests - Wall 3

The stainless steel (ER308) horizontal tensile test specimens had an average ultimate tensile strength of 75.7 ksi. A t-test was conducted to compare the horizontal tensile strength in wall 1 and wall 3. There was not a significant difference in the tensile strength in wall 1 (M=76.0 ksi., SD=2.54 ksi.) and wall 3 (M=72.4 ksi., SD=3.23 ksi.); t(3)=0.59, p=0.5964). Therefore, the steel (ER308) deposition process is repeatable when considering tensile strength parallel to the deposited layers. Additionally, the stainless steel (ER308) horizontal tensile tests had consistent toughness

The tensile test results for the stainless steel specimens that were oriented perpendicular to the deposited layers are shown in Figure 81 and in Figure 82. The vertical stainless steel (ER308) specimens had an average ultimate tensile strength of 57.3 ksi. A t-test was conducted to compare the vertical tensile strength in wall 2 and wall 4. There was not a significant difference in the tensile strength in wall 2 (M=61.5 ksi., SD=6.68 ksi.) and wall 4 (M=57.9 ksi., SD=12.3 ksi.); t(4)=0.676, p=0.536).

Therefore, the stainless steel (ER308) deposition process is repeatable when considering tensile strength perpendicular to the deposited layers.
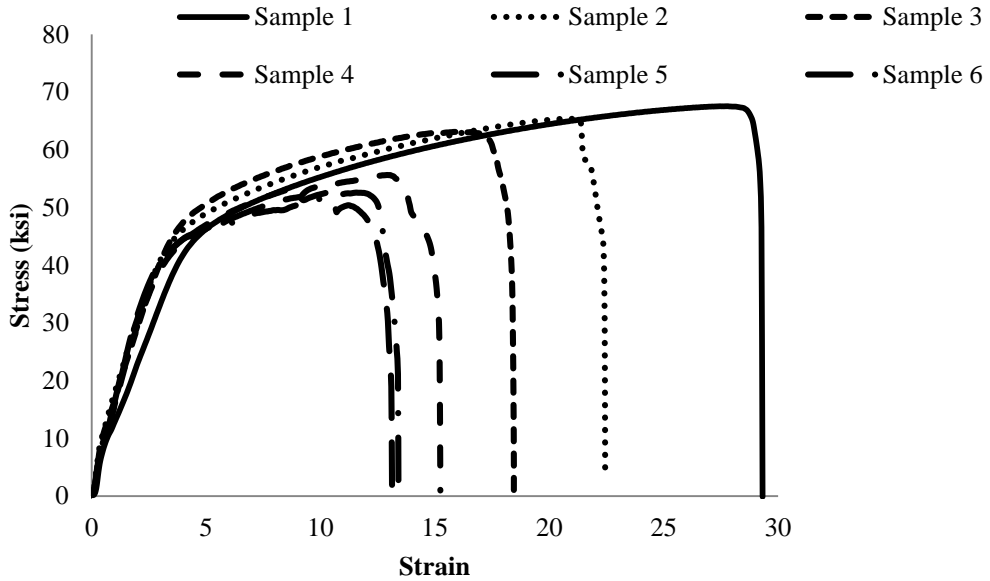
Figure 81: Stainless Steel (ER308) Vertical Tensile Tests - Wall 2
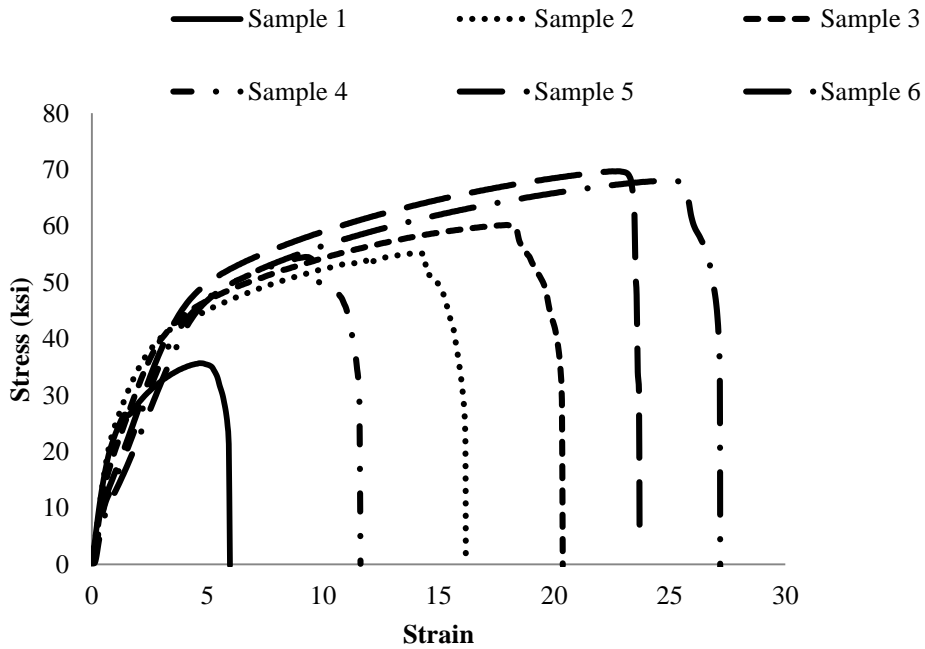
Figure 82: Stainless Steel (ER308) Vertical Tensile Tests - Wall 4

The wire manufacture's specified tensile strength for the stainless steel wire after deposition was specified to be 88 ksi. Figure 83 shows the average ultimate tensile strengths for the stainless steel wall sections compared to the manufacture's specification. The horizontal test specimens were 14% less than the material specification and the vertical test specimens were 34% less.
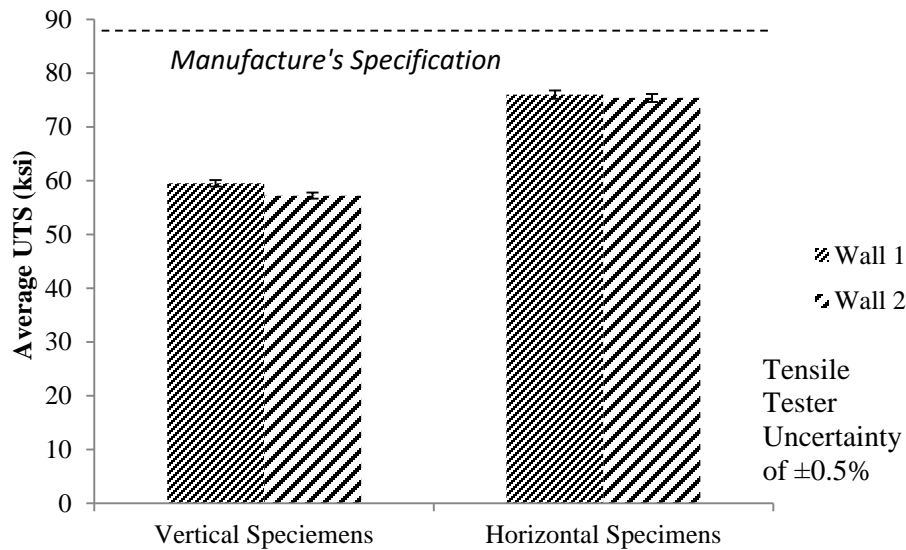
Figure 83: Stainless Steel (ER308) Tensile Test Results

Microstructure Examination Results

Photographs of the microstructure were compared to pictures of traditional steel weld microstructures. As shown in Figure 84, the microstructure of a steel weld is typically acicular ferrite.
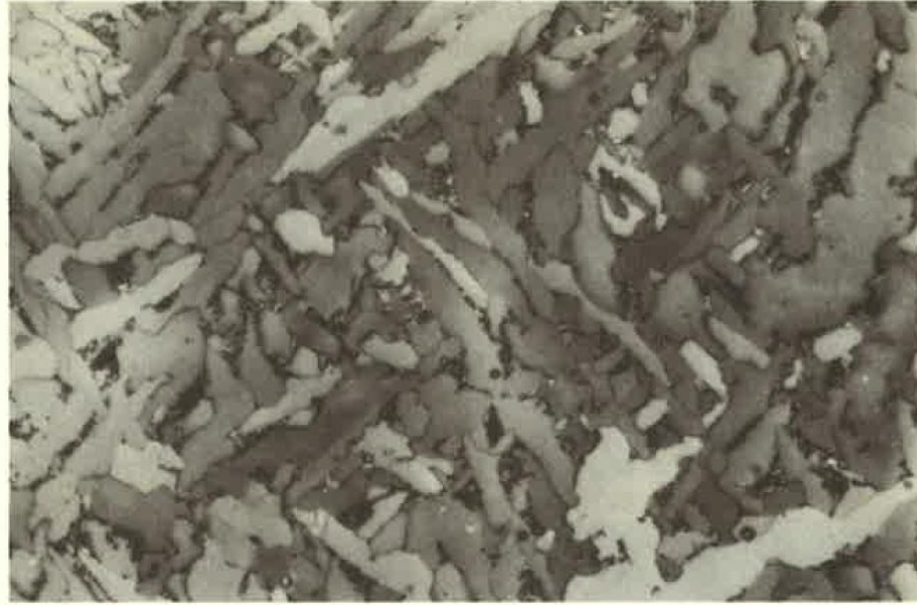
Figure 84: Acicular ferrite plus carbides in submerged arc weld metal [43]

Samples of steel deposits from the middle of a deposited bead etched with 2% Nital are shown in Figure 85 and in Figure 86. In both specimens, the grain structure is acicular ferrite with some regions of pearlite and bainite. The black spots are porosity and some hard oxide particles.
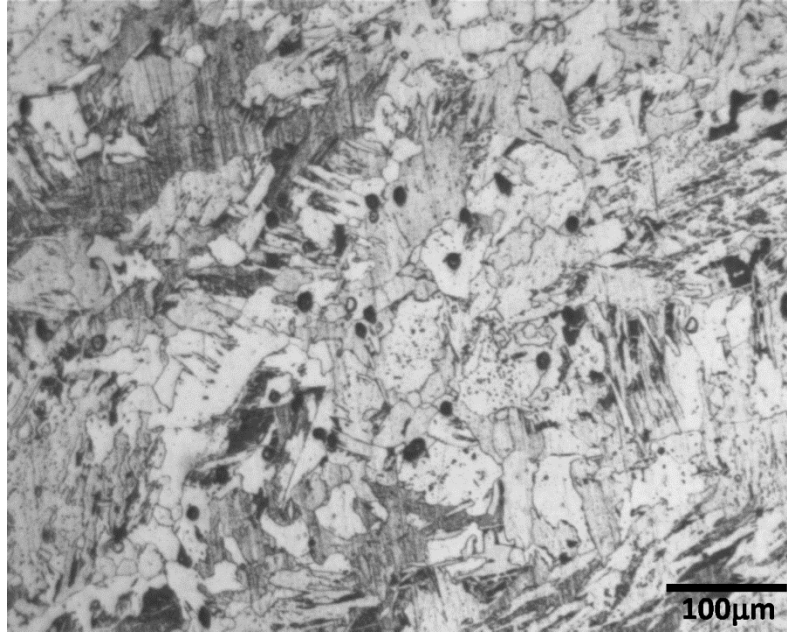
Figure 85: Microstructure of Deposited Steel (ER70S-6) Specimen 1-2 Etched with 2%

Nital
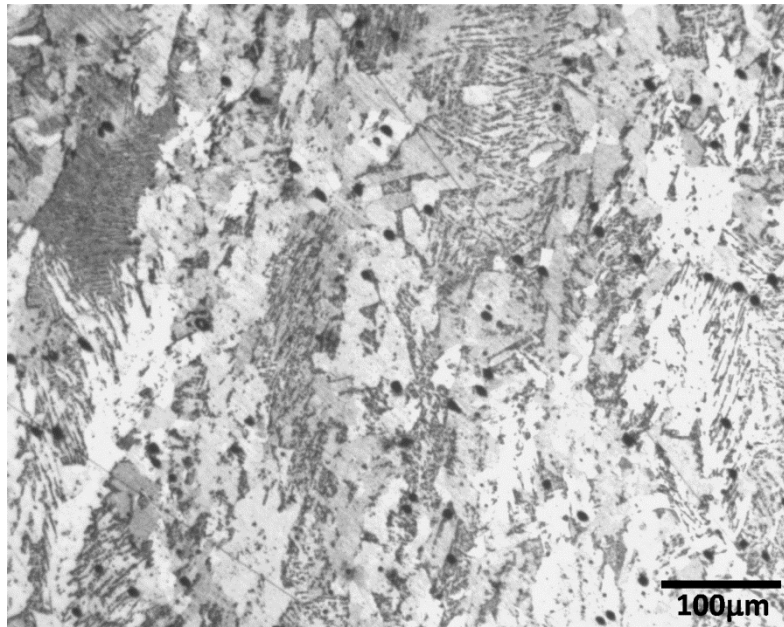
Figure 86: Microstructure of Deposited Steel (ER70S-6) Specimen 1-4 Etched with 2%

Nital

Further magnification of a sample taken from the middle of a deposited bead is shown in Figure 87. The grain boundaries are clearly seen as well as the dark gray pearlite regions.
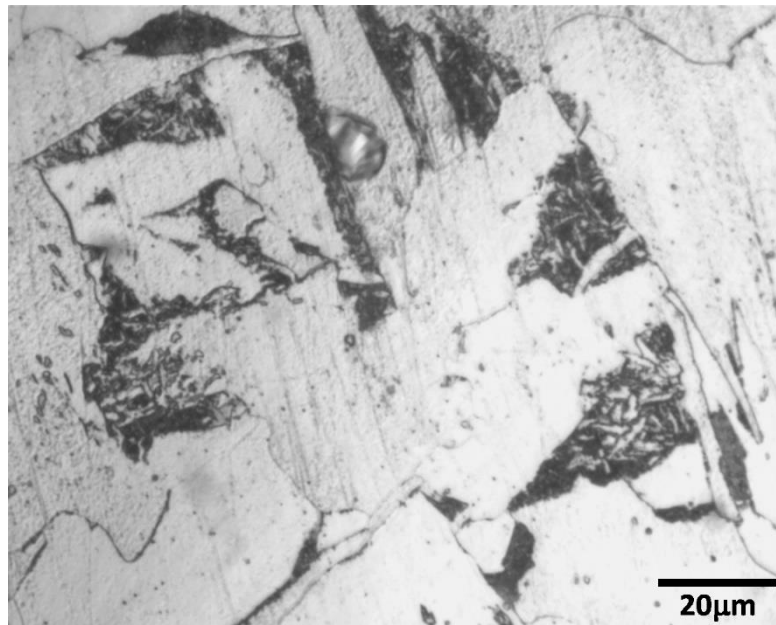
Figure 87: Microstructure of Deposited Steel (ER70S-6) Specimen 3-2 Etched with 2% Nital

When examining an un-etched specimen as shown in Figure 88, small dark spots were shown surrounded by a dark gray region. The small dark spots were hard oxide particles from the deposition and cooling process. The dark gray regions surrounding the small dark spots were smaller oxide particles created by the polishing process. A large hole is also observed in the top of the specimen pictured in Figure 88.
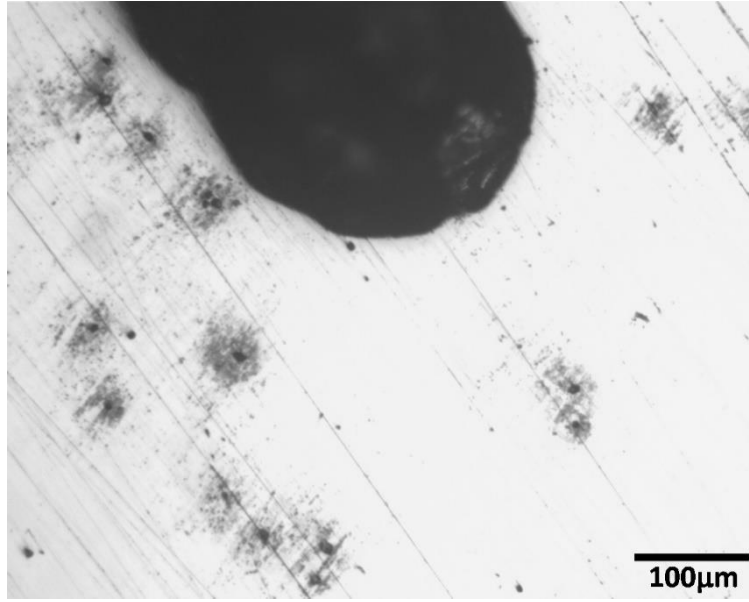
Figure 88: Microstructure of Un-etched Deposited Steel (ER70S-6) Specimen

The region between adjacent layers was also examined as shown in Figure 89 and in Figure 90. While poorly etched, Figure 89 shows an interface between layers without voids. The better etched sample shown in Figure 90 shows an interface between layers with porosity as evidenced by two black voids. Additionally, a light region of different grain structure is shown on the interface between the voids. This light colored region is evident in both Figure 89 and Figure 90 and is at the interface between the two layers.
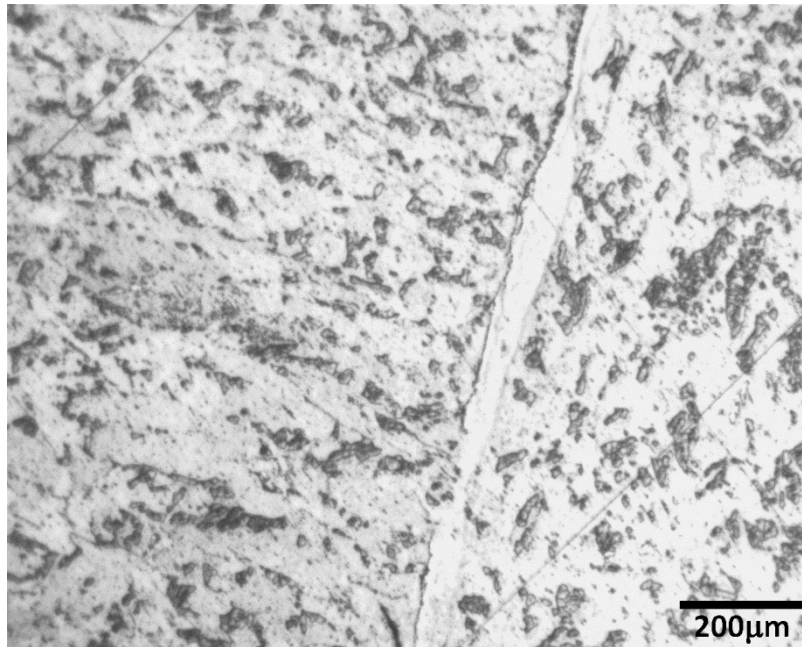
Figure 89: Interface between Deposited Steel (ER70S-6) Layers Etched with 2% Nital
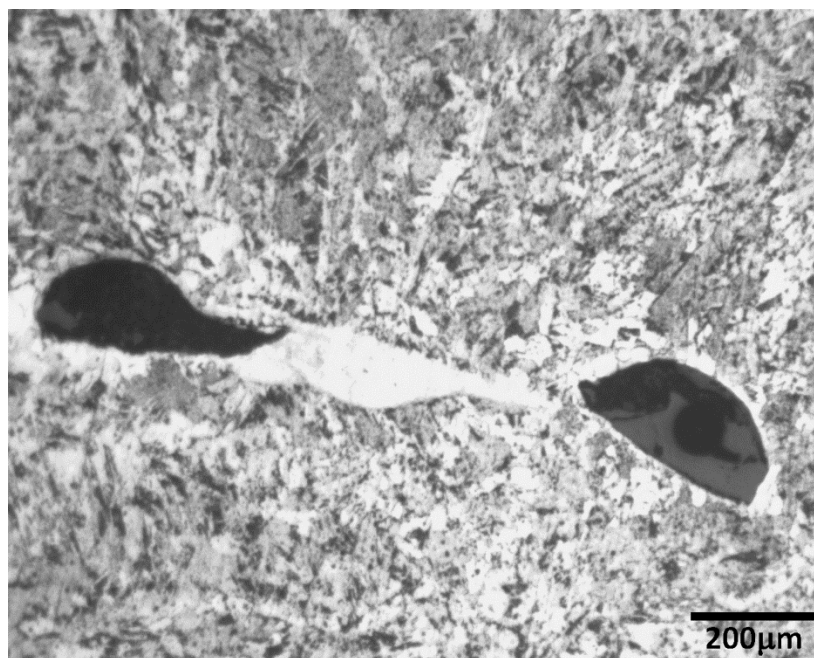
Figure 90: Interface and Porosity between Deposited Steel (ER70S-6) Layers Etched with

2% Nital

Slicing Software Results

When comparing slicing software options, *Kisslicer* was found to be very stable and capable of producing reliable G-code. However, *Kisslicer* was particular about the *.stl* that was inputted and was not capable of slicing a poor *.stl* file. *Slic3r* was found to have more features. However, it did occasionally crash or produce erroneous G-code. Both slicing software options were viable options for future use.

Heat Treatment Results

When examining the surface hardness of the deposited walls, there was no difference observed between the bottom, middle, and top locations as shown in Figure 91. After heat treating, the samples were tempered and not as hard. The average surface hardness before heat treating was 100.8 Rockwell B, and the average surface hardness after heat treating was 94.0 Rockwell B. The hardness test had an uncertainty of $\pm$ 2 Rockwell B.
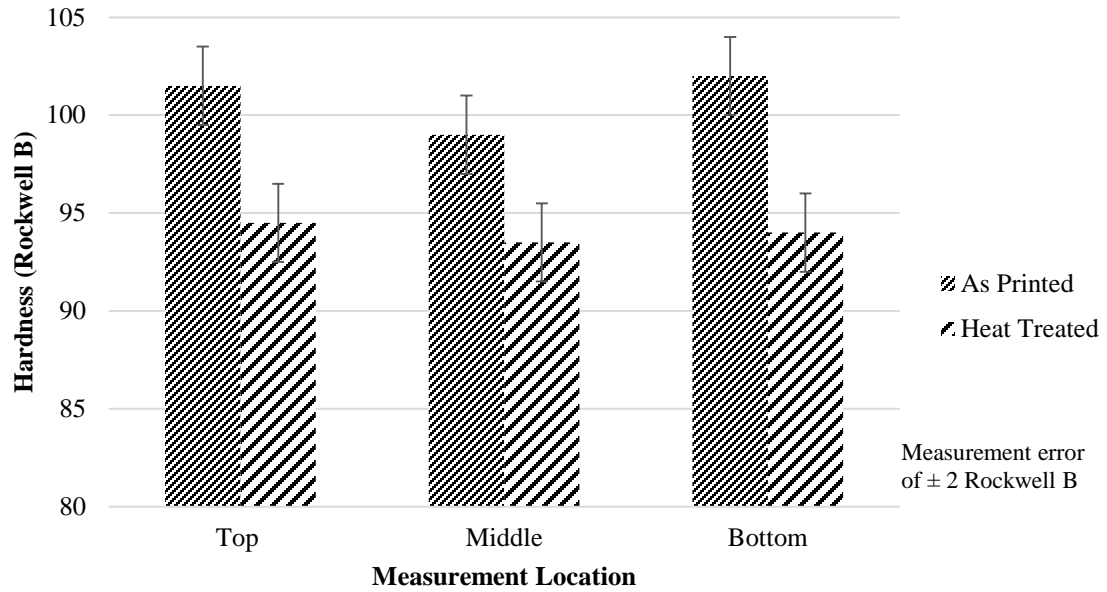
Figure 91: Steel (ER70S-6) Heat Treatment Results

Because surface hardness was not dependent upon location upon the specimen, the grain structure was examined only at the middle of the samples. The microstructure of an untreated sample is shown in Figure 92 and a heated treated sample is shown in Figure 93. The heat treated sample was observed to have more consistent structure and not have dark regions.
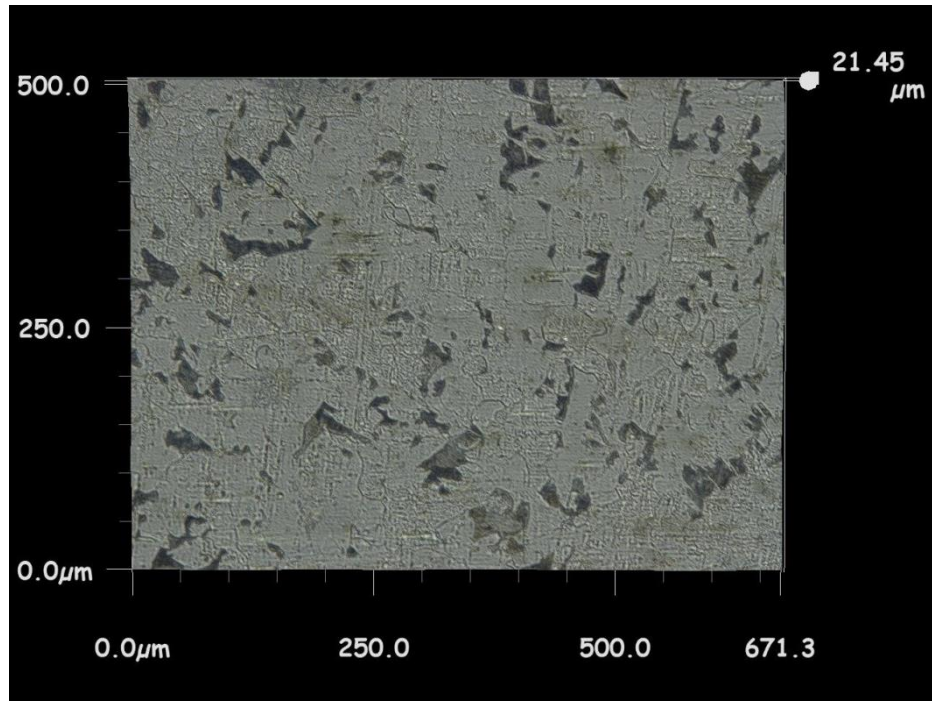
Figure 92: Microstructure of Untreated Steel (ER70S-6) Sample Etched with Nital
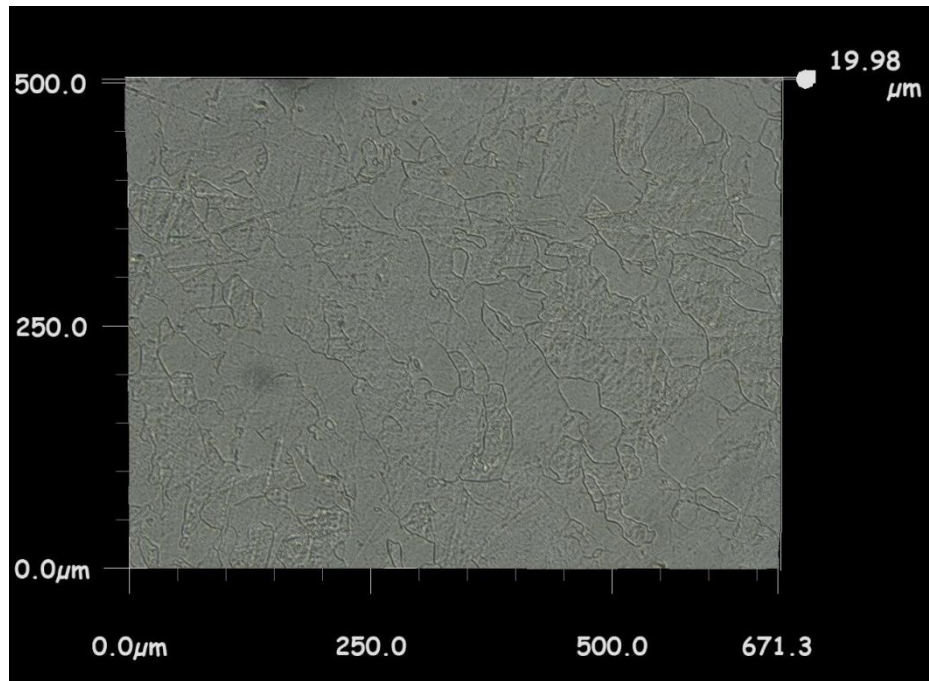
Figure 93: Microstructure of Heat Treated Steel (ER70S-6) Sample Etched with Nital

To ensure that the dark regions of the untreated sample's microstructure were not voids, the 3D microscope was used. Figure 94illustrates that the dark regions were not voids.
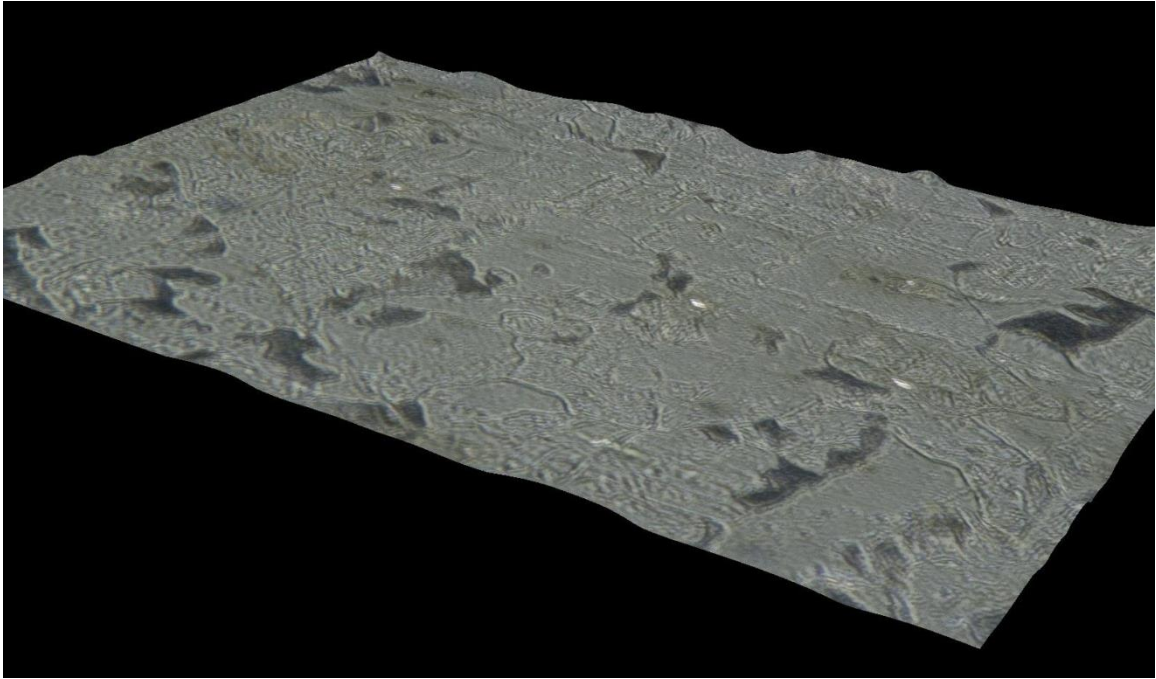
Figure 94: 3D Microstructure of Untreated Steel (ER70S-6) Sample Etched with Nital

The 3D microscope was also used to examine voids found in the surface of the samples as shown in Figure 95 and in Figure 96. The voids in both images were found at the interface between layers. These images also illustrated that the dark regions of microstructure present in the untreated samples are not voids.
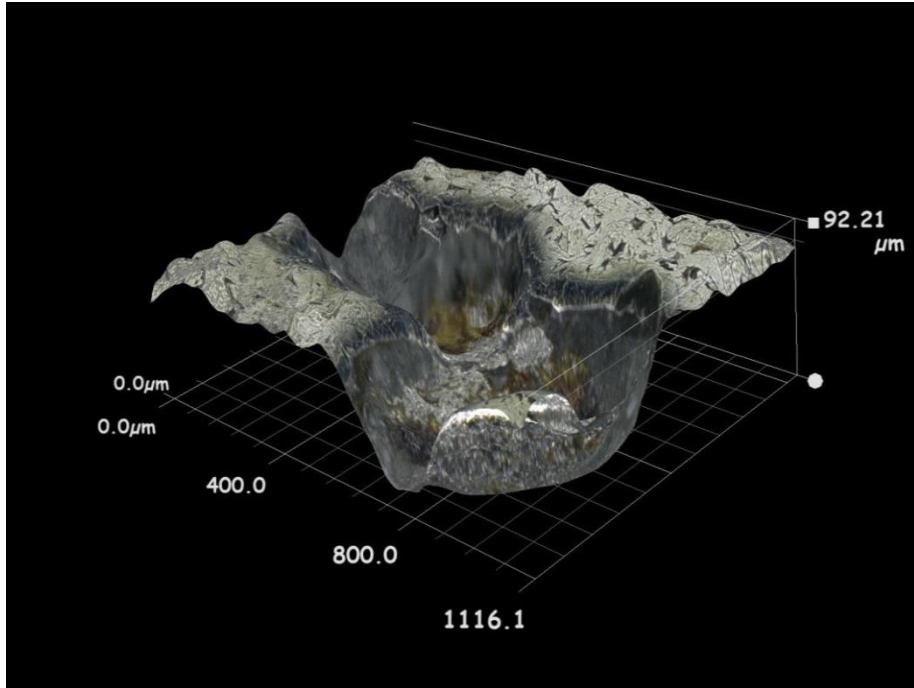
Figure 95: 3D Microscopy of Void in Untreated Steel (ER70S-6) Sample Etched with
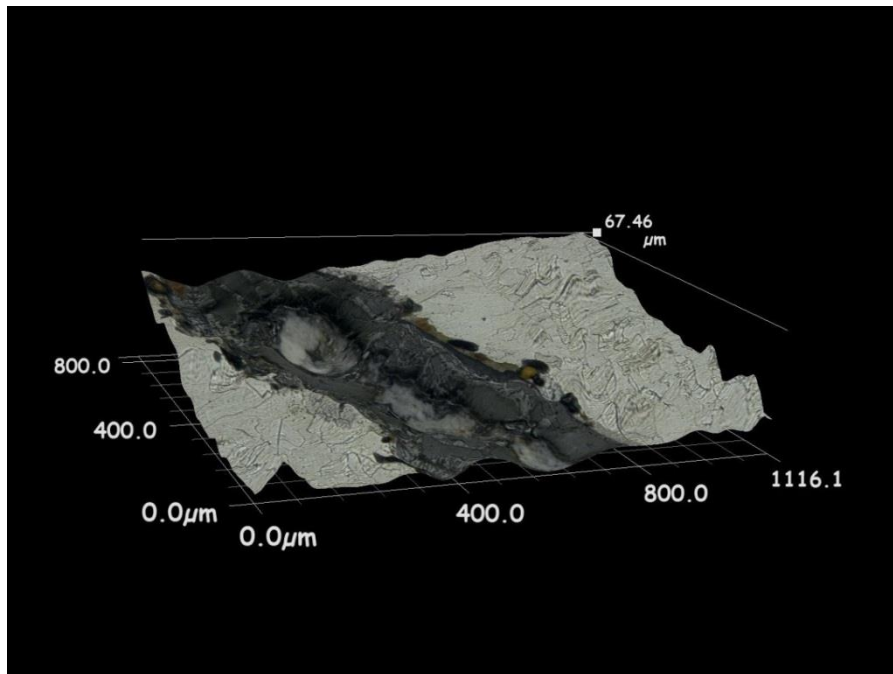
Nital

Figure 96: 3D Microscopy of Void in Heat Treated Steel (ER70S-6) Sample Etched with

Nital

Build Plate Evaluation Results

For the steel wire, the first build plate material considered was a steel build plate. The steel build plate did not allow easy removal of the deposited structure. A band saw was used to remove the deposited structure. The remaining deposits on the steel build plate where then removed with an upright milling machine. Additionally, it was observed that the steel build plate would be warped after the deposition process. The magnitude and direction of warping was dependent upon how much material was deposited and the geometry of the part.

Table 5: Build Plate Materials Results

Wire material	Build plate material	Removable?	Reusable?
A-36 Steel	A-36 Steel	No	No
A-36 Steel	Aluminum	No	No
A-36 Steel	Titanium	Yes	No
A-36 Steel	Chrome alloy foil	No	No
A-36 Steel	Tungsten sheet	Yes	No
A-36 Steel	99.5% Tungsten Bar	Yes	Yes
A-36 Steel	Graphite	Yes	Yes
Aluminum	Aluminum	No	No
Aluminum	A-36 Steel	Yes	Yes

Another material considered for the steel wire was aluminum. When deposited, the steel melted the aluminum and the build plate was not removable or reusable. Titanium was also considered as a build plate material for the steel wire. As shown in

Figure 97, the deposited steel structure did not bond to the titanium enough to prevent warping.

Figure 97: Steel (ER70S-6) Cooling on Titanium Build Plate

After cooling, the warped steel structure was easily removed from the titanium. Upon examination, as shown in Figure 98, the titanium build plate was pitted eroded. The titanium build plate was not reusable without resurfacing.
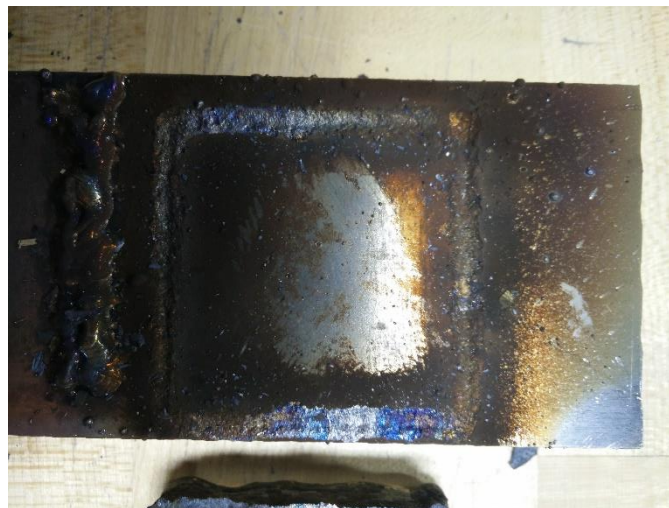
Figure 98: Pitted Titanium Build Plate after Use

Another build plate considered for steel deposition was a chrome alloy foil. The foil was clamped to a steel build plate. As shown in Figure 99, the deposited steel burned

through the foil and was securely bonded to the steel substrate beneath the foil. The chrome alloy foil did not appear to effect or influence the deposition process.

Figure 99: Steel (ER70S-6) Deposited on Chrome Alloy Foil

Tungsten sheet metal was also considered as a build plate for the steel wire. The steel was readily deposited to the 99.5% tungsten sheet as shown in Figure 100. During cooling, the thin tungsten sheet began to crack as shown in Figure 101. The tungsten sheet separated from the steel deposit after cooling. The steel deposit was therefore removable from the tungsten sheet but the tungsten sheet was not reusable.
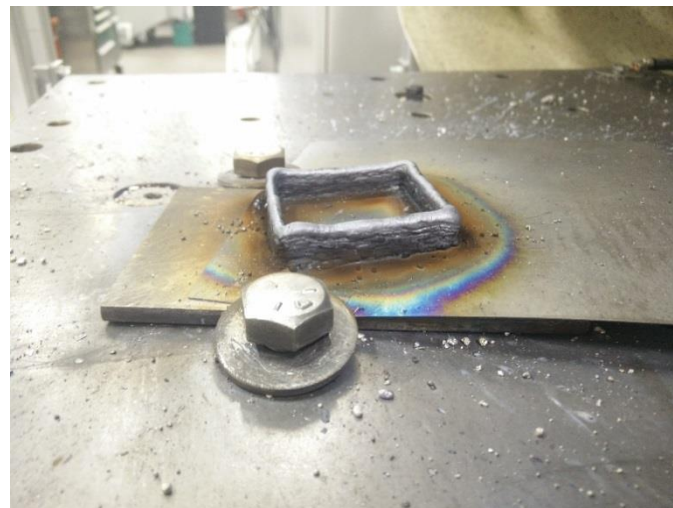
Figure 100: Steel (ER70S-6) Deposited on Tungsten Sheet
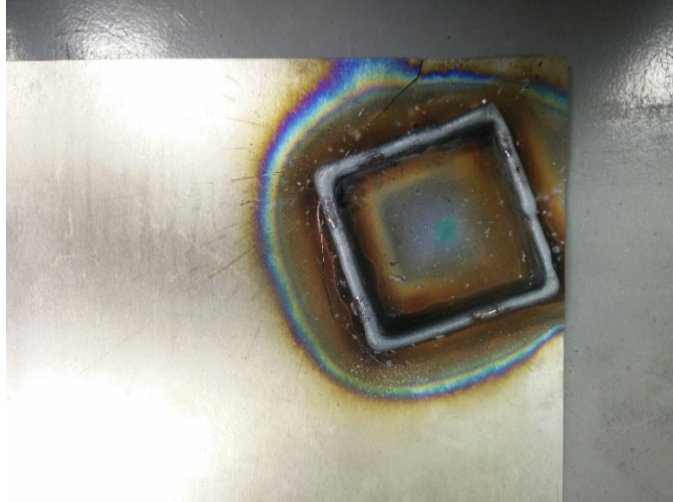
Figure 101: Tungsten Sheet Cracking during Cooling

Because the tungsten sheet was removable from the steel deposit, a thicker tungsten bar was used as a build plate. The tungsten bar (99.5% tungsten) was used twice, and each time the deposit was removable as shown in Figure 102. The after separation with light force from a cold chisel, the tungsten bar was not pitted or warped and could be reused. A heaver piece of tungsten appears to be a good baseplate for steel deposition.

Figure 102: Tungsten Build Plate

The final material considered as a build plate for the steel wire was a graphite bar. When printing, the steel did not bond to the graphite as shown in Figure 103. While the steel deposit was easily removed, it did not bond well enough to the graphite to prevent sliding during the build process. The graphite was undamaged and could be reused.

Figure 103: Graphite Build Plate

For building objects with aluminum wire, an A-36 steel and an aluminum build plate were considered. The aluminum build plate was not removable or reusable. However, the steel build plate allowed removal of the aluminum deposit with a hammer and cold chisel. Additionally, the A-36 steel build plate was reusable although warped from the high heat process. A thicker build plate would mitigate the warping effects.

VII. Discussion

Analysis of the results found in the previous chapter allows a greater understanding of the process, its advantages, and improvement opportunities. A discussion of the results from each aspect of the project is found below.

Geometry Discussion

When examining the geometry evaluation results, material buildup was observed on the corners of the square objects. This material buildup is also observed in FDM additive manufacturing and was caused by a combination of factors. One cause was the machine slowing in the corners (because instantaneous accelerations are not possible). Another cause was that the deposited layer has a set width that is compressed during a corner with a radius less than the width of the layer.

Additionally, material buildup was observed at the layer change point. This material buildup was exacerbated when the layer change points were not randomized. The material buildup was not observed when the machine was spiraling upward to continuously build the object. The material buildup at layer change point was not caused by the action of moving upwards because the welder was not depositing material during travel moves. Rather, it was caused by the start and stop points at the weld bead. Build up was observed when the machine started depositing a bead and a lack of material was observed when machine stopped depositing a bead. This behavior was a combination of heat buildup inside the deposit, the internal welder controls controlling the deposit start

power, and the melt pool being pushed during deposition. Increased control of this material buildup is critical for improving the process.

The spiraling approach of constant layer change was effective for mitigating excessive material buildup. However, the spiraling approach presents additional issues. One of which is excessive heat buildup causing uneven surface features throughout the part. Another issue of the spiraling technique is that it can only be applied to objects with a single continuous perimeter.

It was also observed that the first layer deposited was critical to the success of subsequent layers. If the first layer was poor and discontinuous it would negatively affect the next layer. The first layer was observed to have different characteristics then subsequent layers. This was because the first layer was deposited upon a room temperature build plate unlike subsequent layers which were deposited upon the recently heated smaller mass of the previous layer. This implies that a heated base plate would improve the consistency of the process.

Creating the bridging walls was found to be the most challenging geometry due to inconsistency in the process. It was not found to be repeatable. While it was possible, difficulties were observed in finding the correct step over distance for the overhanging layers. Additionally, it was impossible to manage heat buildup during the creation of the overhanging layers.

Wire Diameter Discussion

It was observed that there was no statistically significant difference in the voltage or current requirements for wire diameters from 0.025 to 0.035 in. Because the welder was programmed from the manufacturer to maintain a constant voltage based upon the

user set voltage value, it was expected that there would be no significant difference in the voltage requirements. Therefore, the welder was performing as expected.

When considering the current required for the different wire diameters, there was no observable difference. The wire diameter change from 0.025 to 0.035 in. is not large enough to create a difference in melting power required that is measureable with the instrumentation.

Tensile Strength Evaluation Discussion

When performing the tensile strength evaluation, both steel and stainless steel materials were stronger in the direction parallel to the layers as opposed to the direction perpendicular to the layers. This type of behavior is typical of additive manufactured parts. Each tensile test specimen, regardless of orientation, exhibited failure along the layer interfaces. Therefore, improvements should be made to the bonding between layers. As a first generation approach, optimization was not a priority although it as a definite possibility.

Also of significance was that the steel tensile test specimens perpendicular to the layers were not repeatable while the equivalent stainless steel specimens were. This implies that the stainless steel process deposition process is more repeatable and consistent than the steel process. This is possibly due to the stainless steel deposition being a cleaner process with less oxidation than the steel. Therefore, improvements could be made to prevent the formation of oxides between the layers of deposition by controlling the atmosphere more accurately.

Microstructure Examination Discussion

Examination of the microstructure also indicates that improvements should be made to the bonding between layers and to prevent the formation of oxides. The microstructure of the steel (ER70S-6) specimens was observed to have multiple spots of porosity and hard oxide particles. Both types of defects were the result of inconsistent deposition due to poor inert gas shielding. Improving the shielding gas to a mix of argon and carbon dioxide would result in a more consistent weld bead and reduce porosity.

Heat Treatment Discussion

After heat treatment, the samples had a softer surface hardness. Therefore, the samples were tempered. To increase the hardenability of the steel objects, more carbon must be added. According the manufacture, the carbon content of the material after deposition is 0.08-0.09 %. This low carbon content was why the material is soft and not very hardenable.

When examining the microstructure after heat treatment, the dark regions of the microstructure had disappeared. To further understand the process, these unknown dark regions should be examined. However, the deposited steel material's hardness and microstructure can be changed with heat treatment.

Build Plate Discussion

While steel was found to be an excellent build plate for aluminum, further experimentation should be done to determine if tungsten is an acceptable build plate for steel deposition. In addition to a larger tungsten build plate, it should be determine how many cycles the tungsten can be reheated before brittle failure. The carbon build plate also needs further examination. Perhaps pins could be inserted into the build plate to

prevent the deposit from sliding during deposition. The machine would deposit material between the pins. After printing, the pins could be easily trimmed. Additionally, sometimes it may be useful to incorporate the build plate into the part's design. The deposited structure might not always need to be removed from the build plate.

VIII. Conclusions and Future Work

A comprehensive literature review was conducted to determine the current state of MIG additive manufacturing technology. From the literature review, research opportunities and important process factors were determined. Using knowledge from the literature review, a MIG based additive manufacturing machine was constructed. After determining the proper operating parameters, numerous geometries were created using the machine. The effects of wire diameter were studied and the tensile strength of the deposited metals was measured. Build plates for the process was evaluated, and the microstructure of the deposited structures was examined. The results of the experiments are listed below.

- A MIG based 3D printer was built using commercial, off-the-shelf parts.

- Software packages were modified to print CAD files by controlling the printer and MIG power source.

- A voltage and current monitor for the MIG power source was implemented and calibrated.

- The constructed machine was capable of creating hollow, solid, and overhanging geometries.

- Steel (ER70S-6), aluminum (ER4043), and stainless steel (ER308) wire in 0.025, 0.030, and 0.035 in. diameters were deposited to create objects.

- The voltage and current requirements for each wire diameter were measured in two different materials. There was no significant difference in the electrical power requirements for different wire diameters within the same materials.

- The tensile strength of steel and stainless steel walls was measured parallel and orthogonal to the layers of deposition. The tensile strength was near the material tensile strength parallel to the layers but was much less orthogonal to the layers.

- The examined microstructure was acicular ferrite. Considerable contaminate and voids were observed. Larger voids were observed at the layer interfaces.

- The hardness and microstructure of the deposited steel structures can be modified with heat treatment.

- An operation manual for the machine was written (Appendix 3).

- The important process parameters were noted, and an experimental record sheet was created for future researchers (Appendix 4).

- Detailed drawings and bill of materials (Appendix 1) were created.

Recommendations for Future Work

As shown in the experiments, future work is necessary to further improve the process. This future work can be divided into machine mechanical improvements, welder improvements, and control improvements.

Several mechanical improvements can be done to improve the 3D printer and are listed below.

- Integrating a milling spindle into the machine. The open architecture of the machine allows for easy implementation of a milling spindle. Adding a milling

spindle would allow production and post-processing to be done on the same machine.

- Adding additional axis to the printer. A trundle could be added to allow the machine use gravity to control the deposition of molten metal. This would allow creation of additional geometries and improve the surface finish

- Improving the build plate. For more consistent deposition of difficult to weld materials like aluminum and copper, a heated build plate would improve the process.

- Controlling the operating environment. In addition to changing the shielding gas mixture, the machine could be fully enclosed to create an inert gas chamber.

The following welder improvements could be made provide greater control of the process.

- A cold water tip cooled MIG gun would assist in the deposition of aluminum and copper.

- A pulsed MIG gun would assist in controlling the heat buildup in the deposit.

- A cold metal transfer MIG process would result in greater control of the weld bead.

The following controls improvements could be made.

- Adding closed loop control based upon sensor feedback. A thermal camera could be used to monitor the previous layer's temperature. Using real time temperature information, the controller could vary the welder's power to ensure consistent layer bonding.

- Adding a visual camera to monitor the deposited layers' width. This information could be used to change the printer's speed to maintain the desired layer width.

The following unfinished objects could be performed.

- Develop an optical system for observation and possible future feedback control.

- Instrument the process with thermocouples to document heat history and future in-process thermal feedback.

- Develop strategy to deal with "slumping" reported by researchers.

- Print an eight-inch diameter, two-inch-high steel skillet with an eight-inch handle.

- Print the casing for a small bore steam engine design.

IX. References

[1]   Pinar, A., Wijnen, B., Anzalone, G. C., Havens, T. C., Sanders, P. G., and Pearce, J. M., 2015, "Low-Cost Open-Source Voltage and Current Monitor for Gas Metal Arc Weld 3D Printing," Journal of Sensors, 2015, pp. 1–8.

[2]   Frazier, W. E., 2014, "Metal Additive Manufacturing: A Review," Journal of Materials Engineering and Performance, **23**(6), pp. 1917–1928.

[3]   Williams, S. W., Martina, F., Addison, A. C., Ding, J., Pardal, G., and Colegrove, P., 2015, "Wire+Arc Additive Manufacturing," Materials Science and Technology, pp. 0–7.

[4]   Anzalone, G. C., Chenlong Zhang, Wijnen, B., Sanders, P. G., and Pearce, J. M., 2013, "A Low-Cost Open-Source Metal 3-D Printer," IEEE Access, 2013, pp. 803–810.

[5]   Miller, 2012, "Guidelines for Gas Metal Arc Welding (GMAW)" [Online]. Available: http://www.millerwelds.com/pdf/mig_handbook.pdf. [Accessed: 13-Aug-2015].

[6]   Fronius, 2011, "Cold Metal Transfer" [Online]. Available: http://www.fronius.com/cps/rde/xbcr/SID-EEBD8E0B-816922C5/fronius_espana/M_06_0001_EN_CMT_leaflet_Feb_2014_aw19_low_44211_snapshot.pdf. [Accessed: 13-Aug-2015].

[7]   Mufti, R. A., 2008, "Mechanical and microstructural investigation of weld based rapid prototyping," Ph.D. thesis, Ghulam Ishaq Khan Institute of Engineering Sciences and Technology.

[8]   Baker, R., 1925, "Method of making decorative articles," U.S. Patent 1533300.

[9]   Eschholz, O. H., 1925, "Ornamental arc welding," U.S. Patent 1533239.

[10]   Shockey, H. K., 1932, "Machine for reclaiming worn brake drums," U.S. Patent 1886503.

[11]   Noble, P., 1933, "Method and apparatus for electric arc welding," U.S. Patent 1898060.

[12]   Carpenter Otis, R., and Kerr, H. J., 1947, "Method and apparatus for metal coating metal pipes by electric fusion," U.S. Patent 2427350.

[13]   White, J. W. D., 1964, "Pressure roller and method of manufacture," U.S. Patent 3156968.

[14]   Ujiie, A., 1971, "Method of and apparatus for constructing substantially circular cross section vessel by welding," U.S. Patent 3558846.

[15]   Brandi, H., and Luckow, H., 1976, "Method of making large structural one-piece parts of metal, particularly one-piece shafts," U.S. Patent 3985995.

[16]   Almeida, P. M. S., 2012, "Process control and development in wire and arc additive manufacturing," Ph.D. thesis, Cranfield University.

[17]   Acheson, R., 1990, "Automatic welding apparatus for weld build-up and method of achieving weld build-up," U.S. Patent 4952769.

[18]   Dickens, P. M., Pridham, M. S., Cobb, R. C., Gibson, I., and Dixon, G., 1992, "Rapid prototyping using 3-D welding," Proc. Solid Freeform Fabrication Symp, DTIC Document, pp. 280–290.

[19]   Spencer, J. D., Dickens, P. M., and Wykes, C. M., 1998, "Rapid prototyping of metal parts by three-dimensional welding," Proceedings of the Institution of Mechanical Engineers, Part B: Journal of Engineering Manufacture, **212**(3), pp. 175–182.

[20]   Rossini, N. S., Dassisti, M., Benyounis, K. Y., and Olabi, A. G., 2012, "Methods of measuring residual stresses in components," Materials & Design, **35**, pp. 572–588.

[21]   Ribeiro, F., Ogunbiyi, B., and Norrish, J., 1997, "Mathematical model of welding parameters for rapid prototyping using robot welding," Science and Technology of Welding and Joining, **2**(5), pp. 185–190.

[22]   Ribeiro, A. F., Norrish, J., and McMaster, R. S., 1994, "Practical case of rapid prototyping using gas metal arc welding."

[23]   Ribeiro, F., 1998, "3d printing with metals," Computing & Control Engineering Journal, **9**(1), pp. 31–38.

[24]   Ribeiro, A. F., and Norrish, J., 1996, "Rapid prototyping using robot welding: slicing system developmens."

[25]   Ribeiro, A. F., and Norrish, J., 1996, "Case study of rapid prototyping robot welding - second 'square to round' shape."

[26]   Ribeiro, A. F., and Norrish, J., 1996, "Metal based rapid prototyping for more complex shapes."

[27]   Norrish, J., 2005, *New Developments in Advanced Welding,* CRC Press ; Woodhead Pub, Boca Raton, FL : Cambridge, England.

[28]   Kovacevic, R., and Beardsley, H., 1998, "Process Control of 3D Welding as a Droplet-Based Rapid Prototyping Technique," Proc. of the SFF Symposium, Univ. of Texas at Austin, Austin TX, pp. 57–64.

[29]   Kmecko, I., Hu, D., and Kovacevic, R., 1999, "Controlling Heat Input, Spatter and Weld Penetration in GMA Welding for Solid Freeform Fabrication," Proceedings of the 10th Solid Freeform Fabrication Symposium.

[30] Zhang, Y., Chen, Y., Li, P., and Male, A. T., 2003, "Weld deposition-based rapid prototyping: a preliminary study," Journal of Materials Processing Technology, **135**(2), pp. 347–357.

[31] Song, Y.-A., Park, S., Hwang, K., Choi, D., and Jee, H., "Welding and Milling Direct Prototyping of Metallic Parts."

[32] Song, Y.-A., Park, S., Choi, D., and Jee, H., 2005, "3D welding and milling: Part I–a direct approach for freeform fabrication of metallic prototypes," International Journal of Machine Tools and Manufacture, **45**(9), pp. 1057–1062.

[33] Song, Y.-A., Park, S., and Chae, S.-W., 2005, "3D welding and milling: part II—optimization of the 3D welding process using an experimental design approach," International Journal of Machine Tools and Manufacture, **45**(9), pp. 1063–1069.

[34] Clark, D., Bache, M. R., and Whittaker, M. T., 2008, "Shaped metal deposition of a nickel alloy for aero engine applications," Journal of Materials Processing Technology, **203**(1-3), pp. 439–448.

[35] "Metal Deposition Technology," Keystone - Synergistic Enterprises, Inc. [Online]. Available: http://keystonehq.com/business-thrust-areas/metal-deposition-technology/. [Accessed: 09-Nov-2015].

[36] "Weld3D - Affordable Metal Additive Manufacturing," Weld3D - Affordable Metal Additive Manufacturing [Online]. Available: http://www.weld3d.com/. [Accessed: 09-Nov-2015].

[37] ASTM International, 2014, "Standard Guide for Evaluating Mechanical Propeties of Metal Materials Made via Additive Manufacturing Processes."

[38]   ASTM International, 2014, "Standard Practice for Reporting Data for Test Specimens Prepared by Additive Manufacturing."

[39]   ASTM International, 2010, "Standard Practice for Steel Castings, Surface Acceptance Standards, Visual Examination."

[40]   ArtSoft, "Mach3" [Online]. Available: http://www.machsupport.com/software/mach3/. [Accessed: 09-Nov-2015].

[41]   Maddox, J., and Roberts, J., 2013, "Measurement and Instrumentation Laboratory Manual."

[42]   Beckworth, T. G., Maragoni, R. D., and Lienhard, J. H., 2007, *Mechanical Measurements*, Prentice Hall.

[43]   Lancaster, J. F., 1999, *Metallurgy of Welding*, Woodhead Publishing Limited.

[44]   "Cura 3D Printing Slicing Software | Ultimaker," Ultimaker.com [Online]. Available: https://ultimaker.com/en/products/cura-software. [Accessed: 10-Nov-2015].

[45]   "MakerBot Desktop Software," MakerBot [Online]. Available: http://www.makerbot.com/desktop. [Accessed: 10-Nov-2015].

Appendix 1: Bill of Materials and Part Drawings

PART	Source	Length (in.)	Quantity	Cost ($)	Total Cost ($)
80/20 beams, brackets, and fasteners	DML			0	0
Sheet metal cover - aluminum	DML			0	0
Misc alumininum bars	DML			0	0
Aluminum angle - 4 in x 4 in. - 1/4 in. thick - 36 in. long -8982K76	DML	1	1	0	0
Fasteners	Local store	1	1	150	150
Aluminum bar to make 80/20 nuts	DML			0	0
Linear Rail LGS20EA - Base	HomeShop CNC	40	2	3.65	292
Linear Rail LGS20EA - Z-axis	HomeShop CNC	27.5	4	3.65	401.5
Linear Rail LGS20EA - X-axis	HomeShop CNC	22	2	3.65	160.6
Wide Carriage LGS20-EA	HomeShop CNC	1	10	59	590
Ballscrew 1605 - Base - 16mm dia.	HomeShop CNC	40	1	1.89	75.6
Ballscrew 1605 - Z-axis - 16mm dia.	HomeShop CNC	26.5	2	1.89	100.17
Ballscrew 1605 - X-axis - 16mm dia.	HomeShop CNC	27	1	1.89	51.03
Ballscrew fixed end machining	HomeShop CNC	1	4	75	300
Ballscrew free end machining	HomeShop CNC	1	2	25	50
Ballscrew fixed end support BK12-C7	HomeShop CNC	1	4	105	420
Ballscrew free end support BF12-C7	HomeShop CNC	1	2	45	90
Ballscrew nut S1605-4-C7 - Square	HomeShop CNC	1	4	99	396
Coupling - EC30 - 3/8 in. to 3/8 in.	HomeShop CNC	1	2	27.5	55
Timing pulley - L-series - 1/2 in. belt width - 0.375 in bore - 1 in. hub dia A 6A 4-12DF05012	SDP-SI	1	3	14.36	43.08
Timing belt - L series - 0.5 in. wide - 76.875 in. long - A 6R 4-205050	SDP-SI	1	1	24.08	24.08

Aluminum plate - 12 in. x 12 in. - 1/4 in. thick	DML			0	0
Duraboard 3000 ceramic insulator - 1 in. thick	DML			0	0
Ceramic unthread shoulder spacer w/ flange - pack of 5 - 92107A461	McMaster	1	2	14.85	29.7
Cover for socket head cap screw - 1/4 in. screw size - 96306A352	McMaster	1	1	6.76	6.76
Steel Plate - 1/2 inch THICK A36 Plate	DML	1	1	0	0
4-Axis Monster CNC Stepper Motor Driver Kit - Ready-to-run	Probotix	1	1	532.29	532.29
Computer and Monitor	DML		1	0	0
RBX-1 3-Channel Opto-Isolated Relay Board	Probotix	1	1	34.95	34.95
C6 - Variable Speed Control Board	CNC4PC	1	1	37.38	37.38
Aluminum sheet metal shielding	DML			0	0
Auto darkening welding helmet - Antra AH6-260-0000	Amazon	1	1	45.95	45.95
Protective fiberglass fabric	McMaster	25	1	7.5	187.5
Velcro Tape - adhesive back	Local store	1	1	15	15
Webcam - Logitech	Amazon	1	2	22.79	45.58
Millermatic MIL951620 MIG Welder with cart	Airgas	1	1	901.24	901.24
Steel build plate - 4 in. x 4 in. x 1/4 in. thick -1388K104	McMaster	1	4	17.04	68.16
Welding tips	Airgas	1	1	20	20
Welding wire - solid	Airgas	1	1	20	20
Argon gas	Airgas	1	1	5	5
CO_2 gas	Airgas	1	1	5	5
Airhose and couplings	DML	1	1	0	0
				Total	5153

16 x Ø .26 THRU ALL
⌴ Ø .43 ▽ .24

4 x Ø .22 THRU ALL
⌴ Ø .39 ▽ .20

4 x Ø .20 THRU ALL

12.0

1.181

7.49

12.0

1.575

2.087

.979

6.89

.50

	UNLESS OTHERWISE SPECIFIED:
	DIMENSIONS ARE IN INCHES
	SURFACE FINISH: As machined
	TOLERANCES:
	  LINEAR:= +/- 0.01, +/- 0.001
	  ANGULAR:
		FINISH:
		
		As machined
					DEBUR AND
					BREAK SHARP
					EDGES
							DO NOT SCALE DRAWING		REVISION	1

	NAME	SIGNATURE	DATE			TITLE:
DRAWN	J. S. Gaddes		11/17/15			
CHK'D						**Build Plate Mount**
APPV'D						
MFG						
Q.A			MATERIAL 6061 T6 Aluminum			DWG NO. 1	A4
			WEIGHT:			SCALE:1:10	SHEET 1 OF 1

4 x ⌀ 0.16 THRU ALL
10-32 UNF THRU ALL

⌀ 0.03 THRU
⌴ ⌀ 1.79 ↧ 0.07

⌀ 1.00 THRU

1.856

1.856

2.008

0.689

3.50

2 x ⌀ 0.35 THRU ALL

4.50

0.250

	NAME	SIGNATURE	DATE			TITLE:		
DRAWN	J.S. Gaddes		11/17/15					
CHK'D								
APP'VD								
MFG								
Q.A								

UNLESS OTHERWISE SPECIFIED:
DIMENSIONS ARE IN INCHES
SURFACE FINISH: As machined
TOLERANCES:
   LINEAR: +/- 0.01, +/- 0.001
   ANGULAR:

FINISH:

As machined

DEBUR AND
BREAK SHARP
EDGES

DO NOT SCALE DRAWING

REVISION   1

TITLE:

Base Motor Mount

MATERIAL
6061 T6

DWG NO.
2

A4

WEIGHT:

SCALE:1:2

SHEET 1 OF 1

4 x ⌀ 0 THRU ALL
M5x0.8 - 6H THRU ALL

2 x ⌀ 0.01 THRU ALL

0.046

0.04

0.018

0.032

0.018

0.08

0.10

UNLESS OTHERWISE SPECIFIED: DIMENSIONS ARE IN INCHES SURFACE FINISH: As machined TOLERANCES: LINEAR: +/- 0.01, +/-0.001 ANGULAR:	FINISH: As Machined			DEBUR AND BREAK SHARP EDGES	DO NOT SCALE DRAWING		REVISION 1

	NAME	SIGNATURE	DATE			TITLE:
DRAWN	J.S. Gaddes		11/17/15			**Base Fixed Ballscrew Mount**
CHK'D						
APPV'D						
MFG						
Q.A			MATERIAL 6061 T6 Aluminum		DWG NO. 3	A4
			WEIGHT:		SCALE:1:1	SHEET 1 OF 1

130

4 x Ø .17 THRU ALL
M5X0.8 - 6H THRU ALL

1.811

.709

2.25

1.299

.689

2 x Ø .35 THRU ALL

3.000

.250

4.00

	NAME	SIGNATURE	DATE		
DRAWN	J.S. Gaddes		11/17/15		
CHK'D					
APPV'D					
MFG					
Q.A					

UNLESS OTHERWISE SPECIFIED:
DIMENSIONS ARE IN INCHES
SURFACE FINISH: As machined
TOLERANCES:
  LINEAR: +/- 0.01, +/- 0.001
ANGULAR:

FINISH:

As Machined

DEBUR AND
BREAK SHARP
EDGES

DO NOT SCALE DRAWING

REVISION   1

TITLE:

Base Free Ballscrew Mount

MATERIAL
6061 T6 Aluminum

DWG NO.
4

A4

WEIGHT:

SCALE:1:1

SHEET 1 OF 1

18.0

11.75

4 x ⌀ 0.60 THRU ALL
⌴ ⌀ 0.90 ▽ 0.25

11.75

18.0

0.50

UNLESS OTHERWISE SPECIFIED: DIMENSIONS ARE IN INCHES SURFACE FINISH: TOLERANCES: LINEAR: +/-0.01, +/-0.001 ANGULAR:		FINISH: As Machined			DEBUR AND BREAK SHARP EDGES		DO NOT SCALE DRAWING		REVISION	1
	NAME	SIGNATURE	DATE			TITLE:				
DRAWN	J.S. Gaddes		11/17/15							
CHK'D							Build Plate			
APPV'D										
MFG										
Q.A				MATERIAL Steel		DWG NO. 5				A4
			WEIGHT:			SCALE:1:10		SHEET 1 OF 1		

4 x ⌀ 0.20 THRU ALL

8 x ⌀ 0.24 THRU ALL

0.197

7.141

0.567

2.087   1.856   0.984

0.683

1.856

1.575

1.181   3.750

0.313

2.031   0.250

5.104

10.21

4 x ⌀ 0.16 THRU ALL
10-32 UNF THRU ALL

⌀ 1.00 THRU
⌀ 1.79 ▽ 0.07

5 x ⌀ 0.26 THRU ALL
∨ ⌀ 0.51 X 100°

0.625

11.708

	NAME	SIGNATURE	DATE			
DRAWN	J.S. Gaddes		11/18/15			
CHK'D						
APPV'D						
MFG						
Q.A						

UNLESS OTHERWISE SPECIFIED:
DIMENSIONS ARE IN INCHES
SURFACE FINISH: As machined
TOLERANCES:
  LINEAR: +/-0.01, +/-0.001
  ANGULAR:

FINISH:
As Machined

DEBUR AND
BREAK SHARP
EDGES

DO NOT SCALE DRAWING

REVISION   1

TITLE:
Carriage Mount Right Upper

MATERIAL
6060 T6 Aluminum

DWG NO.
6

A4

WEIGHT:

SCALE:1:5   SHEET 1 OF 1

133

5 x ∅ 0.20 ▽ 1.40
1/4-20 UNC ▽ 0.50

4 x ∅ 0.20 THRU ALL
1/4-20 UNC THRU ALL

5.104

2.55

0.250

2.552

5.104

11.708

9.520

3.500

0.979

1.094

0.625

3.125

4 x ∅ 0.20 THRU ALL
1/4-20 UNC THRU ALL

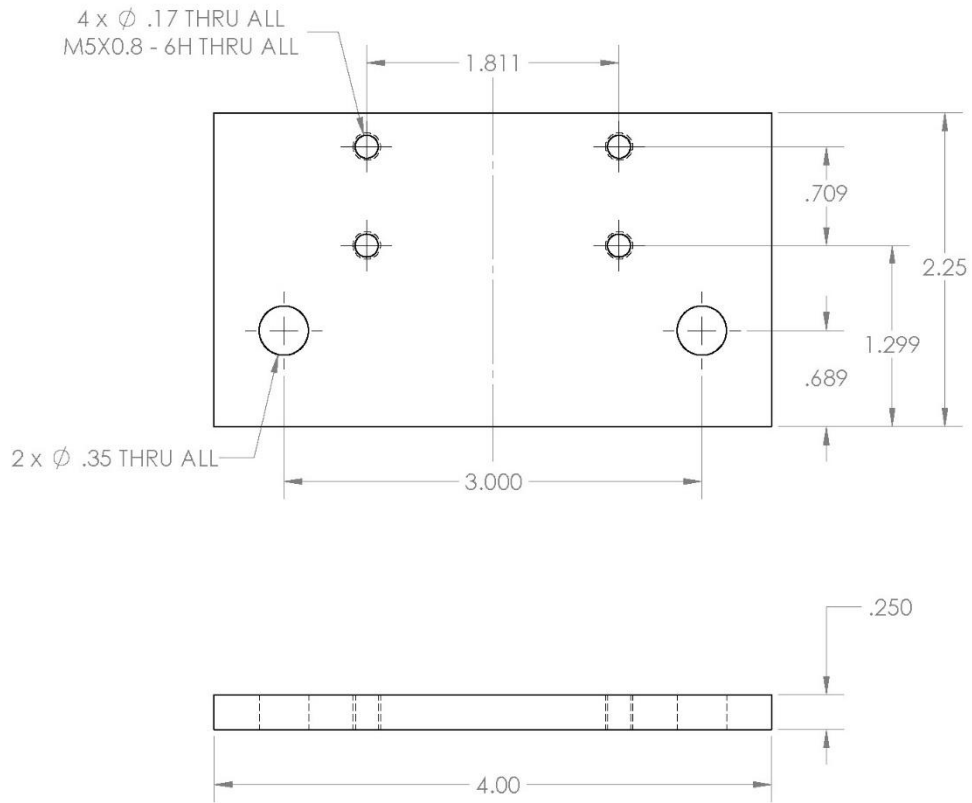|	NAME	SIGNATURE	DATE				TITLE:		
DRAWN	J.S. Gaddes		11/17/15						
CHK'D							Carriage Mount Left Lower		
APPV'D									
MFG									
Q.A									

UNLESS OTHERWISE SPECIFIED:
DIMENSIONS ARE IN INCHES
SURFACE FINISH: As machined
TOLERANCES:
 LINEAR: +/-0.01, +/-0.001
 ANGULAR:

FINISH:
As Machined

DEBUR AND
BREAK SHARP
EDGES

DO NOT SCALE DRAWING

REVISION   1

MATERIAL:
6061 T6 Aluminum

DWG NO.
7

A4

WEIGHT:

SCALE:1:5

SHEET 1 OF 1

134

4 x Ø 0.20 THRU ALL

8 x Ø 0.24 THRU ALL

3.571

2.087

1.575

1.493

1.181

3.750

0.313

0.984

5.104

5 x Ø 0.26 THRU ALL
⌵ Ø 0.51 X 100°

10.208

11.708

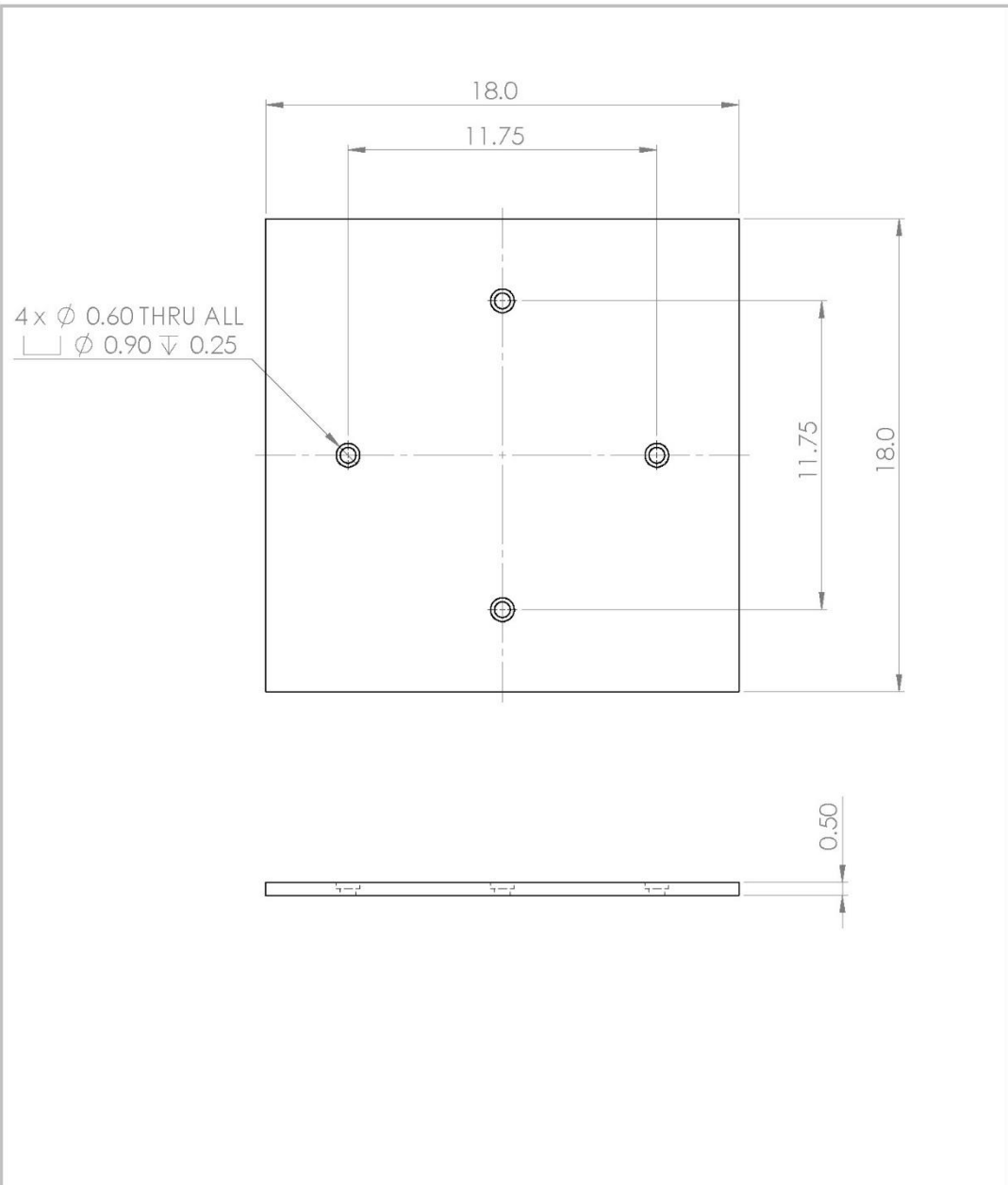|	NAME	SIGNATURE	DATE			TITLE:		
DRAWN	J. S. Gaddes		11/17/15					
CHK'D						Carriage Mount Left Upper		
APPV'D								
MFG								
Q.A						DWG NO.		A4

UNLESS OTHERWISE SPECIFIED:
DIMENSIONS ARE IN INCHES
SURFACE FINISH: As machined
TOLERANCES:
  LINEAR: +/-0.01, +/-0.001
  ANGULAR:

FINISH:

As Machined

DEBUR AND
BREAK SHARP
EDGES

DO NOT SCALE DRAWING

REVISION   1

MATERIAL:
6061 T6 Aluminum

DWG NO.
8

WEIGHT:

SCALE:1:5

SHEET 1 OF 1

135

5 x Ø 0.20 ▽ 1.40
1/4-20 UNC ▽ 0.50

4 x Ø 0.21 THRU ALL
1/4-28 UNF THRU ALL

1.094

0.979

11.708

5.104

2.55

2.552

0.250

5.104

3.500

9.520

0.625

3.125

4 x Ø 0.21 THRU ALL
1/4-28 UNF THRU ALL

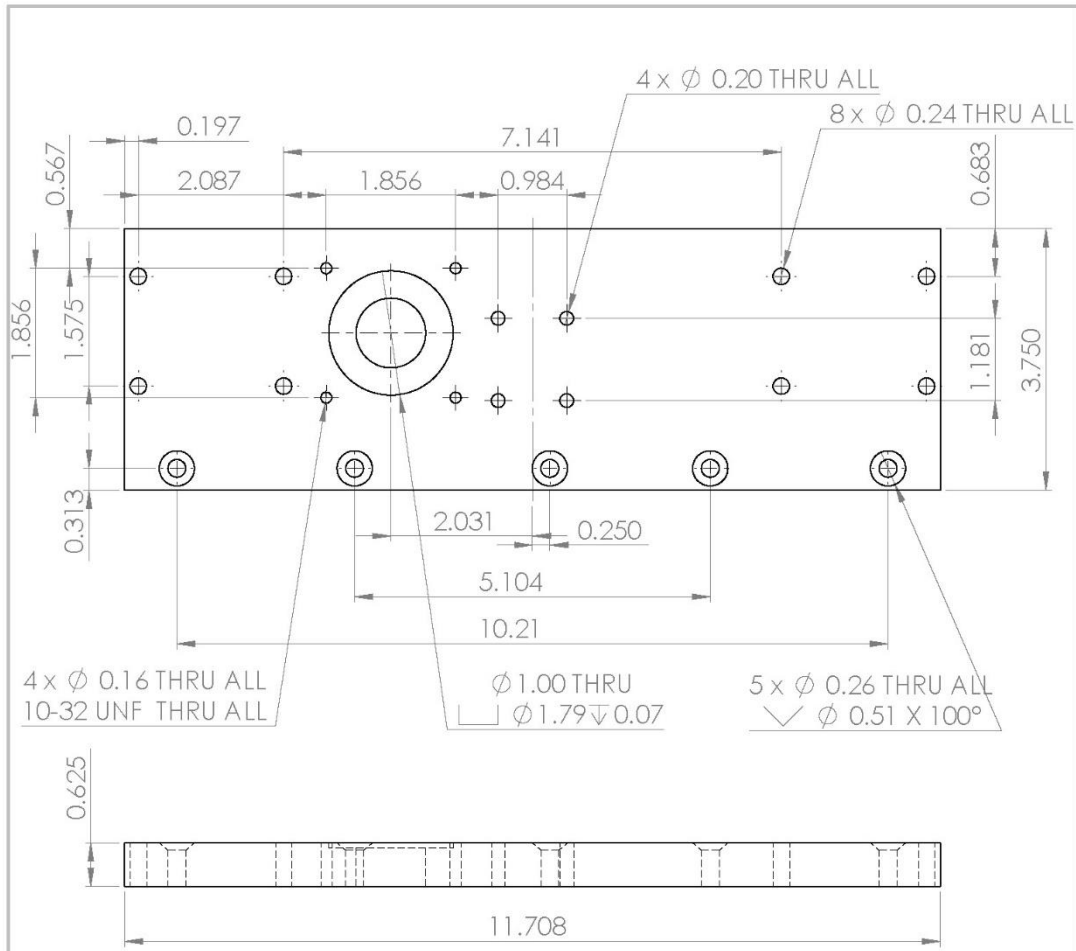|	NAME	SIGNATURE	DATE				TITLE:
DRAWN	J. S. Gaddes		11/17/15				
CHK'D							
APPV'D							
MFG							
Q.A							

UNLESS OTHERWISE SPECIFIED:
DIMENSIONS ARE IN INCHES
SURFACE FINISH: As machined
TOLERANCES:
  LINEAR: +/- 0.01, +/-0.001
  ANGULAR:

FINISH:

As Machined

DEBUR AND
BREAK SHARP
EDGES

DO NOT SCALE DRAWING

REVISION   1

TITLE:
Carriage Mount Right Lower

MATERIAL:
6061 T6 Aluminum

DWG NO.
9

A4

WEIGHT:

SCALE:1:5   SHEET 1 OF 1

2 x ⌀ 0.20 THRU ALL
M6x1.0 - 6H THRU ALL

4 x ⌀ 0.26 THRU ALL

2.500

1.750

0.907

1.811

3.500

0.646

UNLESS OTHERWISE SPECIFIED: DIMENSIONS ARE IN INCHES SURFACE FINISH: As machined TOLERANCES: LINEAR: +/-0.01, +/-0.001 ANGULAR:	FINISH:			DEBUR AND BREAK SHARP EDGES		DO NOT SCALE DRAWING		REVISION	1
	As Machined								
	NAME	SIGNATURE	DATE			TITLE:			
DRAWN	J. S. Gaddes		11/18/15						
CHK'D						Free Side Carriage Rail Mount			
APPV'D									
MFG									
Q.A			MATERIAL			DWG NO.			A4
			6061 T6 Aluminum			10			
			WEIGHT:			SCALE:1:2		SHEET 1 OF 1	

137

4 x ⌀ 0.26 THRU ALL

4 x ⌀ 0.20 THRU ALL
M6x1.0 - 6H THRU ALL

2.500

1.750

0.375

1.811

3.500

4.250
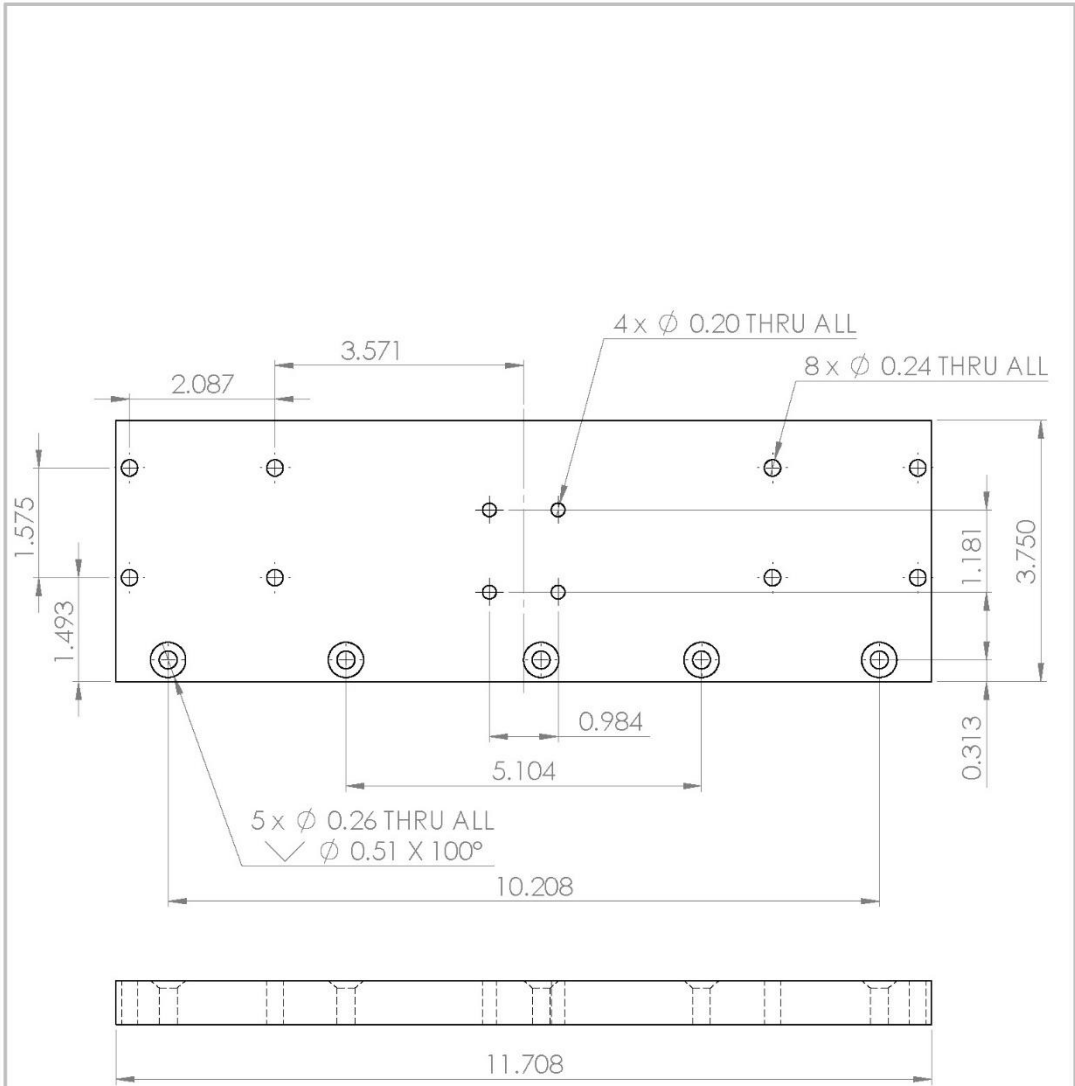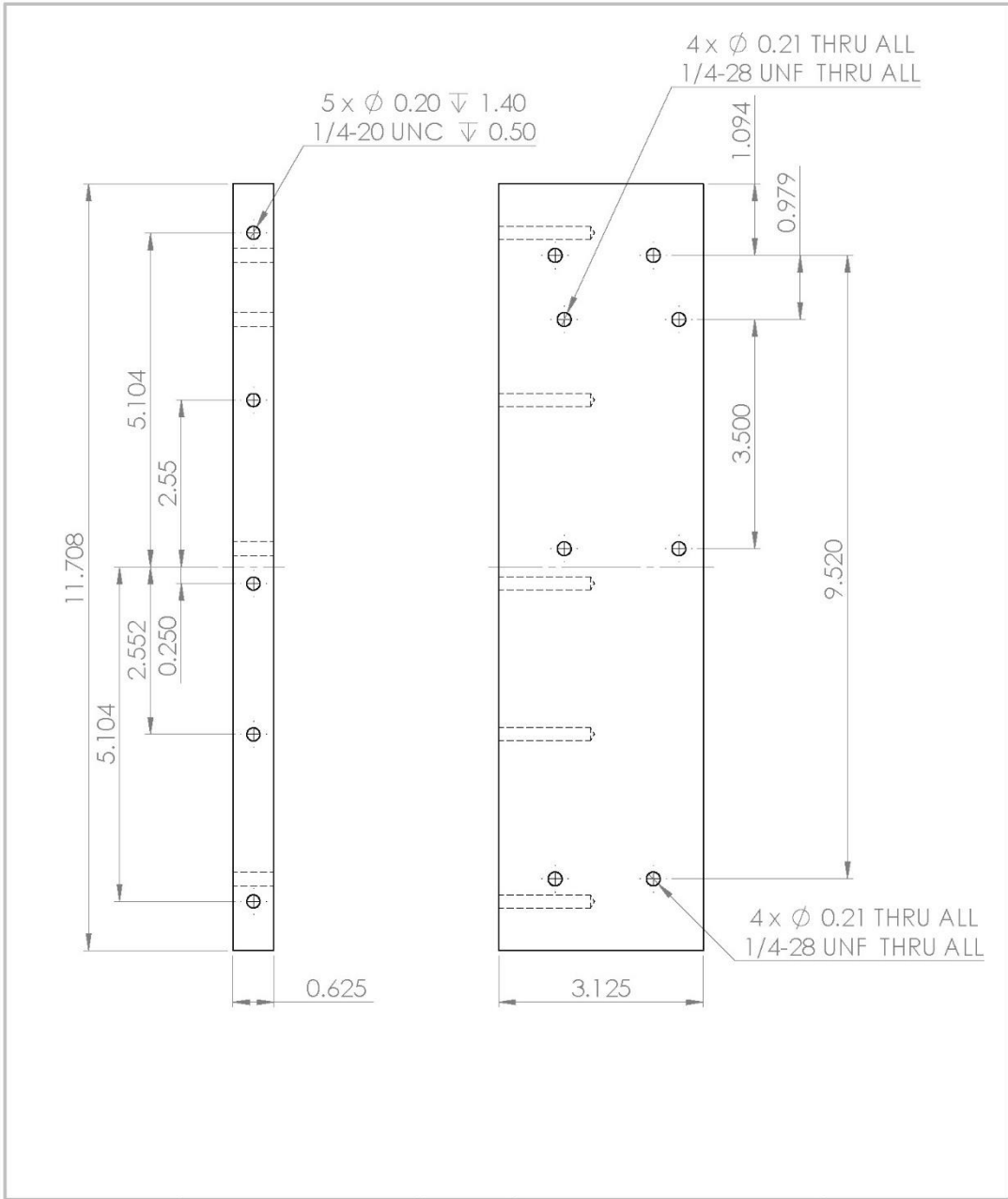
0.512

0.395

0.646

| | | UNLESS OTHERWISE SPECIFIED: DIMENSIONS ARE IN INCHES SURFACE FINISH: As machined TOLERANCES: LINEAR: +/-0.01, +/-0.001 ANGULAR: | FINISH: As Machined | | DEBUR AND BREAK SHARP EDGES | | DO NOT SCALE DRAWING | | REVISION | 1 |

	NAME	SIGNATURE	DATE			TITLE:
DRAWN	J.S. Gaddes		11/18/15			
CHK'D						Motor Mount Side Carriage Rail Mount
APPV'D						
MFG						
Q.A			MATERIAL 6061 T6 Aluminum			DWG NO. 11

A4

WEIGHT:

SCALE:1:2

SHEET 1 OF 1

138

2 x ⌀ 0.33 THRU ALL
⌴ ⌀ 0.59 ▽ 0.31

4 x ⌀ 0.20 THRU ALL
M6x1.0 - 6H THRU ALL

0.512

0.811

1.811

3.11

3.91

0.625

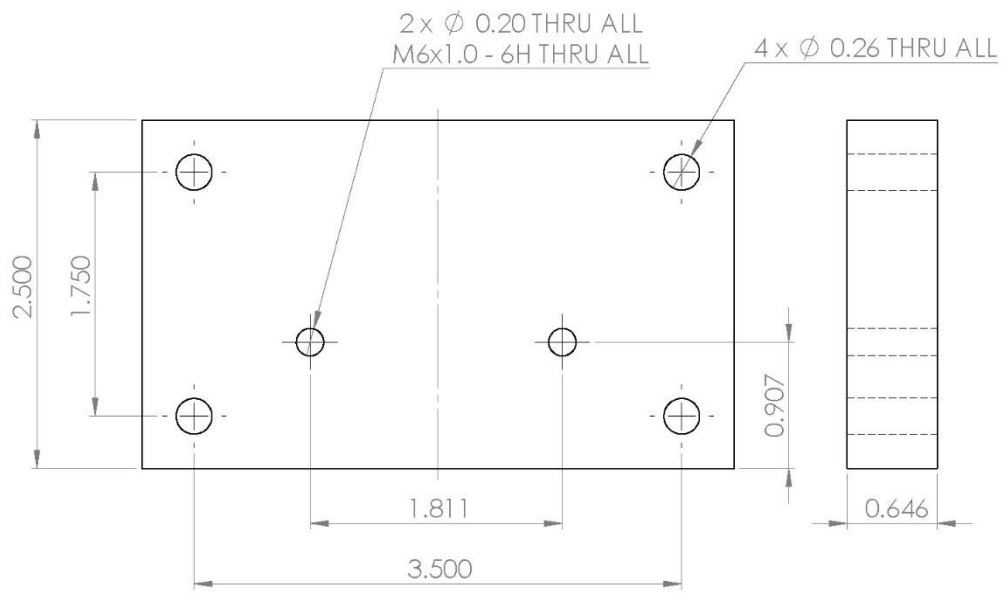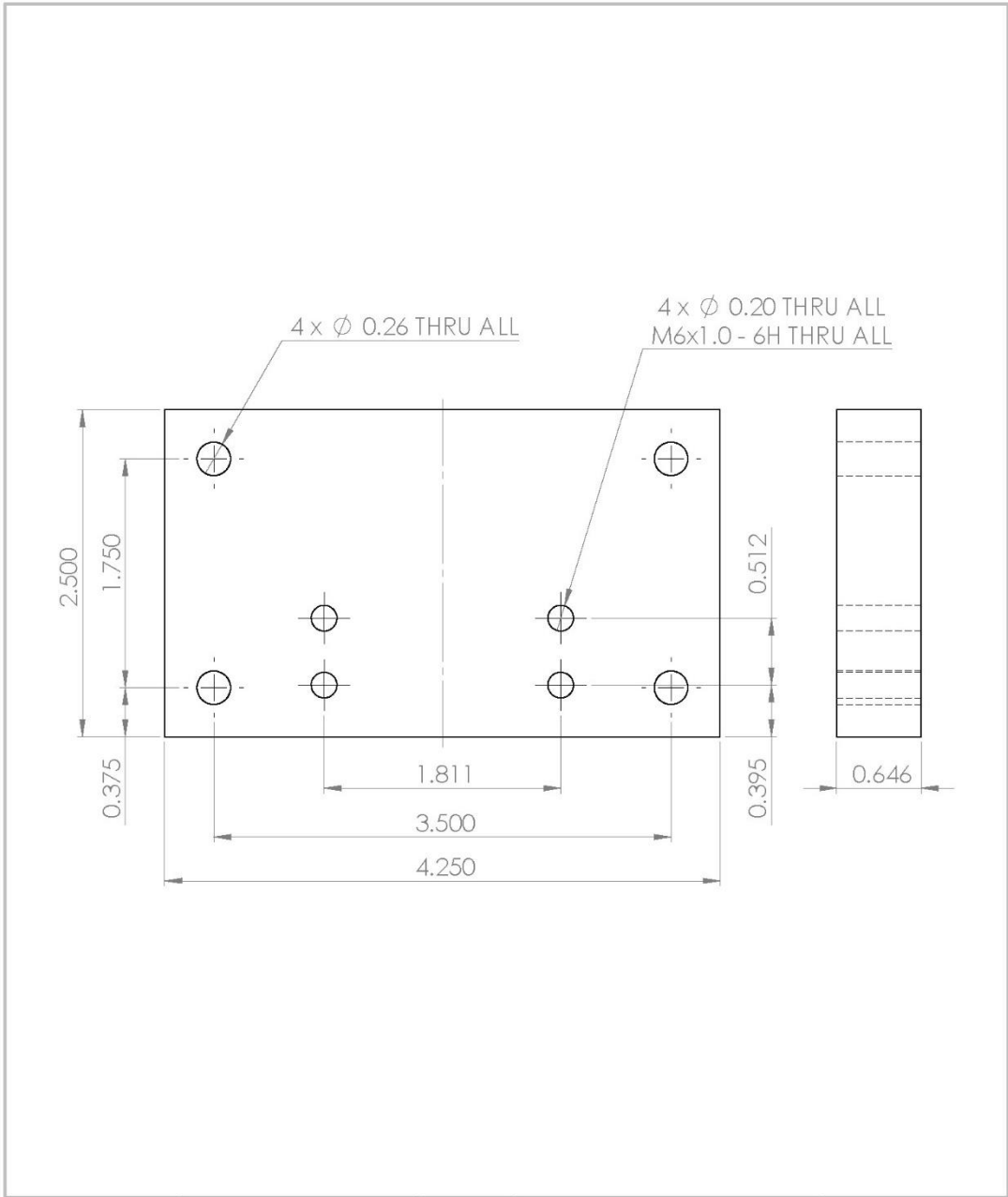|	NAME	SIGNATURE	DATE			TITLE:		
DRAWN	J.S. Gaddes		11/18/15			Vertical Axis Ball Screw Mount		
CHK'D								
APPV'D								
MFG								
Q.A					MATERIAL 6061 T6 Aluminum	DWG NO. 12		A4
				WEIGHT:		SCALE:1:1		SHEET 1 OF 1

UNLESS OTHERWISE SPECIFIED:
DIMENSIONS ARE IN INCHES
SURFACE FINISH: As Machined
TOLERANCES:
   LINEAR: +/- 0.01, +/-0.001
   ANGULAR:

FINISH:

As Machined

DEBUR AND
BREAK SHARP
EDGES

DO NOT SCALE DRAWING

REVISION   1

4 x Ø 0.16 THRU ALL
10-32 UNF THRU ALL

Ø 1.00 THRU
Ø 1.79 ▽ 0.07

1.856

1.856

1.126

0.625 X 1.63

1.00

6.00

1.50

0.313

2.00

4.00

0.25

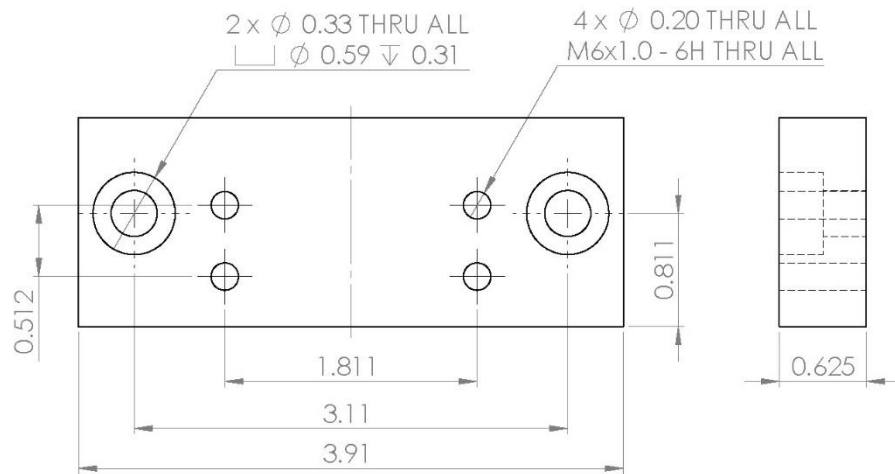|	NAME	SIGNATURE	DATE			TITLE:		
DRAWN	J.S. Gaddes		11/18/15					
CHK'D						Z-Axis Motor Mount		
APPV'D								
MFG								
Q.A						DWG NO.	13	A4

UNLESS OTHERWISE SPECIFIED:
DIMENSIONS ARE IN INCHES
SURFACE FINISH: As machined
TOLERANCES:
LINEAR: +/-0.01, +/-0.001
ANGULAR:

FINISH:
As Machined

DEBUR AND
BREAK SHARP
EDGES

DO NOT SCALE DRAWING   REVISION   1

MATERIAL
6061 T6 Aluminum

WEIGHT:

SCALE:1:2

SHEET 1 OF 1

4 x Ø 0.17 THRU ALL
M5x0.8 - 6H THRU ALL

2.362

1.287

1.500

0.500

4 x Ø 0.27 THRU ALL
⌴ Ø 0.44 ▽ 0.25

29.00

1.00

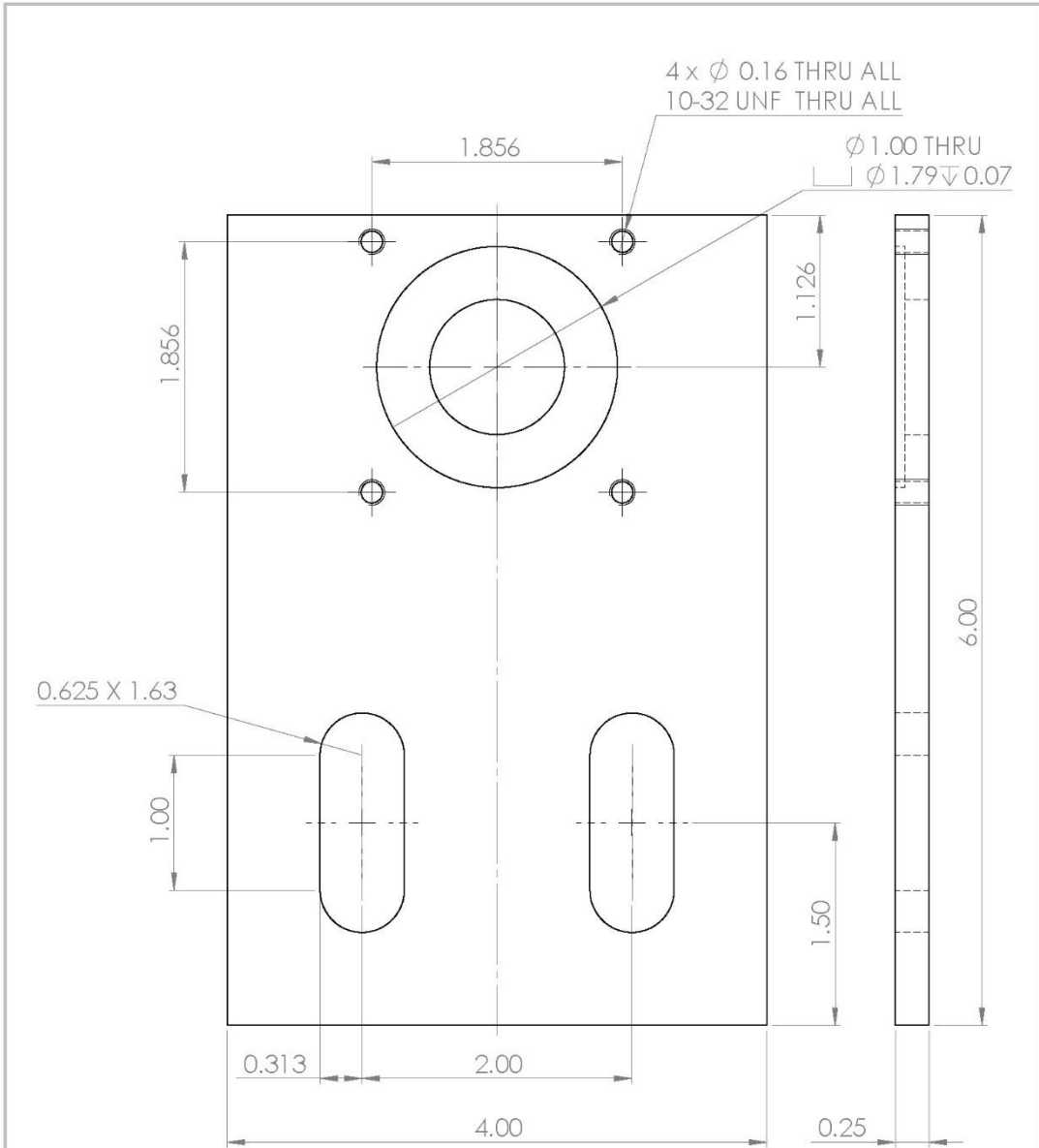|	NAME	SIGNATURE	DATE				
DRAWN	J.S. Gaddes		11/18/15				
CHK'D							
APPV'D							
MFG							
Q.A							

UNLESS OTHERWISE SPECIFIED:
DIMENSIONS ARE IN INCHES
SURFACE FINISH: As machined
TOLERANCES:
   LINEAR: +/- 0.01, +/-0.001
   ANGULAR:

FINISH:

As Machined

DEBUR AND
BREAK SHARP
EDGES

DO NOT SCALE DRAWING

REVISION   1

TITLE:

Z Carriage Long End Bar

MATERIAL
6061 T6 Aluminum

DWG NO.

14

A4

WEIGHT:

SCALE:1:10

SHEET 1 OF 1

2.087   7.316

1.575

1.213

1.181

4 x ⌀ 0.25 THRU ALL
⌴ ⌀ 0.43 ▽ 0.24

4 x ⌀ 0.21 THRU ALL
⌴ ⌀ 0.39 ▽ 0.20

0.984   3.977

0.625

12.883

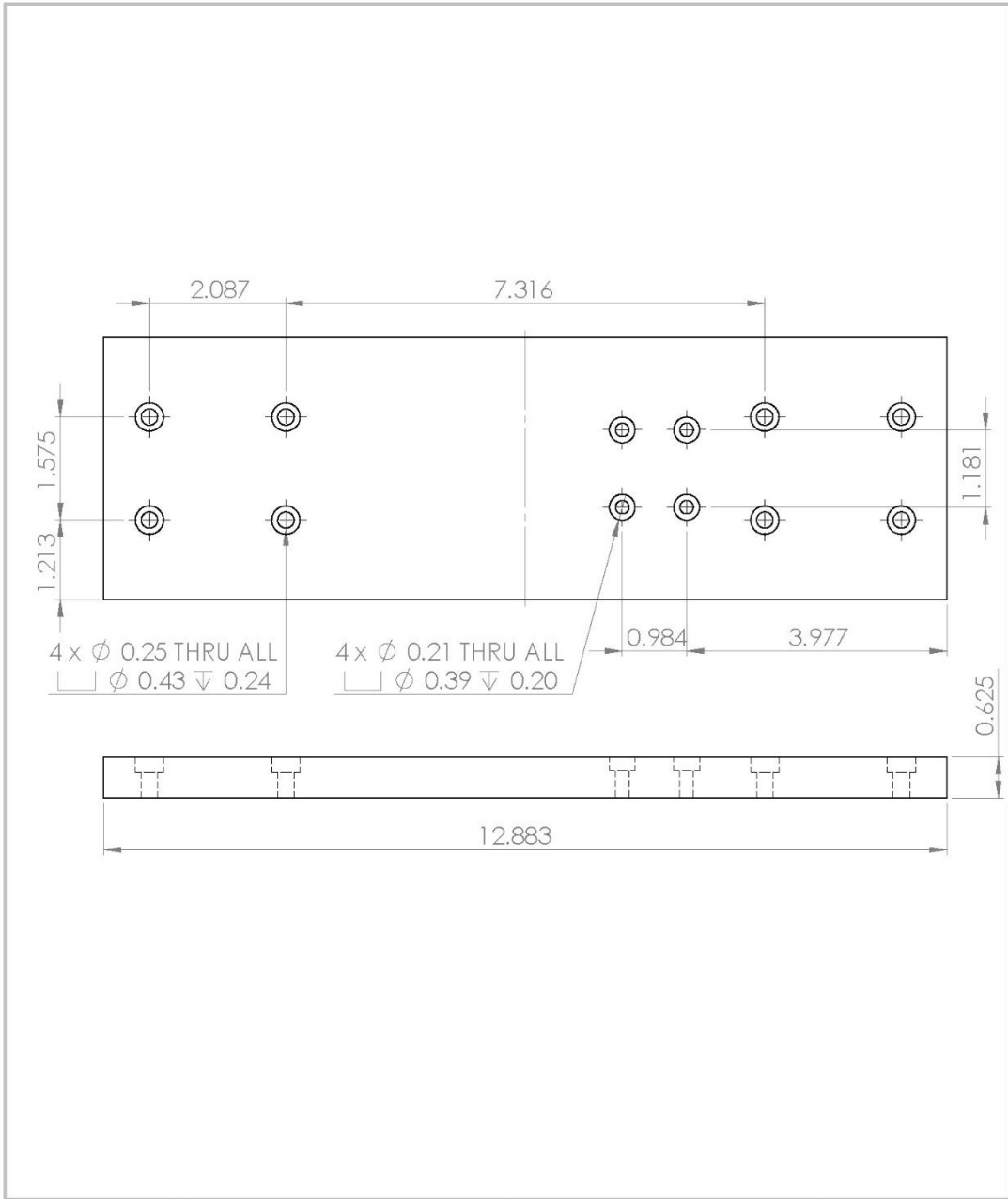|	NAME	SIGNATURE	DATE				TITLE:		
DRAWN	J.S. Gaddes		11/18/15						
CHK'D									
APP'VD									
MFG									
Q.A									

UNLESS OTHERWISE SPECIFIED:
DIMENSIONS ARE IN INCHES
SURFACE FINISH: As machined
TOLERANCES:
  LINEAR: +/- 0.01, +/-0.001
ANGULAR:

FINISH:

As Machined

DEBUR AND
BREAK SHARP
EDGES

DO NOT SCALE DRAWING   REVISION   1

TITLE:

Carriage Base

MATERIAL
6061 T6 Aluminum

DWG NO.

15

A4

WEIGHT: SCALE:1:5   SHEET 1 OF 1

Appendix 2: Arduino Code

The Arduino code for the voltage and current monitor is presented below. The code was original written by Pinar *et, al* and was modified to include a timer which was used to correlate to the print time [1].

```
#define NUM_AVG 250
void setup() {
Serial.begin(115200);
}
void loop() {
double vin = 0;
double iin = 0;
double timer = 0;
for(int a=0; a<NUM_AVG; a++) {
vin = vin + analogRead(1);
iin = iin + analogRead(2);
}
vin = vin / NUM_AVG;
iin = iin / NUM_AVG;
vin = vin * 5 / 1024;
iin = iin * 5 / 1024;
double i = -1.022 * iin * iin + 52.08 * iin + 0.0024;
double v = 10.48407 * vin;
timer = millis();
Serial.print(v);
Serial.print(",");
Serial.print('\t');
Serial.println(i);
Serial.print('\t');
Serial.print(timer,0);
Serial.print(",");
Serial.print('\t');
}
```

Appendix 3: Operation Manual

Hardware, Software, and Controls Overview

As outlined in the machine construction process, the 3D printer is comprised of hardware, software, and controls.

Hardware refers to the machine's mechanics, the welder, the wire feed mechanism, the computer, the stepper motor drivers and relays, and the voltage/current monitor. The Millermatic 190 welder was slightly modified for use with the 3D printer. The wire feed speed can be varied and the power can be turned on and off with the *Mach3* control software. The voltage is manually set with control knob on the front of the welder. The other knob which controls the wire feed speed is disabled because the wire feed speed is controlled by the *Mach3* control software.

The wire feed mechanism is a modified Spoolmate 100. The wire feed mechanism receives wire from a spool mounted to the rear of the machine. There are two electrically isolated spool holders. One spool holder is capable of holding 4 in. diameter spools and the other spool holder is capable of holding 8 in. diameter spools. The wire is fed from the spool, through a PTFE tube, and into the wire feed mechanism.

The computer, which is running Windows 7 and is not connected to the internet, is responsible for preparing the CAD model, controlling the printer, and recording the voltage/current. The CAD model is prepared by either the *Slic3r* or *Kisslicer* software packages. These software packages are capable of the importing a *.stl* file and exporting the machine control code called G-code. The G-code is then modified with a text editor (like *Notepad*) and imported into the *Mach3* control software. The *Mach3* control

144

software is CNC software that interprets the G-code and sends electronic pulses to stepper motor drivers and relays.

The stepper motor drivers and relays interface with the computer via a parallel port cable. The stepper motor drivers and relays send power to the motors and enable/disable the printer based upon the signals received from *Mach3*.

The voltage/current monitor is mounted inside of the welder and is easily observable and removable via the access door on the welder. The voltage/current monitor operates with the ±15 VDC power supply and has two green LEDs that indicate that the monitor is operational. The voltage/current sends the measured voltage and current to the Arduino Uno. The Arduino Uno receives the analog signal from the voltage/current monitor, processes the information, and sends the measured values to the computer via the USB serial port. By monitoring the serial port on the computer (COM 4), the voltage and current values can be observed in real time and recorded. The *sdp.exe* software is used to observe and record the data.

Turning on the Machine

The machine requires two electrical power inputs. The welder requires 240 Volts and the power strip which distributes power requires 110 Volts. The welder is turned on with a switch on the rear of the unit. The computer is turned on with the power button on the front. The computer monitor is turned on with the power button on the front. The stepper motor drivers are turned on with a red switch on the front of the stepper motor driver enclosure. The ±15 VDC power supply for the voltage/current monitor is turned on with a switch on the front. When operation of the machine is finished, it should be turned off.

Preparing and Slicing the CAD Model

The CAD model must be in the *.stl* file format before it is imported into the *Slic3r* or *Kisslicer* slicing software packages. The *.stl* must be in millimeter units. After importing the *.stl* file, the model is sliced and the gcode is generated based upon the slicing parameters. These parameters are saved in profiles that are loaded through the slicing software. Multiple profiles have been created. The slicing process results in a *.gcode* file that must be slightly modified before it can be read by *Mach3*.

Post Processing the G-code

Because the slicing software was originally purposed for FDM 3D printing, the created G-code must be edited before it can be imported into *Mach3*. A text editor, like *Notepad*, can be used to perform the find and replace the text. The necessary modifications, based upon the slicing software, are outlined in Table 6. Additionally, the command "M3 Sxxxxx" must be inserted at the top of the G-code to indicate the correct wire feed speed. After post processing, the G-code can be imported into *Mach3*.

Table 6: G-code Post Process Text Replacement

Slicing Software	"Find" Text	"Replace" Text
Slic3r	M11	M8
Slic3r	M10	M9
Slic3r	E	A
Kisslicer	M101	M8
Kisslicer	M103	M9

A list of all of the custom G-codes and M-codes for the machine and their function is outlined in Table 7. It is important to note that the *M3* command must be issued with a speed to enable the spindle. However, the welder does not turn on the wire feed and power until the *M8* command is issued.

Table 7: Custom Machine Commands

Command	Code
Enable wire feed (spindle)	M3
Disable wire feed (spindle)	M5
Set wire feed speed	Sxxxxx
Feed wire and turn on weld power	M8
Stop wire feed and turn off weld power	M9

Loading the Wire

The welding wire is stored on a spool mounted to the rear of the machine. After removing and replacing the spool, the wire must be fed through the PTFE tubing. Care must be taken to not let the wire rapid unspool or kink. From the PTFE tubing, the wire is fed into the feed mechanism. The red lever must be depressed to release the drive rollers and allow the wire to be fed. The wire must be fed through the feed mechanism and the copper welding tip. The copper welding tip and splatter shield may require removal to feed the wire. When changing the copper welding tip, care must be taken to not over tight and strip the soft threads. However, the tip must be tight enough to provide good electrical contact and not loosen during the machine's operation.

After inserting the wire through the feed mechanism, the wire path must be inspected to make sure there are no kinks and that the drive rollers are correctly engaged. The drive rollers must grip the wire and not slip. However, care must be taken when feeding soft materials (like aluminum) to ensure that the wire is not so deformed by the grip process that it will not easily feed through the copper welding tip. The gripping force applied by the drive rollers to the wire can be adjusted by turning the recessed flathead screw on the front of the drive mechanism. Turning the screw counter-clockwise applies more force to the wire.

Loading the Build Plate

The build plate is securely attached to the steel platform by ½-13 bolts and washers. To prevent toxic fumes, care must be to ensure that the bolts and washers are not plated. Additionally, the build plate should clean and in good electrical contact with the steel platform.

Setting the Gas Flow Rate

The shielding gas flow rate is controllable with the regulator attached to the shielding gas tank. The regulator reads the gas flow rate when the machine is in operation. The gas flow rate should be set between 20 and 30 CFH.

Preparing *Mach3* for Printing

After loading the G-code into *Mach3* CNC software, the machine must be jogged into position and zeroed at the appropriate location. The G-code assumes that the center of the sliced CAD model is at the *x,y,z* locations of 0,0,0. The machine is jogged into position (presumable on the center of the buildplate) using the arrow keys on the keyboard, and the *Zero Axis* button is pressed to set the coordinates to zero. The

machines *z-axis* is jogged using the *page up* and *page down* keys. After the machine is zero, the G-code is ready to be run.

Measuring the Voltage and Current

The voltage/current monitor begins recording when the *sdp.exe* application is started. The application displays the real time measurement values and records the values to a text file that is saved in the same file directory as the *.sdp* executable. After each session, the saved file must be renamed after closing the *sdp.exe* application or it will be appended when the software is restarted. The saved text file includes three columns of text that can be imported into *Excel* or *MATLAB*. The first column contains a time counter that counts in milliseconds, the second column contains the voltage measurement, and the third column contains the current measurement.

Varying Parameters during Machine Operation

If desired, two significant parameters can varied during the machine's operation. The machine's motion feed rate is modified by changing "Feed Rate" slider. The wire feed rate is modified by changing "Spindle Speed" slider. The machines voltage can be varied by turning the control knob on the front of the welder. The shielding gas flow rate can be changed by turning the control valve on the regulator.

Appendix 4: Experimental Record Sheet

Run number:		**Date:**	
Description:		**Time:**	
Environment	Ambient Temperature:		
	Base plate temperature:		
	Shielding gas composition:		
	Shielding gas temperature:		
	Shielding gas flow rate:		
	Sheilding gas application:		
Material	Base plate material:		
	Base plate thickness:		
	Wire material:		
	Wire diameter:		
Slicing Parameters	Slicing software used:		
	Slicing profile name:		
	CAD model name:		
	Layer height:		
	Perimeter layer width:		
	Infill layer width:		
	Number of perimeters:		
	Infill percentage:		
	Infill pattern:		
	Pause time after layer change:		
	Spiral perimeter:		
	Number of solid top layers:		
	Number of solid bottom layers:		
	Perimeter feed rate:		
	Infill feed rate:		
	Wire (spindle) feed rate:		
Welder Parameters	Welder voltage:		
	Wire stickout:		
	Wire offset:		
Miscellaneous	Build duration:		
	Recorded video file name:		
	Voltage/current file name::		
Notes and Observations			